Technische Universität München
TUM School of Medicine and Health

Elucidating the Role of Innate Immunity during Intestinal Inflammation in XIAP deficiency

Madeleine Müller-Foxworth

Vollständiger Abdruck der von der TUM School of Medicine and Health der Technischen Universität München zur Erlangung eines Doctor of Philosophy (Ph.D.) genehmigten Dissertation.

Vorsitz: Prof. Dr. Marc Schmidt-Supprian

Betreuer: Prof. Dr. Percy A. Knolle

Prüfende der Dissertation:
1. TUM Junior Fellow Dr. Jan P. Böttcher
2. Prof. Dr. Dietmar Zehn

Die Dissertation wurde am 05.03.2024 bei der Technischen Universität München eingereicht und durch die TUM School of Medicine and Health am 08.07.2024 angenommen.

Acknowledgements

Though a PhD title may be awarded to a single person, it is a shared achievement shaped by the support of an entire community. This echoes the African belief that raising a child takes a whole village.

First, I sincerely Prof. Percy Knolle and Dr. Monica Yabal for their trust and guidance. I am also grateful to my long-time colleague, Adam Wahida; though we are quite different, our collaboration has enriched my experience. Heartfelt thanks go to Dr. Caterina Branca, a brilliant scientist and friend; everyone should be lucky enough to have an Italian friend like her.

I also want to thank my research partners, including Valentina Brunner, Markus Tschurtschenthaler, Marijana Basic and her team, Laura Griewahn, and Ulrich Maurer. Their scientific support and collaboration have been invaluable. Thanks as well to the core facility teams, notably Dr. Katja Steiger, Olga Seelbach, Silke Hegenbarth, and Savvoula Michailidou, and to the dedicated animal facility staff who ensured high welfare standards in our experiments.

Beyond colleagues, I have gained friends across various labs who have brightened my journey: Tina, Monique, Jan, Fabi, Selin, Linsey, Basti, Charlotte, Evi, Charlie, and Giuliana. Their support often inspires me to keep going.

Finally, I am most grateful to my family, who have always provided unconditional love: my parents, Brigitta and Rainer; my sisters, Kathi and Johannah; my brother-in-law, Markus; and my husband, Joshua. They do not simply call me to pursue my career, but to live my life. Resilience is nurtured by those who believe in you. I could not have done this without them.

Table of Contents

List of Abbreviations

A

Adgre1 = Adhesion G Protein-Coupled Receptor E1 (F4/80)

AIM2 = Absent in Melanoma 2

AMP = anti-microbial peptide

ANOVA = Analysis of Variance

B

BayBioMS = Bayerisches Zentrum für Biomolekulare MassenSpektrometrie

BIR = Baculoviral IAP Repeat

BIRC4 = Baculoviral IAP Repeat Containing 4

Bmi1 = B-Cell-Specific Moloney Murine Leukaemia Virus Integration Site 1

BMP = Bone Morphogenic Protein

Bst2 = Bone Marrow Stromal Antigen 2

C

CARD = Caspase Activation and Recruitment Domain

CASPx = caspase-x

CCRx = C-C Chemokine Receptor Type x

Clecx = C-type Lectin Domain Containing x

CDx = Cluster of Differentiation x

CEP = Comparative Experimental Pathology Department

CLR = C-type Lectin Receptor

Csf1r, M-CSF R = Macrophage Colony-Stimulating Factor Receptor

Csf2ra, Csf2rb, GM-CSF R = Granulocyte-Macrophage Colony-Stimulating Factor Receptor

CXCR3 = C-X3-C Motif Chemokine Receptor 1

D

D = Day

DAMP = Danger-Associated Molecular Pattern

DAP = Diaminopimelic Acid

DC / cDCx / pDC = dendritic cell / conventional DC type x / plasmacytoid DC

DC–SIGN = Dendritic Cell-Specific Intercellular adhesion molecule-3-Grabbing Non-integrin

DD = Death Domain

DIABLO = Direct IAP-Binding protein with Low pI

DNA = Deoxyribonucleic acid

Dpp4 = Dipeptidyl peptidase 4

E

EO IBD = early-onset IBD

F

Fcgrx = Fc gamma receptor x

Fcgr1 = High-affinity immunoglobulin gamma Fc receptor

Flt3 = Fms-like tyrosine kinase 3

FMT = faecal material transplant

FOXP3 = Forkhead box P3

G

GALT = gut-associated lymphoid tissue

gf = germfree

GI = gastrointestinal

GSDMx = Gasdermin x

GWAS = Genome-wide association Studies

H

HDAC = histone deacetylase

H&E = Haematoxylin-Eosin

HILIC = hydrophilic interaction liquid chromatography

HLH = haemophagocytic lymphohistiocytosis

HMI = high metabolic independence

HSCT = haematopoietic stem cell transplantation

I

cIAPx = cellular inhibitor of apoptosis protein x
IBD = Inflammatory Bowel Disease
IBDU = IBD unclassified
ICAM1 = Intercellular Adhesion Molecule 1
IE = intraepithelial
IEC = intestinal epithelial cell
IEL = intraepithelial lymphocytes
IET = intraepithelial T cell
IFNy = Interferon gamma
IHC = Immunohistochemistry
IκBKG = Inhibitor of Nuclear Factor Kappa-B Kinase subunit gamma
ILx = Interleukin x
IL10R = Interleukin 10 Receptor
Irfx = Interferon regulatory factor x
ITGAE/M/X = Intergrin alpha E/M/X
ITM2C = Integral Membrane Protein 2C

K

KEGG = Kyoto Encyclopedia of Genes and Genomes

L

Lgr5 = Leucin-rich Repeat-containing G-Protein Coupled Receptor 5
Ln / mLn = lymph node / mesenteric Ln
LP = Lamina propria
LPS = lipopolysaccharide
Ly6x = Lymphocyte antigen 6 complex, locus x
LUBAC = Linear Ub Chain Assembly Complex

M

M cell = microfold cell
Mafb = v-Maf avian musculoaponeurotic fibrosarcoma oncogene homolog B
MAMP = microbe-associated molecular pattern
MAP3K7 = Mitogen-activated Protein Kinase Kinase Kinase 7
MDP = muramyl dipeptide
MEFV = Mediterranean Fever
MHCII = Major Histocompatibility Cluster II
MLKL = Mixed Lineage Kinase Domain Like Pseudokinase
Mo/Mac = monocyte/macrophage
MS = mass spectrometry
MUC2 = Mucin2
MyD88 = Myeloid Differentiation primary response 88

N

NFκB = Nuclear Factor Kappa-Light-Chain-Enhancer of Activated B Cells
NLR = NOD-Like Receptor
NLRP3 = NOD-Like Receptor Family Pyrin Domain Containing 3
NLRC4 = NOD-Like Receptor Family CARD Domain Containing 3
NODx = Nucleotide-binding Oligomerization Domain-containing protein x

O

zOTU = zero-radius operational taxonomic unit

P

PAMP = pathogen-associated molecular pattern
PAS = Periodic acid – Schiff
PC = Phosphatidylcholine
PCA = Principle Component Analysis
pH = potential of hydrogen
PE = Phosphatidylethanolamine
Plet1 = Placenta-expressed transcript 1
PMT = photomultiplier tube
PRR = Pattern Recognition Receptor
PTGDS = Prostaglandin D2 Synthase
Ptprc = Protein tyrosine phosphatase, receptor type, C
PYCARD = PYD and CARD Domain Containing

R

RegIII = Regenerating Islet-Derived Protein 3

RING = Really Interesting New Gene

RIPKx = Receptor Interacting Serine/Threonine Kinase x

RNA / bulkRNAseq / scRNAseq = ribonucleic acid / bulk RNA sequencing / single cell RNA sequencing

RT = room temperature

S

SCFA = short-chain fatty acid

SCID = severe combined immunodeficiency syndrome

SEM = Standard Error of the Mean

Siglech = Sialic acid binding Ig-like lectin H

Sirpα = Signal-regulatory protein alpha

SMAC = Second Mitochondria-derived Activator of Caspases

SN = supernatant

SNP = Single Nucleotide Polymorphism

SOX4 = SRY-Box Transcription Factor 4

SPF = specific-pathogen-free

STATx = Signal Transducer and Activator of Transcription x

STRING = Search Toll for the Retrieval of Interacting Genes/Proteins

T

TCR = T cell receptor

TF = Transcription factor

TLRx = Toll-like Receptor x

TNF = Tumour Necrosis Factor

TNFRx = TNF receptor x

TNFRSFx = TNF receptor superfamily x

TRADD = TNFR1-associated death domain protein

TRAFx = TNF receptor-associated factor x

U

Ub = Ubiquitin

UBA =

UC = Ulcerative Colitis

UEA1 = Ulex europaeus agglutinin-1

UMAP = uniform Manifold Approximation and Projection

UV = ultraviolet

V

VEO IBD = very early-onset IBD

W

Wt = wild type

X

Xcr1 = X-C motif Chemokine Receptor 1

XIAP = X-linked inhibitor of apoptosis protein

XLP2 = X-linked lymphoproliferative syndrome 2

Z

ZBP1 = Z-DNA binding protein 1

Zbtb46 = Zinc finger and BTB domain-containing Protein 46

Abstract

Inflammatory bowel disease (IBD) is a chronic multifactorial disease phenotype, affecting over five million people worldwide. Patients suffer lifelong disease relapses, with limited and cost-intensive treatment options, such as the use of anti-TNF biologics. Monogenic IBD, such as caused by mutations in the gene encoding the X-linked inhibitor of apoptosis protein XIAP, is often particularly severe and can manifest already in infancy. Approximately 4% of early-onset IBD cases can be linked to XIAP deficiency, but the exact disease mechanism remains elusive.

I employed a mouse model featuring a genetic deletion of *Xiap* and systematically exposed these mice to microbiota. Young germfree *Xiap*$^{-/-}$ mice developed the first signs of tissue inflammation in the terminal small intestine, ileum, and microbial dysbiosis within 15 days of conventionalisation. Transcriptomics and protein surface marker-based experimental methods identified unique subsets of CD209a^{+} dendritic cells (DC) located in the ileal epithelium and Lamina propria, whose loss was dependent on TNF (tumour necrosis factor) signalling via TNF-receptor 2 downstream of TLR (toll-like receptor) 5 and correlated with tissue inflammation. I propose the existence of a plasmacytoid DC (pDC)-like pre-conventional DC (cDC) 2 subset, functionally adapting to the tissue environment, and activated by exposure to intestinal luminal antigens.

Additionally, I could show that *Xiap*$^{-/-}$ mice failed to establish adequate numbers of certain bacterial families, such as Bifidobacteriacae and Verrucomicrobiaceae, representing the first signs of dysbiosis. I enhanced these findings by discovering changes in the caecal metabolic profile, particularly regarding amino acid synthesis and cell membrane components.

My work sheds light on the central role of XIAP in mediating a local innate immune cell response to microbial stimuli, which contributes to the Crohn's-like ileitis observed in both *Xiap*$^{-/-}$ mice, and XIAP-deficient patients. In the future, it might contribute to refining treatment options for IBD patients, as it elucidates a lesser-known mechanism of inflammatory cell death downstream of TNF signalling via TNFR2 and suggests a path for the use of microbiota-based therapy options.

Zusammenfassung

Weltweit sind mehr als 5 Millionen Patienten von chronisch-entzündlichen Darmerkrankungen, IBD, betroffen. Durch die vielen Faktoren, sowohl genetische als auch Lebensstil-bedingte, die in das Krankheitsbild hineinspielen, ist die Ermittlung eines genauen Krankheitsursprungs schwer. Trotz kostenaufwändiger Therapieoptionen, etwa der Behandlung mit Anti-TNF-Biologika, leiden die Patienten oft ein Leben lang unter Rückfällen. Seltener sind Fälle monogener IBD, die auf die Mutation eines einzelnen Gens zurückgeführt werden. Diese sind besonders schwerwiegend, und können bereits im Säuglings- oder Kleinkindalter auftreten. Bei etwa 4% dieser jungen IBD-Patienten lassen sich die Symptome mit einem Defizit im sogenannten *X-linked inhibitor of apoptosis*-Gen XIAP erklären. Über den molekularen Wirkmechanismus dieses Apoptose-Inhibitor-Proteins in IBD ist jedoch wenig bekannt.

Durch die systematische Besiedelung keimfreier *Xiap*-defizienter Mäuse mit einem Mikrobiom konnte ich erste Anzeichen von Gewebsentzündung im terminalen Dünndarm, Ileum, innerhalb von 15 Tagen induzieren. Außerdem zeigten diese Mäuse Anzeichen einer sich entwickelnden Dysbiose, und daraus folgend Veränderungen des metabolischen Profils im Blinddarm. Durch eine Kombination von transkriptom- und proteinmarker-basierten Methoden konnte ich spezialisierte Subpopulationen von CD209a-expremierenden dendritischen Zellen (DC) identifizieren, die sich durch die sie umgebenden Zytokine funktionell an ihre Verortung im intraepithelialen Raum, oder der Lamina propria des Ileums anpassen. Ich postuliere daher, dass die lokale Entzündung der Villi des Dünndarms mit dem TNFR2-abhängigen Zelltod dieser DC korreliert, welche in Abwesenheit von XIAP auf eine Aktivierung des TLR5 mit luminalen Flagellinen reagieren. Die sich ausbildende mikrobielle Dysbiose war vor allem von einer reduzierten Menge an Bakterien im Allgemeinen, und dem Verlust einzelner Bakterien-Familien, beispielsweise Bifidobacteriaceae und Verrucomicrobiaceae, geprägt.

Mit Hilfe der hier präsentierten Forschungsergebnisse liefere ich einen Beitrag zum Verständnis der Rolle von XIAP in der Vermittlung adäquater lokaler Immunzellaktivierung. Ich hoffe zudem, dass ich durch meine Erkenntnisse um die molekularen Mechanismen, welche zu hyperentzündlichen Immunzell-Reaktionen auf mikrobielle Reize in Abwesenheit von XIAP führen, welche sowohl dem Morbus

Crohn-ähnlichen Phänotyp im Dünndarm von *Xiap*$^{-/-}$ Mäusen, als auch XIAP-defizienter Patienten zu Grunde liegen, auch allgemein zum Fortschritt im Feld der entzündlichen Darmerkrankungen beitragen kann.

Die neuartige Entdeckung, welche entzündlichen Zelltod als Konsequenz von aberranter TNF-Signalgebung vermittelt durch TNFR2 in den Vordergrund rückt, eröffnet potentiell Wege für neue Anti-TNF-basierte Therapieoptionen. Eine zusätzliche Errungenschaft könnte in der gezielten mikrobiellen Besiedelung oder Gabe von bestimmten Metaboliten liegen, um einer patienten-eigenen Dysbiose entgegenzuwirken.

Introduction

Intestinal tissue physiology and mucosal immunity

The gastrointestinal (GI) system is a complex network of organs vital for digesting food, absorbing nutrients and water, and eliminating waste. In mammals, the GI tract includes several organs: the mouth, oesophagus, stomach, small intestine (which is divided into the duodenum, jejunum, and ileum), large intestine, and rectum, as well as the liver, gallbladder, and pancreas. Each of these organs contributes to the breakdown of food and the retention of both macronutrients and micronutrients. The GI system serves as a crucial regulator of an organism's health, highlighted by the increasing research focus on the gut-brain axis, now frequently referred to as the microbiota-gut-brain axis.

Though less intuitive, an essential function of this vast interface lies in mucosal immunity since the GI tract is a primary entry point for various antigen-rich environmental components. The intestine provides the most significant contribution to the immune system, housing specialised innate and adaptive immune cell populations[1,2] in the lumen-facing mucosal epithelium and the densely populated Lamina propria (LP)[3]. Specialised epithelial M cells transport antigens from the intestinal lumen to immune cells in Peyer's Patches, part of the gut-associated lymphoid tissue (GALT)[4].

Understanding the compartmentalisation of the intestine is essential to fully understand its role both in health and disease. It leads to varied physiological conditions that impact specific immunological processes[5]. The anatomical makeup of the surrounding tissue shapes the intestinal niches. For instance, Paneth cells are found in the crypts of Lieberkühn in the small intestine, where they carry out innate immune-like functions. However, they are absent from the colon. Additionally, extrinsic factors such as pH and oxygen gradients play a significant role in determining the composition of the immune cell populations, and local commensal microbiota.[6]

Given that this thesis focuses on the ileum, the terminal segment of the small intestine, subsequent chapters will primarily examine the specific conditions in this niche. **Figure 1** illustrates the general tissue architecture of the small intestine. While many aspects of mucosal immunity could be discussed, the following sections will

concentrate on those most relevant to the experimental results presented in the chapter “Results.”

The contribution of intestinal epithelial cells to mucosal immunity

Intestinal mucosal immunity arises from the interplay of three main factors: the integrity of the intestinal epithelial barrier, the diverse immune cell populations within the tissue, and the contribution of the commensal microbiome. Perturbations in the latter are discussed in a subsequent chapter.

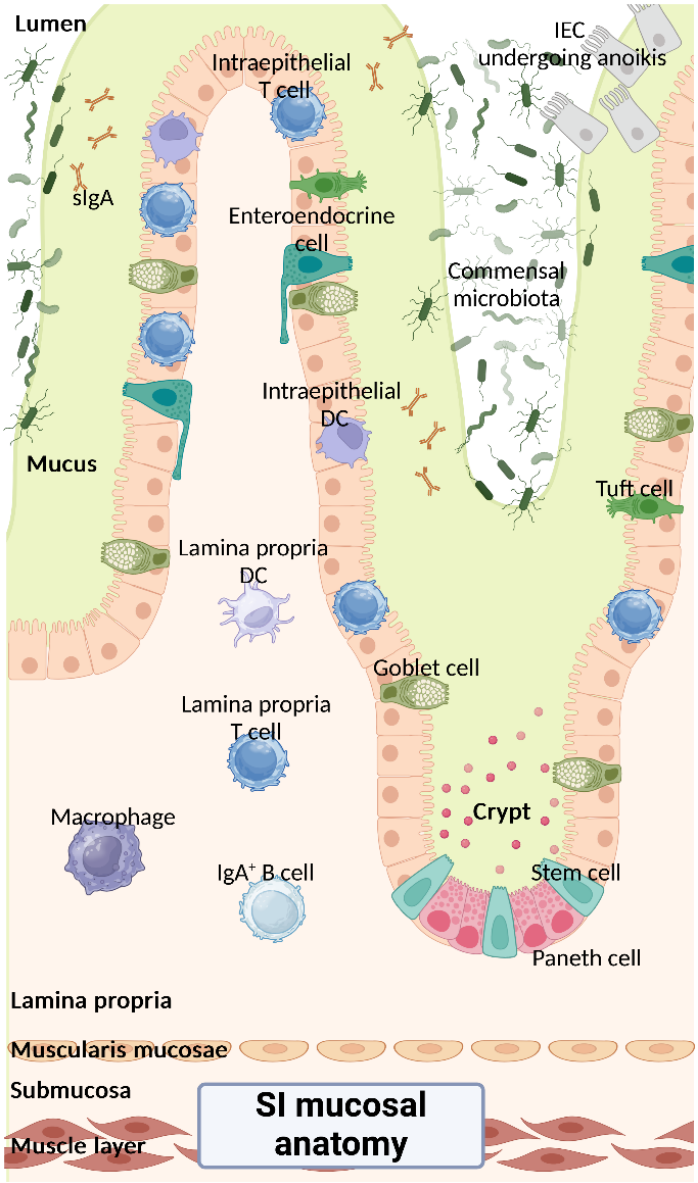

Figure 1. Illustration of the intestinal mucosal anatomy and immune cell repertoire of the small intestine. This figure depicts the commensal microbiome (dark green) within a protective mucus layer (light green) made of proteoglycans, that serves as a barrier to pathogens and a habitat for some microbiota. Goblet cells (grass green) produce this mucus layer. The small intestine is lined with villi composed of columnar intestinal epithelial cells (IECs, orange), each with a microvilli-covered brush

border. These villi are interspersed with crypts of Lieberkühn, containing intestinal stem cells (turquoise) at the crypt base, replenishing IECs shed from the villus top. Paneth cells (dark red) in the crypts produce antimicrobial peptides (AMPs, red) to prevent bacterial invasion.

Intraepithelial lymphocytes (blue) are specialised T cells closely associated with the epithelium. Specific dendritic cells (DCs, lilac) also integrate into the epithelium, expressing tight junction markers and projecting dendrite-like protrusions into the lumen for antigen sampling.[7] The lamina propria (LP) beneath the epithelium contains diverse innate and adaptive immune cells, which this thesis discusses in detail. Figure generated using Biorender.

As illustrated in **Figure 1**, the intestinal epithelium consists of a single layer of columnar epithelial cells. Traditionally viewed primarily as a physical barrier between the intestinal lumen and underlying tissues, recent discoveries highlight the active role of specialised epithelial cell types in maintaining intestinal health, re-positioning the epithelium as a potential therapeutic target for intestinal diseases.[8]

Intestinal epithelial cell (IEC) development begins in the crypts of Lieberkühn, where long-lived stem cells are interspersed with Paneth cells—specialised innate immune-like epithelial cells considered the guardians of the crypt. Stem cells can be identified by leucine-rich repeat-containing G-protein coupled receptor 5 (Lgr5)[9] markers and Bmi1 (B-Cell-Specific Moloney Murine Leukemia Virus Integration Site 1)[10]. As stem cells divide and differentiate, they migrate upward along the villus toward the lumen. A unique retrograde movement of these cells occurs at the crypt periphery, primarily in the small intestine, which plays a critical role in replenishing the stem cell pool.[11]

The upward differentiation of epithelial cells is regulated by gradients of Wnt/β-Catenin expression, and signals from Paneth cells, including R-spondin, Notch, and bone morphogenetic protein (BMP), which help maintain stem cell identity.[12] Once a stem cell exits the crypt, specifically from position +5 above the most distal stem cell, it enters the transit amplifying zone. As cells progress along the villus, they encounter various transcription factor gradients that promote terminal differentiation.[13] Within a few days (typically 2 to 5), downregulation of integrin expression leads to a form of programmed non-inflammatory cell death called anoikis[14], resulting in cell shedding into the intestinal lumen.

Paneth cells support the stem cell niche and produce antimicrobial peptides (AMPs), as shown in **Figure 1**. Their distinct morphology, characterised by acidophilic granules, contains crucial components such as α-defensins, lysozyme, tumour necrosis factor (TNF), RegIII (Regenerating Islet-Derived), immunoglobulin A, matrix metalloproteinase-7, and interleukin (IL)-1β.[15] Given their vital role in maintaining

intestinal epithelial integrity, Paneth cell dysfunction has been linked to several intestinal pathologies, such as inflammatory bowel disease (IBD)[16], particularly Crohn's Disease (CD)[17].

The protective mucus layer separating luminal content from the epithelial surface is crucial for intestinal health. Intestinal mucus, composed of glycoproteins[18], is produced by Goblet cells and serves as both a nutrient source and a biological niche for microbiota associated with the epithelium. The molecule Mucin2 (MUC2)[19] is the primary constituent of intestinal mucus. The diversity of Goblet cell types and mucus consistency across intestinal compartments contributes to localised microbial diversity. Adequate mucus production is essential for intestinal function; reduced Goblet cell numbers or functionality is associated with infections and inflammatory conditions, such as CD.[20]

Intestinal immune cell diversity

The following chapter emphasizes the role of myeloid populations, specifically macrophages and dendritic cells, central to the experimental results presented herein. Knowledge about the role of specialised immune subpopulations is rapidly evolving, particularly with advancements in single-cell transcriptomics.

The intestinal epithelium harbours unique sets of immune cells that exploit their close proximity to the intestinal lumen to survey antigens and relay this information to other immune cells located deeper in the tissue, such as in the LP. The immune cell populations in the small intestine can be categorised into two groups based on their compartmental residency: intraepithelial lymphocytes (IEL) and Lamina propria lymphocytes (LPL). However, the term "lymphocyte" can be misleading, as it suggests a focus solely on adaptive immune cells, while both innate and adaptive immune cells contribute to these compartments.

Adaptive immune cells, particularly specialised T cell populations, are key to maintaining intestinal homeostasis. A large proportion of the small intestinal T cell repertoire is TCRγδ$^+$ that play a prominent role in immune surveillance at mucosal surfaces with high antigen exposure.[21] Accordingly, these TCRγδ$^+$ T cells are concentrated in the intestinal epithelium, and their dysregulation has been implicated in IBD pathogenesis.[22] Located primarily in the Lamina propria (LP), regulatory T cells are essential for intestinal immune tolerance, functionally supported by tolerogenic DC

populations.[23] As this thesis focuses on myeloid populations, further details on T cell functions and their contributions to IBD pathology lie outside its scope.

Myeloid cell subtypes include granulocytes (neutrophils, eosinophils, basophils) and circulating monocytes, which may differentiate into DC and macrophages upon migrating to tissues in response to cytokine gradients.[24] The different types of myeloid immune cells are essential to the innate immune system, and originate from a common progenitor in the bone marrow[25]. Protein markers, including cytokine receptors and transcription factors, have helped classify specific myeloid identities over time.[26] Myeloid cell identities and functions have been found to be shaped by their tissue environment and local homeostasis[27] and certain macrophage and DC populations are self-renewing in specific tissues[28].

Granulocyte subtypes each have specialised functions. Neutrophils, as rapid responders to inflammation, perform phagocytosis and release extracellular traps. Eosinophils and basophils mediate responses to allergens and parasites.[29] Eosinophils are linked to asthma via granules containing peroxidases and MBP, while basophils, with histamine- and heparin-rich granules, affect vascular permeability in allergic reactions.

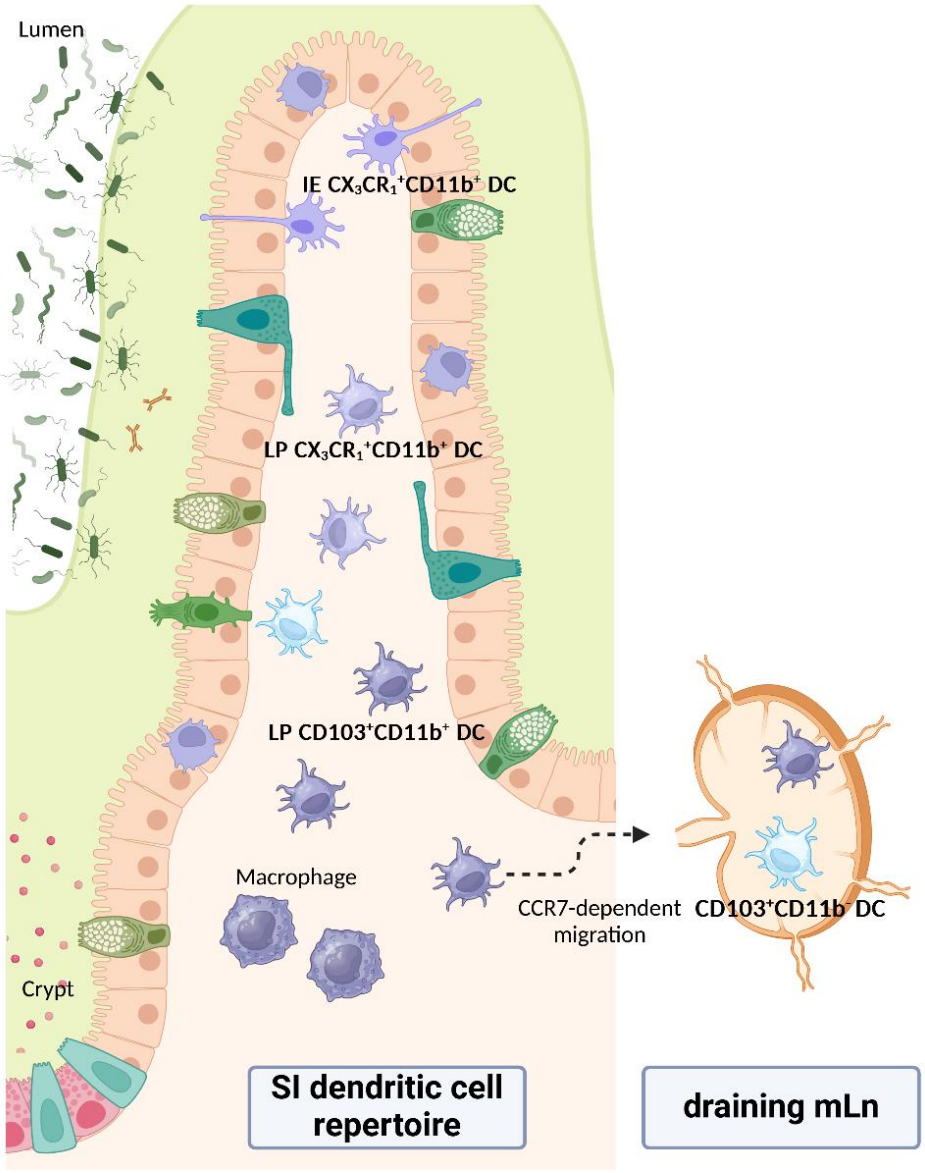

Figure 2. Overview of small intestinal intraepithelial (IE) and lamina propria (LP) myeloid populations, focusing on dendritic cell (DC) subtypes. Depicted are myeloid cell populations (lilac) closely associated with the epithelium. DCs extend dendrites across the epithelium to sample luminal antigens by upregulating tight junction markers like Claudin-4 and Zona occludens-2.[7] In the LP, DC subpopulations, differentiated by markers CD11b (violet) and CD103 (light blue), regulate immune tolerance versus response, including T cell differentiation in the LP and mesenteric lymph nodes (mLn). Figure generated using Biorender.

Figure 2 displays diverse dendritic cell (DC) populations within their intestinal tissue compartments. Both the intestinal epithelium (IE) and LP are densely populated with immune cells that maintain the critical balance between immune tolerance and activation. Conventional DC (cDC) capture and process antigens, presenting them to naïve T cells with co-stimulatory molecules to induce T cell activation and differentiation. Due to constant antigen exposure from food, foreign substances, and the intestinal microbiome, the intestine is a unique environment optimised to retain

high immune tolerance.[30] This tolerance relies largely on high levels of the anti-inflammatory Interleukin (IL)-10,[31,32] which mitigates inflammation and is linked to one of the most prominent monogenic IBD phenotypes, as detailed in a later chapter.

Macrophages and DC, key antigen-presenting cells, facilitate the transition from innate to adaptive immunity. Hence, both macrophages and DC play a pivotal role in intestinal homeostasis.[33] On a molecular level, both cell types express MHCII[34,35] and CD11c, participating in antigen presentation. Generally, it was understood that murine macrophages can be differentiated from DC by the expression of CD64 and F4/80[36,37]. CD11b expression distinguishes DC from macrophages in lymphoid tissue, while CD103 indicates tissue residency in DC located in non-lymphoid tissue. However, distinguishing monocyte-derived DC from true macrophages, either by phenotype or function, remains challenging.[38,39] Conventional DC (cDC1 and cDC2) are marked by XCR1 and CD172a (SIRPα), respectively.[40,41] While either $CD11b^+$ or $CD103^+$ DC are found in various organs, double-positive $CD11b^+CD103^+$ DC are unique to the intestine.[42] Intestinal subtypes of cDC2 are traditionally further differentiated by markers such as the chemokine-receptor CX_3CR_1 or ESAM (Endothelial Cell-Selective Adhesion Molecule).[43,44]

Hinging on discoveries such as illustrated in the paper by Papaioannou *et al.*[45], previous dogmas around DC ontogeny are being challenged. Broader access to large transcriptomic datasets at single cell level has unveiled a broader picture of myeloid diversity, in particular with respect to the heterogeneity of cDC2. An attempt to give an overview of the latest developments is depicted in **Figure 3**. This also illustrates the fluidity of DC identity, as different pre-cursors can display different DC identities along their ontogenetic development, and previously established markers, such as CD64 or F4/80 might have to be revisited. Since it has been shown that the distinct cytokine environments in certain tissue niches or upon certain tissue states (i.e. tissue homeostasis versus inflammation) can vastly influence the phenotype and function of myeloid cells, the predominant question to ask has become whether cell identity can be determined purely based on the expression of certain markers.[80,47]

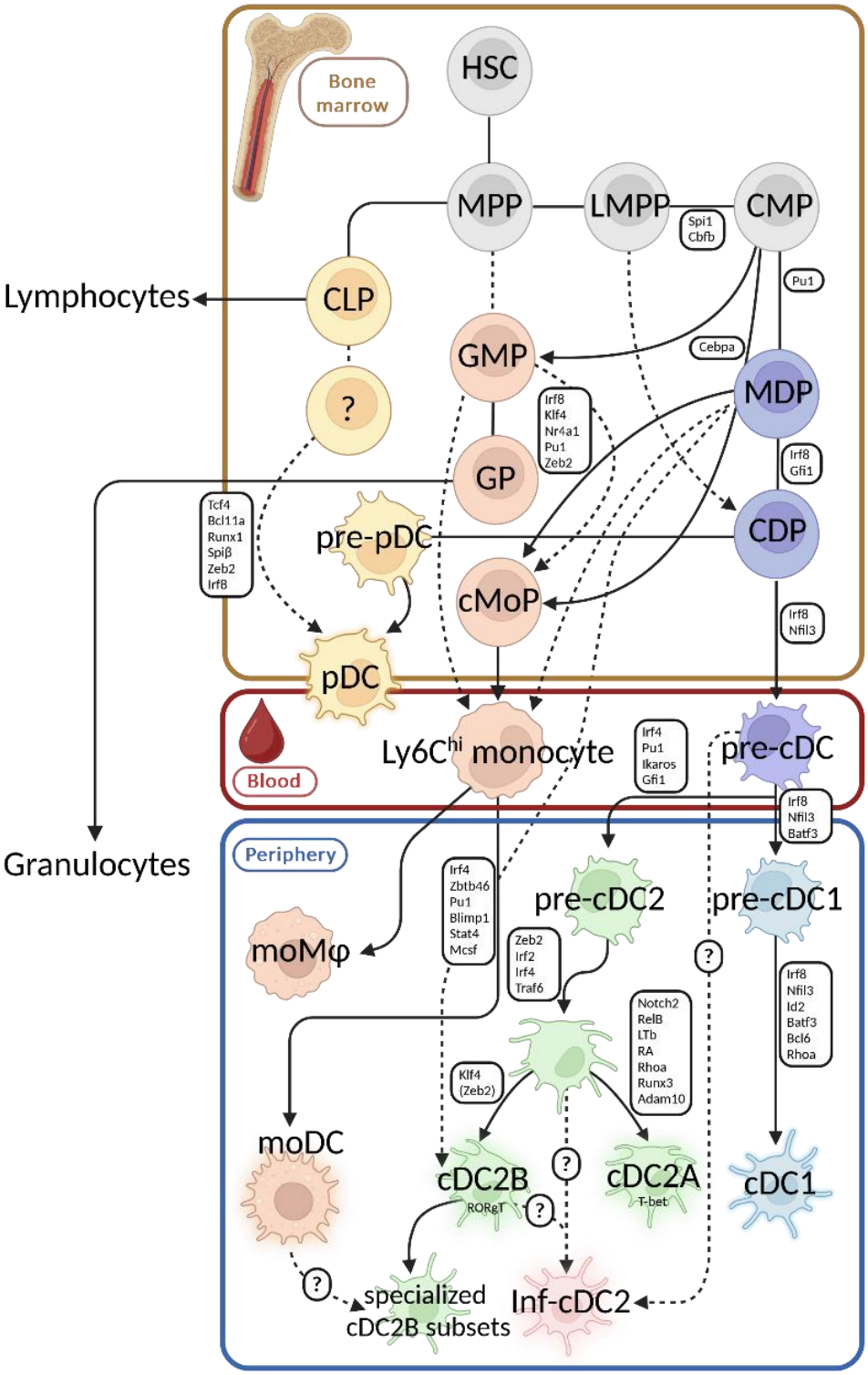
Bone marrow
HSC
MPP
LMPP
CMP
Spi1
Cbfb
Pu1
Lymphocytes
CLP
GMP
Cebpa
MDP
?
Irf8
Klf4
Nr4a1
Pu1
Zeb2
Irf8
Gfi1
GP
Tcf4
Bcl11a
Runx1
Spiβ
Zeb2
Irf8
pre-pDC
CDP
cMoP
Irf8
Nfil3
pDC
Blood
Ly6C^hi monocyte
Irf4
Pu1
Ikaros
Gfi1
pre-cDC
Irf8
Nfil3
Batf3
Granulocytes
Periphery
Irf4
Zbtb46
Pu1
Blimp1
Stat4
Mcsf
pre-cDC2
pre-cDC1
moMφ
Zeb2
Irf2
Irf4
Traf6
?
Irf8
Nfil3
Id2
Batf3
Bcl6
Rhoa
Notch2
RelB
LTb
RA
Rhoa
Runx3
Adam10
Klf4
(Zeb2)
moDC
cDC2B
RORgT
?
?
cDC2A
T-bet
cDC1
?
specialized
cDC2B subsets
Inf-cDC2

	cDC1 (Ccr7 DC?)	ESAM^{high} cDC2A	ESAM^{low} cDC2B (DC3?)	Inf-cDC2	cDC3 (cDC2B?)	MoDC	pDC (tDC?/preDC2?)
General surface markers	CD11c, MHCII, CD26, FLT3	CD11c, MHCII, CD26, FLT3	CD11c, MHCII, CD26, FLT3	CD11c, MHCII, CD26, FLT3		CD11c, MHCII	
Specific (surface) markers	CD8, CD24, CD36, CD103, CD205, Clec9a, Langerin, Necl2, Xcr1	CD11b, CD209a, CD172a (Sirpα), DCIR2, CD4, CD103, ESAM, F4/80	CD11b, CD209a, CD172a (Sirpα), DCIR2, CD14, Ccr2, CD64, Cx3cr1, Ly6C, Clec10a, Clec12a, Mgl2, (F4/80)	CD11b, CD172a (Sirpα), Ccr2, CD64, DC-SIGN (CD209a), Ly6C, Mar-1	Clec10a, Tmem176a, Tmem176b, Lyz2, Ccl9, Hpgd, Clec4a3, Clec12a, Cd209a, Cd7, Mdh2, Ppp1r14a, Ccl5, Pglyrp1, Rgs2, CD16/32+ DC3 = T-bet-DC2B?	CD11b, CD209a, CD172a (Sirpα), CD14, Ccr2, CD64, Cx3cr1, Ly6C, CD16/32, CD88, CD115, CD206, F4/80, Mar-1, MerTK	Siglech, B220, CD11b, CD16/32, Sca-1, CD117, Ly6C
Transcription factors	Batf3, Gfi1, Id2, Ikaros, Irf8, Nfil3, Notch2, Pu.1, Stat3, Zbtb46	Gfi1, Ikaros, Irf2, Irf4, Notch2, Pu.1, Stat3, T-bet?, Traf6, Zbtb46	Gfi1, Ikaros, Irf4, Klf4, Pu.1, (RorγT), Zbtb46, (Zeb2), LysM	Irf4, Irf8, Zbtb46	Irf7, Irf8	Gfi1, Ikaros, Irf8, Klf4, Pu.1, Zbtb46	Irf7, Irf8
Differentiation/ survival factors	Adam10, Flt3, Gm-Csf, Rhoa	Adam10, Flt3, Gm-Csf, Ltβr, Ra, Relb, Rhoa	Flt3, Gm-Csf		Il1b, Csf1r = M-Csf	Gm-Csf, Il-4 (*in vitro*), M-Csf (*in vitro*)	
Function	Ag cross presentation, Type I immune response	Notch2-cDC2: Bacterial + fungal infections, Type 3 responses, T-bet cDC2: tissue repair develop from pDC-like tDC?	Klf4-cDC2: Type 2 responses, parasite infections, allergens, RorγT-cDC2: pro-inflammatory	CD4+ T cell priming, Type 2 responses, Ag cross presentation		local T cell reactivation, Th1 and Th17 responses during infection	
Cytokines	IFNγ, IL-12	IFN-III, IL-6, IL-23, TGFβ	IL-4, IL-12, IL-33, TNF	IFN-I, IL-12, TNF		IL-12, IL-23, iNOS, TNF	
Human equivalent	CD141 (BDCA3), cDC1: BATF3, BTLA, CD11c, CD26, CD117, CLEC9A, IRF8, MHCII, NECL1, XCR1	CD1c (BDCA1) cDC2: BCLA1, CD11b, CD11c, CD26, CLEC10A, MHCII, IRF4, SIRPα	CD1c^{low} cDC2: CD5, CD11b, CD11c, CD26, CLEC4A, CLEC10A, MHCII, IRF4, SIRPα	Inf-DC (DC3?): CD1c, CD11b, CD11c, CD26, CD64, CD141, CD163	BM cDC3 (DC2B?): CFN1, LST1, CPF, S100A9, MNDA, CSTA, LGALS2, CLEC10A, S100A8, VCAN	MoDC: CD11b, CD11c, CD14, CD16, CD64, CD86, CD115, CLEC4A, MHCII, SIRPα	BM pDC: JCHAIN, GZMB, MZB1, IGKC, SERP1NF1, ITM2C, PTPRS, IRF7, CLIC3, PTGDS

Figure 3. Ongoing developments in the field of DC ontogeny, classification and function. The upper panel illustrates recent insights into myeloid cell haematopoiesis, highlighting DC population heterogeneity. The transcription factor IRF8 is expressed by macrophage and DC precursors (MDP) and pre-pDC, while both MDP and common monocyte precursors (cMoP) contribute to the Ly6C^{high} monocyte pool, which can differentiate into either *bona fide* macrophages or monocyte-derived DCs (moDC) in tissues. moDCs express transcription factors associated with cDC2 fate, such as ZBTB46 and IRF4, potentially contributing to a cDC2 subset.

The lower panel displays the complexity of surface markers and transcription factors used for cell identity determination, primarily focusing on murine myelopoiesis, as markers and derived populations differ between species. moDCs also express cDC2 markers (e.g., CD172a) and macrophage markers like MAR-1, MerTK, and F4/80. Inflammatory cDC2 (inf-cDC2) additionally express the macrophage marker CD64. Relationships among pDC, tDC, and pre-DC2 are under investigation, with marker expression showing high tissue specificity. Figure generated using Biorender, table manually amended from Backer *et al.*[39], Liu *et al.*[48], Dutertre[49], Minutti *et al*.[50]

Bosteels *et al*. identified a subset of cDC2 in the lung which, in response to respiratory virus infection, upregulated markers typical of cDC1 and macrophages, such as CD64 and MAR-1, calling these cells "inflammatory cDC2", a concept initially proposed by Brown *et al*.[51,52] Rivera *et al.* found specific cDC2 subsets in the intestine that adopted a niche-specific phenotype after colonising the epithelium, with reduced pro-inflammatory gene expression and increased antimicrobial peptide expression.[53] Supporting the fluidity in DC phenotypes, recent studies have shown that the transcription factors IRF8 and IRF4, initially thought to separate cDC1 and cDC2 lineages[54], are more dynamically expressed during cell maturation; IRF8, for instance, is expressed in all DC precursors before cDC2 fate is determined.[55]

Additionally, emerging markers for immature DC and DC precursors have led to a proposal of the reclassification of pDC-like cells as pre-DC2 within tissue-specific

contexts[56], and the proposal of a new third cDC population, termed cDC3.[48] Recent studies have also stirred debate by proposing that pDC might be reclassified as innate lymphoid cells.[57,58]

A primary function of DC, particularly those protruding through the epithelium to sample the intestinal lumen, is antigen presentation, which mediates a balanced immune response to microbiota-derived antigens and metabolites, maintaining tolerance and inflammation in the intestine. Hence, microbiome composition metabolites heavily influence mucosal immunity and intestinal homeostasis[59], a subject covered in the following chapter.

Introduction of the intestinal microbiome

Research interest in the intestinal microbiome and its contribution to host health has accelerated significantly over the past few decades. The commensal microbiome is understood to act as an intermediary, supplying essential metabolites derived from food constituents that are metabolically indigestible to the host. Thus, a delicate balance between the tolerance of beneficial species and defence against pathogenic invaders that may harm the host must be maintained.

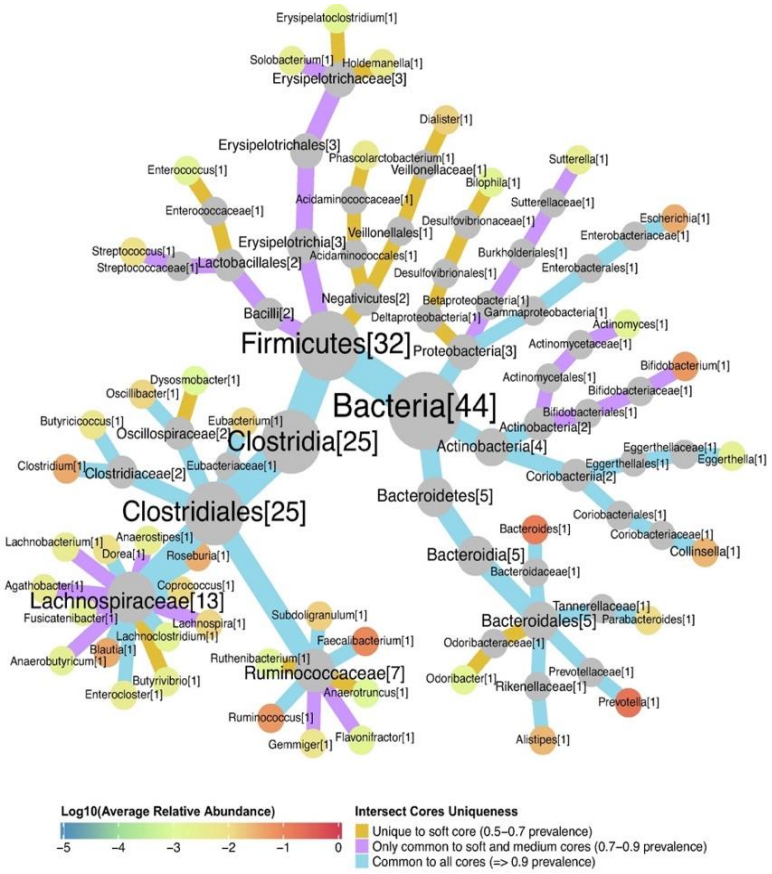

Figure 4: Universal (life style and country of origin independent) phylogenetic core bacterial genera in the human intestinal microbiome. Depicted is a core taxa analysis based on dataset enrichment of whole-genome shot gun sequencing of 545 publicly available faecal samples from healthy donors of various nationalities, ethnicities, living spaces and life style choices as published by Piquer-Esteban *et al*[60]. Numbers in parentheses indicate how many core taxa are assigned at the respective taxonomic level. Colours of edges indicate uniqueness of indicated taxon, and the colours of nodes indicate $\log_{10}$ of average relative abundance.

The dominant contributors to the human microbiome are members of the phyla Firmicutes, Bacteroidetes, Actinobacteria, Proteobacteria, and Verrucomicrobia. **Figure 4** illustrates the most common taxa analysed in an in-depth meta-analysis, which includes a large pool of samples with high ethnic diversity.[60] Approximately 90% of detected species can be assigned to the Firmicutes and Bacteroidetes phyla. Members of Firmicutes, predominantly the genus Lactobacillus, are known for their role as probiotics contributing to intestinal homeostasis. Other genera, such as Bacillus, Enterococcus, Ruminicoccus, and Clostridium, are recognised for producing short-chain fatty acids (SCFA).[61] Bacteroides, also members of Bacteroidetes, contribute significantly to the digestion of dietary fibre and polysaccharides.[62] Actinobacteria also contribute to digestion, with Bifidobacterium, a prominent probiotic, contributing to developing a healthy microbiome, particularly in infants.[63]

Proteobacteria is a diverse phylum consisting of facultative pathobionts, which are species generally considered harmless commensals but that may contribute to disease under specific circumstances.[64] Changes in the abundance of Proteobacteria are often correlated with dysbiotic phenotypes, as many members can display pathogenic properties.[65,66] *Akkermansia muciniphila*, a prominent member of the Verrucomicrobia, has garnered research attention due to its role in feeding on the mucus layer produced by the host; loss of *Akkermansia* abundance is often linked to epithelial barrier breakdown resulting from decreased mucus production.[67]

Many species that contribute to the complex human intestinal microbiome still need to be discovered due to limitations in replicating the unique conditions in which these bacterial species thrive.[68] Current research focuses on generating reference collections and minimal consortia that reflect complex compositions using a limited number of representative species and their defined functions.[69] It is widely accepted that changes in microbiome composition, such as the loss of certain species and the subsequent overgrowth of others, play as crucial a role in host intestinal homeostasis as the host's physiology.[70] Therefore, the diagnosis and therapy of intestinal inflammatory diseases, particularly IBD, are understood to be intrinsically linked to microbial dysbiosis.

A significant debate persists regarding whether microbial dysbiosis in IBD patients is a cause or merely a consequence of changes in tissue conditions.[71] The definition of dysbiosis requires a clear definition and understanding of eubiosis, which remains challenging. Though core taxa have been defined[72,73], aided by advances in bioinformatics tools, compositions vary significantly among individuals from different ethnic backgrounds, origins, and lifestyles.[74] It is of note that despite some general overlaps, one can scarcely speak of a uniform intestinal microbiome, as local composition depends heavily on the unique conditions present at the sampling site.[75]

The intestine serves as a unique interface for immunological exchange, distinct from other organs.[76] First-line interactions between innate immune cells and bacteria occur via pattern recognition receptors (PRR) on the cell surface, which detect distinct molecules indicating the presence of microbes through microbe-associated molecular patterns (MAMP) or pathogen-associated molecular patterns (PAMP). [77] TLR, a class of PRR, are transmembrane proteins located on either the outer cell membrane or intracellular endosomal membranes. TLR can recognise various bacterial or viral

PAMPs, exemplified by the interaction between TLR4 and LPS (lipopolysaccharide), a component of gram-negative bacteria. The downstream consequence of TLR induction includes the upregulation of TNF production and activation of NFκB signalling. Another class of PRR, the nucleotide-binding oligomerisation domain-like receptors (NLR), are cytoplasmic receptors detecting intracellular signals, including bacterial and viral RNA, and danger-associated molecular patterns (DAMPs). NLR are involved in inflammasome formation, a central process in programmed inflammatory cell death, as discussed below. XIAP-related pathologies have been linked to defective downstream signalling resulting from NOD2 engagement (as will be discussed in a later chapter). Lastly, C-type lectin receptors (CLR), a group of cell surface protein receptors heavily exploited for identifying immune cell subtypes (such as the unique expression of the CLR XCR1 by cDC1), recognise sugar moieties on microbial surfaces. The mannose receptor CD206, characteristic of type 2 macrophages, and DC-SIGN (Dendritic Cell-Specific Intercellular adhesion molecule-3-Grabbing Non-integrin, also known as CD209) in humans, or its murine homologue SIGNR5 (Specific Intracellular adhesion molecule-3-Grabbing non-integrin Receptor 5, also known as CD209a), are prominent CLR. The engagement of CLR triggers MAPK and NFκB signalling pathways, leading to increased cytokine production.

In the following chapter, I will outline how the aforementioned PRR-PAMP interactions, associated with specific pathogenic bacteria, may lead to aberrant immune responses due to dysbiotic changes in microbiome composition.

The relationship between microbiome diversity, dysbiosis, and intestinal inflammation

The loss of microbial diversity is widely accepted as a hallmark of dysbiosis.[78,79] It remains debated whether changes in microbial composition and ensuing dysbiosis occur due to developing intestinal inflammation or whether microbial alterations lead to inflammatory pathogenesis. To determine taxonomic composition and diversity, microbiota perturbations in human stool samples are monitored through 16S rRNA sequencing data.[80] Similar analyses are conducted on caecal and colonic samples from mice.[81] Intestinal inflammation in patients has been associated with a loss of Firmicutes, particularly Clostridia species.[82] Furthermore, the loss of beneficial species can lead to the overgrowth of previously low-abundance species, potentially driving inflammatory reactions and the establishment of pathogenic species.[83]

The mere presence of a bacterial species does not provide insight into their function or downstream influence on host metabolism; thus, establishing IBD-specific meta-transcriptomic and metabolic signatures has become a focal point of recent investigations.[82,84] Decreased levels of beneficial metabolites, such as SCFA and vitamins that cannot be produced by eukaryotic host cells, have been linked to IBD.[85] Interestingly, some metabolites, such as amino acids and products of nucleotide synthesis pathways, were increased in patient stool samples. Recent publications postulate that certain species driving a dysbiotic phenotype are characterised by high metabolic independence (HMI).[86,87] Watson *et al.* observed that colonisation after faecal microbiota transplantation (FMT) favours bacteria whose genomes encode the entirety of 33 metabolic modules, enabling them to produce essential metabolites independently of external supply. Among these biosynthesis pathways are various amino acid synthesis pathways. Crucially, they determined that the biosynthetic pathways distinguishing bacteria that colonised well versus those that poorly colonised post FMT were enriched in the genomes of IBD patients, suggesting a quantifiable disease marker through metagenomic analysis. This was corroborated by Veseli *et al.*, who explored using HMI enrichment as a minimally invasive prediction tool by training a metagenomic classifier on a large dataset of publicly available human metagenomes to differentiate healthy controls from IBD samples, achieving over 85% accuracy. However, neither study confirmed the increased presence of specific metabolites in their samples, and it is unclear how the authors would differentiate between the enrichment of metabolic modules stemming from bacterial metabolism versus host eukaryotic input, as many of the 33 described biosynthesis pathways are not exclusive to bacteria.

The re-establishment of a “healthy” microbiome via FMT has garnered significant clinical interest over the years, leading to the establishment of more facilities to provide this treatment option.[88,89] However, preclinical research in experimental mice has suggested the existence of a critical window in an organism’s lifespan for establishing a healthy microbiota, and interference with this process, such as through antibiotic administration, may render the host acutely sensitive to further microbial disturbances later in life.[90] This is corroborated by observations indicating that antibiotic treatment in human infants may adversely affect their ability to establish a fully functioning immune system, leaving them susceptible to further infections or intestinal inflammation.[91,92]

Ultimately, the causal relationship among microbial dysbiosis, aberrant mucosal immune reactions, and the complex phenotype of intestinal inflammation remains to be fully elucidated.

Inflammatory Bowel Disease

Historical development of IBD burden

Inflammatory Bowel Disease (IBD) is a chronic inflammatory autoimmune condition affecting the digestive system from the mouth to the anus. The primary forms are Ulcerative Colitis (UC) and Crohn's Disease (CD).[93] UC is characterised by crypt abscess formation in the colon, leading to continuous inflammation due to immune cell infiltration in the Lamina propria.[94] In contrast, CD features discontinuous fistulating inflammation throughout the gastrointestinal tract, forming granuloma.[94] Patients with atypical symptoms are classified as having IBD unclassified (IBDU), also referred to as indeterminate colitis. Various clinical classifications have emerged over the years to capture this complex disease.[95]

As outlined by Kaplan and Windsor, data on IBD incidence and prevalence in Europe spans nearly 270 years.[96] By the end of 2016, over 0.3% of the population in Europe, North America, and Oceania were estimated to have some form of IBD, with individual countries reporting much higher prevalence.[97,98] Highly industrialised nations like Norway, Germany, the USA, and Canada exhibit the highest disease rates. Interestingly, while IBD incidence appears to have stabilised in these regions, prevalence remains elevated. This pattern correlates with industrialisation and "westernisation" in parts of Africa, South America, and Asia, where steep increases in IBD incidence have been noted. It is projected that by 2030, about 1% of the Western population will be affected by IBD, posing a significant burden on healthcare and underscoring the importance of research into prevention and treatment.

The multifactorial pathogenesis of conventional IBD

IBD arises from a complex interplay of intrinsic genetic vulnerabilities and extrinsic environmental factors.[99] Genome-wide association studies (GWAS) have identified over 230 risk loci, many influencing genes involved in host-microbiota interactions, mainly variations of the pattern recognition receptor NOD2.[100,101] Onset typically

occurs in late adolescence to early adulthood, around ages 15 to 35, seen in the Oxford IBD cohort depicted in **Figure 5**. Lifestyle choices and environmental factors further influence disease outcomes.[102] Factors such as diet, hygiene, and exposure to mutagens like cigarette smoke or UV light play a role, and even chronically elevated stress levels can exacerbate IBD symptoms. As discussed in the previous chapter, the unique composition of each patient's commensal microbiome adds further complexity to the IBD pathology.

Various therapeutic options exist for IBD patients, ranging from traditional anti-inflammatory medications like sulfasalazine[103] and corticosteroids[104], to immune modulators like thiopurines[105] and methotrexate[106]. As anti-TNF therapies (Infliximab, Adalimumab, Golimumab)[107], anti-IL-12/23 therapies (Ustekinumab, Mirikizumab), and anti-Integrin therapies aiming to prevent excessive leukocyte adhesion, have become widely available, the popularity of this therapy option has seen a sharp uptake[108]. However, although anti-TNF biologics play a crucial role in IBD treatment nowadays, only 60% of patients respond to the treatment long-term.[109]

Stem cell transplantation options include haematopoietic, mesenchymal, and intestinal epithelial stem cells, serving as more drastic measures if other therapy options remain unsuccessful.[110] Surgical resection of inflamed tissue remains a last resort, but complete recovery from IBD is unlikely, necessitating lifelong monitoring for flare-ups.[111]

Emerging therapies increasingly focus on the intestinal microbiome's role in homeostasis, as discussed in the previous chapter. Antibiotics aim to reduce dysbiotic microbiota, while pre-, pro-, and post-biotics[112] and FMT[113] are being explored to restore a healthy microbial community.

The influence of genetics in early-onset IBD

So-called paediatric onset or very early-onset (VEO) IBD cases remain rare, though interestingly, studies have reported increasing IBD incidences in children.[114,115] 25% of IBD cases develop in childhood and adolescence (before the age of 18), including a small minority developing during infancy. Unlike multifactorial adult-onset IBD, early-onset (EO) IBD is often classified as monogenic or Mendelian-disorder-associated IBD. The penetrance of different polymorphisms leading to such IBD varies[116], though

comprehensive studies including different ethnicities are rare. About 75 risk genes for paediatric onset IBD have been identified.[117]

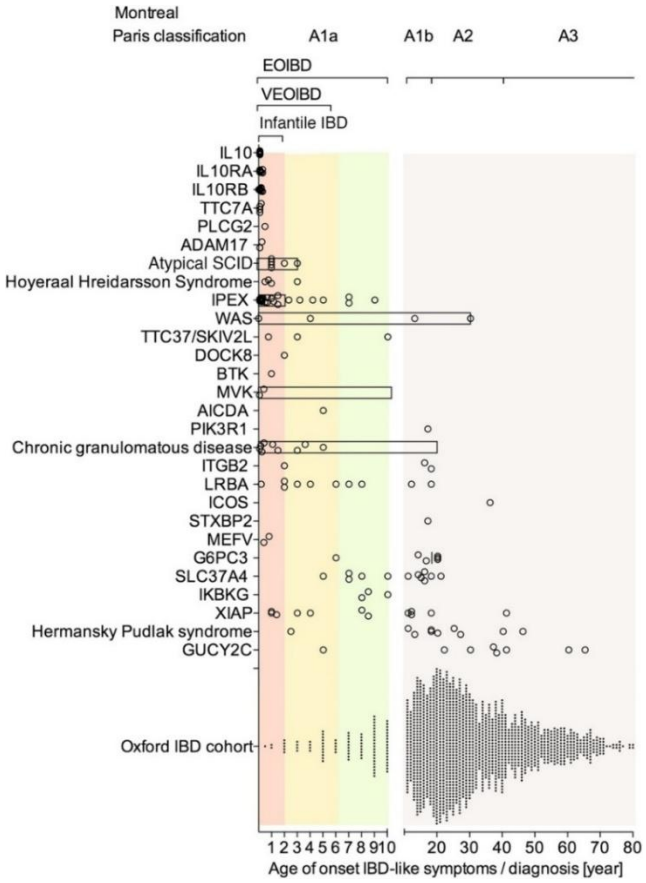

Figure 5. Meta analyses of the age of IBD onset in patients diagnosed with monogenic IBD in comparison to the Oxford IBD cohort. Atypical severe combined immune deficiency (SCID), Hoyeraal-Hreindarsson syndrome, Chronic granulomatous disease and Hermansky-Pudlak syndrome encompass multiple genetic defects of similar symptomatic. The Oxford IBD cohort consists of n = 1605 patients diagnosed with Crohn's Disease, UC and IBDU. Dots and circles represent individual cases, if individual data was not available, age range is represented as bar. Figure as depicted in Uhlig *et al.*[118]

Figure 5 from Uhlig *et al.* illustrates the age of onset in patients with various monogenic IBD risk loci compared to a large cohort primarily consisting of adult-onset IBD.[118] More than 63% of children with variations in these loci develop very early-onset (VEO) IBD, with symptoms appearing before age 6. Studying these cases is crucial as paediatric-onset IBD is often severe and therapeutic success is low. Systematic studies are limited due to the disease's rarity, and unclear diagnostic and therapeutic guidelines hinder treatment. Identifying the genetic defect enables more personalised care, including experimental treatments like CRISPR-Cas9 gene editing tools.[117] Unfortunately, surgical resection and, in cases of immune cell-driven phenotypes, hematopoietic stem cell transplantation are often the only viable options, despite their

risks. Additionally, 76% of monogenic IBD patients develop severe extraintestinal comorbidities, such as infections, dermatological issues, and autoimmune conditions like arthritis or type 1 Diabetes mellitus.

Notably, deficiencies in the gene encoding the anti-inflammatory cytokine Interleukin 10 (IL-10) or its receptors lead to neonatal-onset IBD, with symptoms manifesting within 28 days after birth.[119] Without IL-10, the immune-dampening effects from for example intestinal epithelial cells and regulatory T cells cannot be achieved, resulting in hyperinflammation. Due to the high penetrance associated with these SNP, an IL-10-deficient mouse model was established as one of the earliest murine models of experimental IBD in 1993.[120]

Another gene leading to early-onset IBD is the so-called X-linked-inhibitor of apoptosis protein (XIAP). As the functions of XIAP are one of the main topics of this thesis, a more detailed account of its role in both health and disease is elaborated on in the following chapter. The general syndrome associated with genetic variations in the gene *BIRC4* encoding XIAP is the immunodeficiency X-linked lymphoproliferative syndrome 2 (XLP2).[121] Its most prominent clinical manifestation is haemophagocytic lymphohistiocytosis, a severe dysregulation of lymphocytes and macrophages, leading to hyperinflammation and hypercytokinaemia, potentially leading to multi-organ failure.[122] The increasing knowledge around monogenic IBD led to the discovery that in about 26% of XLP2 patients, the disease manifests as severe Crohn's Disease-like symptoms early in life[219], and about 4% of cases of early-onset IBD can be ultimately traced back to a deficiency in XIAP.[125] Disease onset is often triggered by environmental factors such as bacterial or viral stimulus, for example in case of an infection with *Clostridium difficile* or *Epstein-Barr* Virus. The exact molecular mechanisms driving intestinal inflammation in the absence of XIAP remain to be uncovered.

The X-linked inhibitor of apoptosis protein in programmed cell death

Introducing XIAP, a member of the IAP family

The so-called X-linked inhibitor of apoptosis protein (XIAP) is the most prominent member of the inhibitor of apoptosis protein (IAP) family, a protein ubiquitously expressed in many cell types.[126] The gene encoding for XIAP is called *BIRC4* in human

and mouse. **Figure 6** illustrates the fact that members of the IAP family retain a highly conserved structure[127], featuring one or more of so-called BIR (Baculoviral IAP Repeat) domains. Different domains of an IAP can act as scaffolds, facilitating protein-protein interactions. IAPs have been found in species from very different kingdoms; 8 different human IAP members are currently known. The first human IAPs discovered were cellular IAP1 and 2 (encoded by *BIRC2* and *BIRC3)*. However, due to the fact that its direct interaction partners remain elusive, and that its absence has been connected to severe human autoimmune pathology, the multifunctional protein XIAP remains a target of elevated scientific interest.

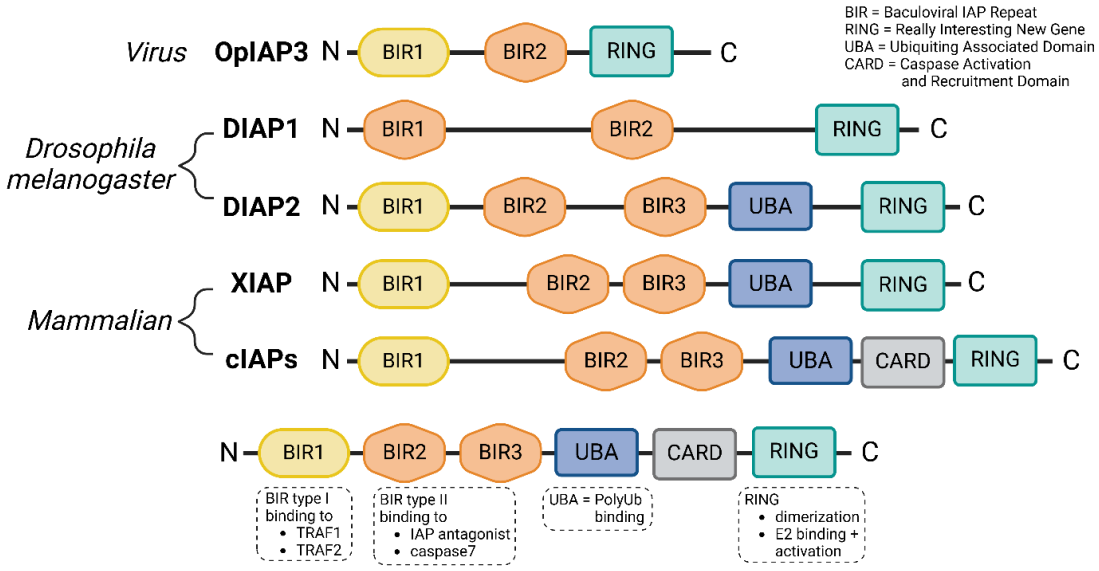

Figure 6. IAP family members exhibit a conserved protein structure that facilitates interactions with multiple partners involved in TNF signalling, cell death mediation, and protein ubiquitylation. All IAPs feature conserved BIR domains, with type 1 BIR domains (in yellow) interacting with TRAF1 and TRAF2 (TNF receptor-associated factors). Type 2 BIR domains (in orange) bind IAP antagonists (e.g., SMAC/DIABLO) and caspases. The UBA (ubiquitin-associated) domain, shown in dark blue, binds polyubiquitin chains. The function of the CARD (caspase activation and recruitment domain, in grey) remains to be fully understood, though it is believed to facilitate protein-protein interactions and caspase activation related to cell death and inflammation. The RING (Really Interesting New Gene) domain, depicted in turquoise, is involved in transferring ubiquitin to substrate proteins via interaction with E2 ubiquitin-conjugating enzymes. Figure generated using Biorender.

Interest in IAPs, especially XIAP, initially focused on their potential as therapeutic targets in cancer therapy. Cancer cells evade apoptosis by overexpressing apoptosis-inhibiting proteins like IAPs. This led to the exploration of "inhibiting the inhibitors" for therapeutic gain.[128,129] XIAP, as shown in **Figure 6**, contains two type II BIR domains that inhibit caspases, crucial initiators of apoptosis.[130] Cancer cells can also evade apoptosis by downregulating apoptosis-promoting proteins, such as SMAC/DIABLO, discovered by Du *et al.* in 2000.[131] SMAC, usually localised in

mitochondria, moves to the cytoplasm to block IAP-caspase interactions, acting as an endogenous IAP antagonist. This insight led to the development of SMAC mimetics for cancer therapy.[132]

The role of XIAP, however, extends beyond caspase inhibition via type II BIR domains. While cIAP1 and 2 also contain BIR2 and BIR3, their capacity to inhibit caspases remains limited, unlike XIAP, which effectively blocks apoptosis.[133] Given the central role of XIAP, researchers anticipated that *Xiap*-deficient mice would experience a strong phenotype resulting from deregulated cell death; however, Harlin *et al.* found no general phenotype beyond increased cIAP1 and 2 expression in these mice, leading to the suggestion of a compensatory mechanisms within the IAP family.[134]

Contrary to findings in mice, human patients with XLP2 syndrome, a rare immunodeficiency linked to BIRC4 mutations, display HLH, splenomegaly, and Crohn's-like IBD, often exacerbated by *Epstein-Barr* Virus infection.[135] Reduced XIAP levels cause excessive lymphocyte apoptosis and decreased natural killer T cell counts, confirming a role for XIAP in lymphocyte homeostasis. Beyond apoptosis, XIAP was shown to function as an E3 ubiquitin ligase via its RING domain, mediating SMAC degradation and inducing a negative feedback loop through self-ubiquitylation, stabilizing apoptosis inhibition.[136]

XIAP also connects to immune signalling via NLR receptors like NOD1 and NOD2, recognising bacterial components (DAP and MDP) and triggering NFκB signalling through RIPK2. In 2009, Krieg *et al*. demonstrated that RIPK2 binds to the BIR2 domain of XIAP, facilitating NOD1/NOD2 interaction.[137] Bertrand *et al.* further confirmed the necessity of cIAPs and RIPK2 in immune cell response, showing their roles in alleviating colitis through NOD2 activation.[138] As mentioned previously, GWAS had identified SNP in NOD2 as a major IBD risk factor[139]. At the same time, Damgaard *et al.* demonstrated that the ubiquitin-ligase activity of XIAP is crucial for an appropriate NFκB response to NOD2 activation, connecting BIRC4 mutations in XLP2 patients to impaired NOD2 signalling and inflammatory cell death, revealing one potential connection between dysregulated XIAP expression and inflammation in IBD.

The connection between XIAP deficiency and inflammatory phenotypes in XLP2 patients remains a significant area of investigation despite the role of XIAP in inhibiting non-inflammatory "silent" cell death.

The central role of XIAP in mediating inflammatory cell death modalities

Cell death pathways were viewed as separate and mutually exclusive; however, recent research highlights their reversibility and interconnectedness, highlighting the role of central mediators like XIAP.

Apoptosis and necrosis were once seen as the two primary cell death forms.[140] Apoptosis is a “silent”, tightly regulated process, initiated either intrinsically via mitochondrial stress or extrinsically through receptor engagement. This process deconstructs the cell internally, limits debris release, and avoids immune activation, making it non-immunogenic and preventing damage to surrounding cells.[141] Necrosis, by contrast, is typically unregulated and results from external damage, causing cell swelling, membrane rupture, and the release of cellular contents that recruit immune cells, trigger inflammation and may affect neighbouring cells.[142]

New insights into cell death reveal programmed inflammatory processes such as necroptosis, which follows TNF signalling and is mediated by RIPK3 and MLKL, leading to controlled membrane disruption.[143] Similarly, pyroptosis is another programmed inflammatory death pathway triggered by NLR family receptors, such as NLRP3 or NLRC4, and involves inflammasome assembly. This activates caspase-1, cleaves Gasdermins (like GSDMD), and releases IL-1β through GSDM pores, marking pyroptotic cell death.[144,145]

A very recent and highly controversial concept in cell death, which I want to outline briefly in this thesis, is the introduction of the term PANoptosis proposed by Kanneganti and colleagues in 2020.[146–148] It assumes the existence of a holistic, integrated cell death concept mediated through a macromolecular protein complex called the PANoptosome[149], a multifaceted cell death machinery supposed to consist of enzymes and signalling molecules from pyroptosis, apoptosis and necroptosis. PANoptosis proposes the execution of cell death programs in a way that exceeds the individual events of each modality itself. Despite the controversy surrounding this hypothesis, its proposal clearly illustrates that the formerly clear distinctions between cell death pathways have become more blurred.

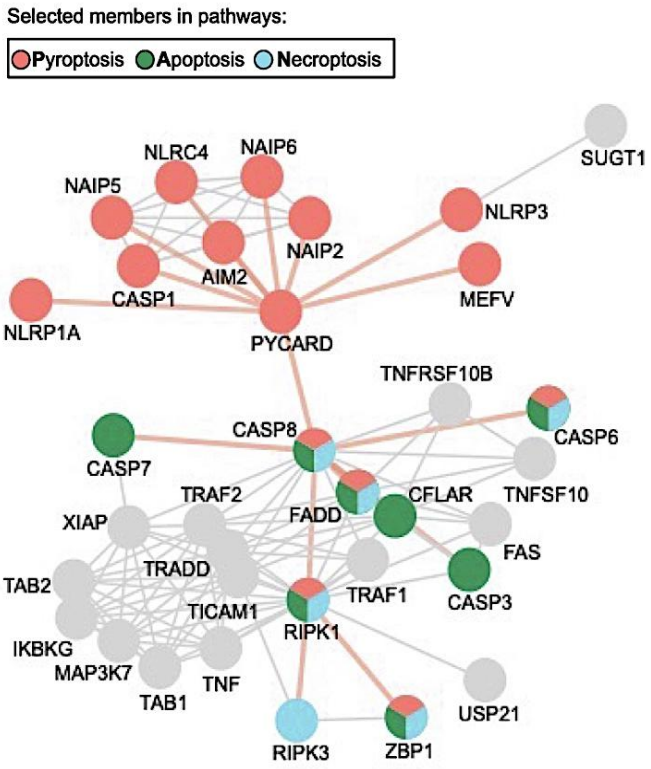

Figure 7. STRING database generated interaction network of seven relevant proteins (AIM2, PYCARD, MEFV, ZBP1, CASP1, CASP8, RIPK3) involved in programmed cell death pathways. Colours indicate central members of respective death modality, apoptosis in green, pyroptosis in red, necroptosis in blue. Figure from Wang and Kanneganti.[146]

As illustrated in **Figure 7**, central proteins involved in apoptosis, necroptosis and pyroptosis can be bioinformatically placed into an interconnected network. Here, one can observe, that XIAP, which would by name suggest being a mere inhibitor of apoptotic cell death, might functionally be placed at the crosstalk of various cell death modalities, including necroptosis and pyroptosis. Furthermore, one can appreciate that XIAP is associated with proteins that define the signalling events downstream of TNF receptor engagement (such as TRAF2 and TRADD) and upstream of NFκB signalling (such as IκBKG and MAP3K7).

TNF and inflammatory cell death signalling in the presence and absence of XIAP

cIAP1 and 2 had been found to bare part of the signalling complex formed downstream of TNFR1 activation, called complex I. cIAP1/2 were found to mediate ubiquitylation of RIPK1 with the help of the enzyme complex LUBAC.[150] The downstream consequences of this interaction are manifold, leading to NFκB-mediated cell survival[151] or apoptosis induction. However, a direct contribution of XIAP to complex 1

was not confirmed. Necroptosis, as an alternative downstream consequence, executed by forming a cell death complex including RIPK1 and RIPK3, could be induced, though again, the interaction with XIAP remains to be demonstrated[152]. Finally, three different studies by Yabal *et al.* in 2014[153], Lawlor *et al.* in 2015[154] and Wicki *et al.* in 2016[155] could elucidate the central role of XIAP in cell death mediation using *in vitro* immune cell systems. In these studies, it was shown that engagement of PRR, concretely the stimulation of TLR4 with its ligand LPS in *Xiap*-deficient myeloid cells, led to the release of IL-1β and that this inflammatory cell death required RIPK3 and was dependent on TNF signalling. Hence, XIAP protected against spontaneous cell death through TNF-induced ubiquitylation of RIPK1, driving necroptotic RIPK3-dependent inflammasome activation and pyroptotic IL-1β release in response to the presence of PAMP that induces TLR signalling.

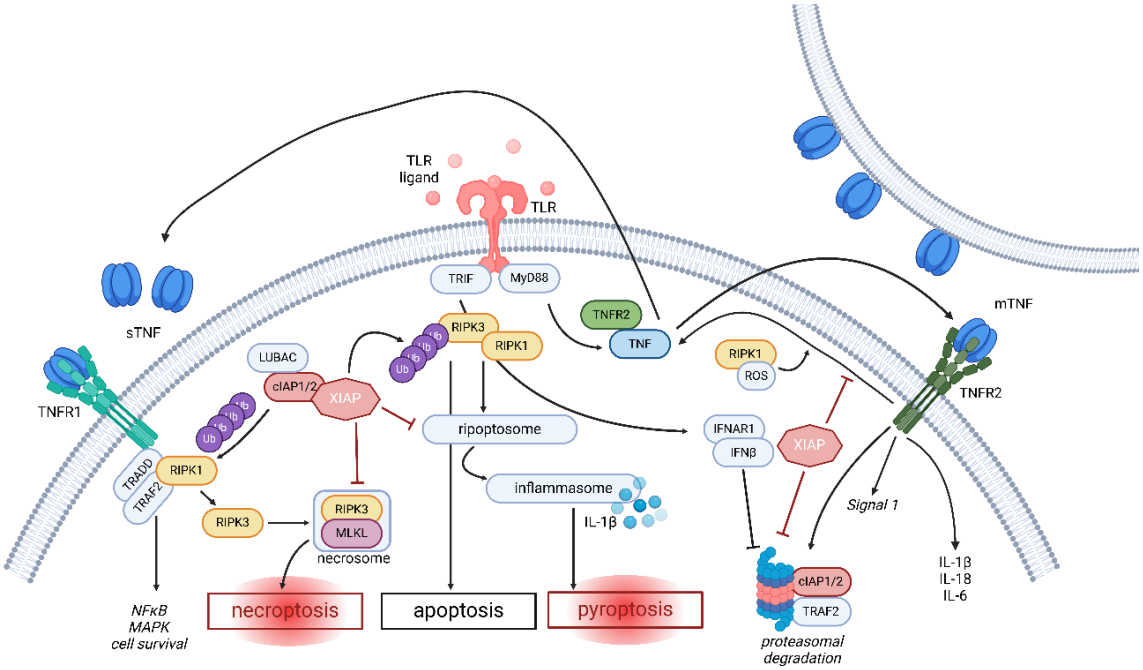

Figure 8. XIAP restrains cell death pathways downstream of TLR/TNFR signalling. XIAP (white on red) inhibits cell death complex formation (e.g., ripoptosome, inflammasome, necrosome) following TLR/TNF signalling. (i) XIAP mediates RIPK1 ubiquitylation (orange) in a RIPK3-dependent (orange) manner downstream of TLR (light red) and TNFR1 (turquoise) signalling, blocking ripoptosome activation. (ii) XIAP also inhibits RIPK3-MLKL (purple)-dependent necroptosis. (iii) TLR ligation through MyD88 (light blue) induces signalling via TNFR2 (dark green), where membrane-bound TNF (higher affinity for TNFR2 than soluble TNF) leads to the proteasomal degradation of cIAP1/2 (red)-TRAF2 (light blue), a process inhibited by XIAP. Without XIAP, loss of the cIAP-TRAF2 complex encourages inflammasome formation and IL-1β maturation. (iiii) In the absence of XIAP, TNFR2-mediated excessive TNF production amplifies TNFR1 signalling, promoting inflammasome formation and increased cell death. Figure created with BioRender

Figure 8 illustrates the current working knowledge on the multiple outcomes determining cell fate downstream of TLR-activation and consequential TNFR signalling via both TNFR1 and TNFR2 in the presence and absence of XIAP. A surprising aspect when further elucidating this signalling cascade was the finding that in the absence of XIAP, activation of TLR-MyD88 (the canonical adaptor protein that associates with the intracellular domain of TLRs) engagement induces the degradation of a cIAP/TRAF2 (Tumour Necrosis Factor Receptor-Associated Factor 2) complex and its association with TNFR2 engagement.[156] Even though TNFR2 does not have an intracellular death domain, the TNFR2-dependent proteasomal degradation of the cIAP/TRAF2 complex in *Xiap* deficiency was shown to unleash RIPK3-dependent NLRP3 inflammasome activation, Il-1β response, and excessive inflammatory cell death.

Aims of this study

The following study aims to identify and define the role of specialised myeloid cell populations in small intestinal inflammation within an XIAP-deficient murine model.

XIAP has emerged as a central regulator in PRR-TNF-induced inflammatory cell death pathways, particularly in the context of pediatric XLP2 patients who exhibit a Crohn's-like intestinal phenotype. By introducing microbiota to young, germfree *Xiap*$^{-/-}$ mice, this study seeks to clarify the cellular mechanisms linking microbial responses, deregulated TNF signalling downstream of XIAP, and intestinal inflammation.

Material and Methods

Material

Antibodies

Antibody target	Fluorochrome	Clone	Manufacturer	Reference number
CD11b	Apc-Vio770	REA592	Miltenyi Biotec	130-113-803
CD11b	BV421	M1/70	Biolegend	101235
CD11b	VioGreen	REA592	Miltenyi Biotec	130-113-811
CD11c	AF488	N418	Biolegend	117311
CD11c	Apc-Fire750	N418	Biolegend	117351
CD11c	Apc	REA754	Miltenyi Biotec	130-110-839
CD11c	eF660	invitrogen	N418	50-0114-82
CD11c	PerCp-Vio700	REA754	Miltenyi Biotec	130-110-842
CD11c	VioBlue	REA754	Miltenyi Biotec	130-110-843
CD26	BV605	BD Bioscience	H194-112	745125
CD26	Pe	REA1196	Miltenyi Biotec	130-122-775
CD26	Pe-Vio770	REA1196	Miltenyi Biotec	130-122-778
CD45	Apc-Vio770	REA737	Miltenyi Biotec	130-110-800
CD45	Fitc	REA737	Miltenyi Biotec	130-110-796
CD64	Pe-Vio770	REA296	Miltenyi Biotec	130-119-659
CD64	PerCp-eFluor710	X54-5/7.1	invitrogen	46-0641-82
CD103	Pe	REA789	Miltenyi Biotec	130-111-685

CD103	Pe-Cy7	2E7	Biolegend	121426
CD103	VioBlue	REA789	Miltenyi Biotec	130-111-998
CD172a	Apc	REA1201	Miltenyi Biotec	130-123-150
CD172a	VioBright515	REA1201	Miltenyi Biotec	130-123-157
CD209a	Pe	MMD3	Biolegend	833003
MHCII	Pe-Vio615	REA813	Miltenyi Biotec	130-112-393
SiglecH	Apc	REA819	Miltenyi Biotec	130-112-297
Xcr1	AF647	ZET	Biolegend	148214
Xcr1	Apc	REA707	Miltenyi Biotec	130-111-373
Xcr1	Pe	REA707	Miltenyi Biotec	130-111-372
Xcr1	PerCp	REA707	Miltenyi Biotec	130-111-377
goat-anti-rabbit IgG (H+L)	AF555	X	invitrogen	A32732
anti-rabbit IgG Fab2	AF594	X	CellSignalling	889S
anti-rabbit IgG Fab2	AF647	X	CellSignalling	4414S
DyLight488 Donkey anti-rabbit IgG	AF488	X	Biolegend	A32732
anti-GFP, rabbit polyclonal	AF488	X	invitrogen	A21311
rabbit-anti-mouse Lysozyme	Fitc	X	Dako	F0372

Buffer compositions

Buffer	**Composition**
Cryo slides coating buffer (heat to 45°C, use cooled and filtered; store slides at -20°C until use)	1000 mL dH_2O + 5 g Gelatine + 0.5 g $CrK(SO_4)_2$
Flow cytometer running buffer (store at 4°C)	500 mL PBS, pH 7.0 (prepared in house from powder, autoclaved before use) + 1 % FBS (heat inactivated, v/v)

	+ 2 mM EDTA (from 0.5M EDTA, prepared in house from powder)
LPDK Digestion buffer (sterile until use, store at up to 4 weeks at 4°C)	Per sample 2.5 mL of HBSS (with Ca^{2+} or Mg^{2+}) + 5% FBS + 100 µL Enzyme D (reconstituted in HBSS (without Ca^{2+} or Mg^{2+}) + 50 µL of Enzyme R (reconstituted in HBSS (without Ca^{2+} or Mg^{2+}) + 12.5 µL of Enzyme A (reconstituted in HBSS (without Ca^{2+} or Mg^{2+})
LPDK Pre-Digestion buffer (sterile until use, store up to 4 weeks at 4°C)	500 mL HBSS (without Ca^{2+} or Mg^{2+}) + 5 mM EDTA (from 0.5M EDTA, prepared in house from powder) + 5% FBS (heat inactivated, v/v) + 1 mM DTT (from 1M DTT, prepared in house from powder) + 10 mM HEPES (from 1M HEPES, prepared in house from powder)
LPDK Washing buffer (sterile until use, store at RT)	500 mL HBSS (without Ca^{2+} or Mg^{2+}) + 10 mM HEPES (from 1M HEPES, prepared in house from powder)
TBS for cryo slides (store at 4°C to prevent molding)	1000 mL ddH_2O + 150 mM NaCl + 100 mM Tris adjust pH to 7.4
TBS-A for cryo slides (store at 4°C to prevent molding)	500 mL TBS (see above) + 0.1% Triton-X-100 (pipette slowly with cut-off pipette tip, v/v)
TBS-B for cryo slides (store at 4°C to prevent molding)	250 mL TBS-A (see above) + 2% BSA (from powder, dissolve at RT by continuous rolling on Western Blot roller)

Buffer compositions used by cooperation partners / Core facilities are not specified in above list. In case of interest, please contact the respective facility.

Commercial kits

Kit name	Manufacturer	Order number	Data sheet version
Lamina propria Dissociation Kit (LPDK), mouse	Miltenyi Biotec	130-097-410	140-003-623.03
MACS Comp Bead Kit, anti-REA	Miltenyi Biotec	130-104-693	140-004-514.06

Sequencing datasets

GSE query #	Species	Details
GSE117772	murine	bulkRNAseq of flagellin stimulated Paneth-cell skewed SI organoids
GSE182934	murine	bulkRNAseq of small intestinal crypts of *Xiap*$^{-/-}$ mice
GSE183885	murine	scRNAseq of small intestinal, colonic and mLn immune cells

RNAseq dataset can be openly accessed at the Gene Expression Omnibus as of August/September 2021.

Laboratory devices

Device	Model	Manufacturer
Centrifuge	Fresco 17, Megafuge 8R, Multifuge X3R	Thermo Fisher Scientific
Confocal microscope	TCS SP8 (HC PL APO CORR CS2 63x/1.30NA objective)	Leica Microsystems
GentleMACS dissociator	Octo Dissociator with Heater sleeves	Miltenyi Biotec
Light microscope	Axioscope 10 (AX 10)	Zeiss
Neubauer counting chamber	N/A	Paul Marienfeld & Co.KG
Spectral cell analyser	SA3800, SP6800	SONY Biotechnology

Mouse lines

Mouse	Strain	Hygiene level
Wt	C57BL/6J	conventional housing (TUM, MRI, Mouse room 1)
gfWt	C57BL/6J	germfree (Hannover School of Medicine)
Xiap$^{-/-}$	Δ-exon 1 and 2 *XIAP-null*[157]	conventional housing (TUM, MRI, Mouse room 1)
gf*Xiap*$^{-/-}$	Δ-exon 1 XIAP-deficient[134]	germfree (Hannover School of Medicine)
Tnf$^{-/-}$	Δ-exon 1 and intron 1 *TNFa Knockout*[158]	conventional housing (TUM, MRI, Mouse room 1)
Tnfr1$^{-/-}$	Δ-exon 2,3,4 *Tnfr1*^{0}/*Tnfr1*^{0}[159]	conventional housing (TUM, MRI, Mouse room 1)
Tnfr2$^{-/-}$	Δ-exon 2 TNF-R2$^{-/-}$[160]	conventional housing (TUM, MRI, Mouse room 1)
Ripk3$^{-/-}$	Δ-exon 1,2,3 *rip3* mutant[161]	conventional housing (TUM, MRI, Mouse room 1)
Mlkl$^{-/-}$	Δ-exon 3 Mlkl$^{-/-}$[144]	conventional housing (TUM, MRI, Mouse room 1)
Irf8-VENUS reporter	*Irf8*-VENUS[162]	SPF (TUM, MRI, Experimental room 4)

All genetically modified mouse lines were generated on a C57Bl/6 background. Double-deficient mice were generated in house by breeding either single male and female, or single male and two females homozygous for either deficiency. Offspring were genotyped from ear punches, and heterozygous mice bred again. All mice were born at about Mendelian ratios, and can be considered as “unbelastete Linie” = unimpaired line according to local animal welfare regulations.

Reagents and Chemicals

Reagent /Chemical / Solution	Manufacturer	Order number
Chromium(III) potassium sulfate dodecahydrate	Merck	10103650250
L-Cysteine hydrochloride monohydrate	Sigma-Aldrich	C7880-100g
Dulbecco's Phosphate Buffered Saline	Sigma-Aldrich	D8537-500ML
DPBS (powdered, without calcium or magnesium)	PAN Biotech	P04-036050P
DPBS (powdered, without calcium or magnesium	Capricorn Scientific	PBS-1A-P50
Dulbecco's Modified Eagle Medium	Sigma-Aldrich	D5796-1L
Dithiothreitol (powdered)	Thermo Fisher Scientific	R0862
EDTA	Roth	8043.1
Ethanol absolute	AppliChem Panreac	A1613,1000GL
Foetal Bovine Serum Supreme	PAN Biotech	P30-3031
Flouromount-G	invitrogen	00-4958-02
Gelatine (powdered)	AppliChem Panreac	1471161210
Hanks' Balanced Salt solution (with sodium bicarbonate, without phenol red)	Sigma-Aldrich	H8264-500mL
HBSS (no calcium, no magnesium, no phenol red)	gibco	14175-095
HBSS (with calcium, with magnesium, without phenol red)	Merck	55037C-1000mL
4-(2-Hydroxyethyl)-1-piperazineethanesulfonic acid (HEPES) Pufferan (powdered)	Roth	HN78.3
Isoflurane CP	cp pharma	4042668012144
2-Mercaptoethanol	Thermo Fisher Scientific	31350010
Normal mouse serum	Merck	NS03L
Paraformaldehyde (powdered)	AppliChem Panreac	1414511211

Percoll	cytiva	17089101
RNAprotect Tissue Reagent	Qiagen	76106
RPMI 1640	Gibco	21875-034
Sodium pyruvate	Thermo Fisher Scientific	11360039
D(+)-Sucrose (powdered)	AppliChem Panreac	A2211,5000
Tissue-Tek O.C.T. Compound	Sakura Finetek Europe	44583
Tris Pufferan (powdered)	Roth	4855.2
Triton-X-100	AppliChem Panreac	A9778
Tween-20	AppliChem Panreac	A4974
Viability dye Apc-eF780, fixable (1:1000)	Thermo Fisher Scientific	65-0865-14
Viability dye eF450, fixable (1:500)	Thermo Fisher Scientific	65-0863-18

Software and Bioinformatic tools

Software	**Version**	**Manufacturer**
Affinity designer	v1.10.6	Serif
Aperio ImageScope	v12.4.6	Leica Biosystems
R package BiocManager (Seurat pipeline, patchwork, tidyverse, hdf5r)	v3.18	Bioconductor
ChatGPT	v4.5	OpenAI LP-C
FlowJo™	v10.8.1 and v10.8.2	BD Bioscience
MetaboAnalyst (MetaboAnalystR package)	v6.0	Xia Lab (McGill University, Canada)
Graphpad prism	v9.5.0 and v9.5.1	GraphPad
Imaris	v9.7.2	Bitplane AG
IMNGS2	Beta test	Core Facility NGS/Microbiome - ZIEL - TUM
Microsoft 365	v16.69.1	Microsoft
Namco Microbiome Explorer (R shiny application)	v1.1	Chair of Experimental Bioinformatics - TUM

RStudio	2023.06.1+524	Posit Software, 2020
SP6800 spectral analyser software	v2.0.2.14140	SONY Biotechnology
Xcms viewer (open source R package)	v0.5.3	Smith Group, Scripps Research Institute

Methods

Mouse strains and animal facilities

Following mouse strains deficient in the depicted genes have been generated and phenotypically characterised previously and were bred in-house according to local animal welfare laws: *Birc4*$^{-/-}$ (hereafter referred to as *Xiap*$^{-/-}$), *Tnf*$^{-/-}$, *Tnfr1*$^{-/-}$, *Tnfr2*$^{-/-}$, *Ripk3*$^{-/-}$, and *Mlkl*$^{-/-}$. To generate double knockout lines, *Xiap*-deficient male and female mice were crossed with the respective sex of *Tnf*$^{-/-}$, *Tnfr1*$^{-/-}$, *Tnfr2*$^{-/-}$, *Ripk3*$^{-/-}$, and *Mlkl*$^{-/-}$ mice. All mice were housed separately by genotype and sex, in addition to exclusive homozygous breeding, mice were regularly genotyped to confirm the retention of genetic deletions. Germfree (gf) Wt and *Xiap*$^{-/-}$ mice were derived and bred under sterile conditions in the Central Animal Facility of Hannover Medical School, Germany. Regular testing according to FELASA standards is performed to ensure sustained gf status. *Irf8*-VENUS reporter mice[162] were generously provided by Dr. Veronika Lukacs-Kornek at the Institute of Molecular Medicine and Experimental Immunology at Universitätsklinikum Bonn and were bred in-house under SPF conditions. All mice were bred and maintained under conventional or SPF conditions at Munich Rechts der Isar, School of Medicine, Technical University of Munich, following FELASA guidelines. Briefly, mice were housed in a 12-hour light-dark cycle at a room temperature of 24°C and 55% humidity, monitored consistently. All cages included enrichment items such as plastic shelters, chewing wood, and bedding nestlets. Water and chow were provided *ad libitum*, and newly weaned mice were given oats. The health status of the mice was closely monitored by trained staff and responsible scientists. At the end of the experiment, mice were euthanised after receiving a brief isoflurane narcosis, and organs were collected for analysis. No sex-specific influences on the evaluated phenotypical parameters were observed previously; therefore, mice of either sex were included in all experiments. All mouse experiments were authorised by the District Government of Upper Bavaria (Vet_02-19-103).

Passive conventionalisation of germfree mice and targeted inoculation via FMT

For the passive colonisation experiment, gf mice were derived under sterile conditions in the Central Animal Facility of Hannover Medical School, transported to the

quarantine room of the conventional housing facility at Munich Rechts der Isar, and placed in clean (but not gf) cages with bedding, enrichment, water, and chow according to regulations. After a 24-hour resting period, pre-selected mice of each genotype were retrieved to establish baseline parameters. Used bedding from adult Wt and *Xiap*$^{-/-}$ mice raised in the conventional facility was transferred to the cages to promote passive colonisation of the gf mice. Cages were changed twice weekly, with used ("dirty") bedding added as needed to ensure consistent colonisation success. To monitor colonisation kinetics, age- and sex-matched mice were retrieved at predetermined time points: 5, 8, and 15 days (endpoint) after their arrival at the conventional housing facility.

For faecal matter transplantation (FMT) in gf mice, Wt and *Xiap*$^{-/-}$ mice were acclimatised to the conventional facility for three weeks before receiving fresh faecal pellets from both Wt and *Xiap*$^{-/-}$ donor mice. After four weeks in the conventional facility, samples were retrieved. Following three weeks of acclimatisation with used bedding from adult Wt and *Xiap*$^{-/-}$ mice, adult gf Wt and *Xiap*$^{-/-}$ mice underwent FMT as described below. Approximately 90 mL of sterile L-cysteine hydrochloride buffer (see "Reagents") was prepared under sterile conditions and stored in 50 mL tubes at room temperature overnight. (0.05 g of L-cysteine hydrochloride was dissolved in 100 mL of autoclaved homemade PBS; the buffer was prepared in a sterile hood and filtered into sterile 50 mL tubes, retaining about 90 mL.) Six fresh faecal pellets per genotype were dissolved in 1800 µL of L-cysteine hydrochloride buffer by crushing them with a large pipette tip. The suspension was pulse-centrifuged at maximum speed for approximately 20 seconds. In accordance with animal welfare laws, 100 µL of the supernatant was orally administered to each Wt and *Xiap*$^{-/-}$ mouse that had been germfree for three weeks and acclimatised to the conventional facility. Mice were returned to their respective cages and regularly monitored to ensure their health status.

16S rRNA sequencing and spiked zOTU analysis of absolute species quantification

16S ribosomal RNA analysis is a state-of-the-art method for determining bacterial abundance and diversity in biological samples. This technique involves sequencing the 16S rRNA gene using a chosen Next Generation Sequencing method, which offers several advantages: the ribosomal subunit is unique to prokaryotic organisms,

allowing for easy differentiation from host-derived contaminations. Furthermore, as the evolution of this gene is particularly slow[163], comparisons with well-curated databases can yield high accuracy in determining phylogenetic origins.

For sample retrieval for 16S rRNA analysis, euthanised mice were opened, and the intestines were extracted. The ileum, caecum, and colon were separated macroscopically, with the ileum defined as the proximal third of the small intestine. All tissue pieces were superficially washed with cold PBS to minimise surface friction. Pre-labelled tubes were kept on ice. Using a 1 mL plastic pipette tip turned to the side to create a flat surface, intestinal contents were scraped from the intestines, applying minimal pressure to prevent tissue damage (as tissue was processed for microscopic analysis and RNA extraction). The entire content of each intestinal compartment was collected and split into two tubes, with part of the sample prepared for metabolome analysis as described below. It is important to note that this method retrieves luminal microbiota, as only the luminal content is collected, not specifically the mucosa-associated microbiota; however, no clear separation is discernible using this technique. Samples were weighed (see Table 1) and stored at -80°C until transfer.

Sample origin	Mean sample weight	Max. sample weight	Min. sample weight
Ileum	97.6 mg	191.3 mg	42.2 mg
Caecum	152.0 mg	355.4 mg	31.3 mg
Colon	94.3 mg	168.1 mg	41.9 mg

Table 1. Sample weight of frozen ileal/caecal/colonic content for 16S rRNA sequencing.

Samples were transferred on dry ice to maintain quality. The sequencing procedure was carried out at the Core Facility Microbiome at the ZIEL – Institute for Food & Health of TUM under the guidance of Dr. Klaus Neuhaus. The procedure generally involves DNA extraction, library construction using appropriate primers to amplify variable regions of the 16S rRNA gene, cleaning the library of known contaminants, and sequencing. Sequencing was performed using an Illumina MiSeq System (Illumina Inc., USA) second-generation sequencer in PE300 mode. To determine absolute species abundances, samples were spiked before analysis. Raw sequencing read data and additional zOTU analysis were processed using the IMNGS2 (Integrated Microbial Next Generation Sequencing, a free platform for global assessment of 16S rRNA gene diversity in microbial ecosystems, available in autumn 2023 at https://www.imngs.org; external users only available in beta test version)[164]

and were generously supplied by Dr. Klaus Neuhaus. Descriptive data analysis and visualisation were generated using NAMCO Microbiome Explorer[165] (v1.1), freely available in summer/autumn 2023 at https://exbio.wzw.tum.de/namco, with additional help from Dr. Monica Matchado and Dr. Alexander Dietrich.

Metabolome and Short chain fatty acid (SCFA) analysis

To assess the functional state of the intestinal microbiota beyond mere composition and species abundances, metabolites from respective samples were measured. For caecal metabolome analysis, euthanised mice were opened, and the intestines were extracted. The caecum was separated macroscopically and washed with cold PBS to reduce surface friction. Pre-labelled tubes were kept on ice. A 1 mL plastic pipette tip was turned sideways to create a flat surface, allowing caecal content to be scraped from the caecum with minimal pressure to avoid tissue damage. In some cases, a small hole was cut into the caecal surface to facilitate content release. The collected content was split into two tubes, with part prepared for 16S rRNA sequencing as described above. Samples were transferred on dry ice to maintain quality. The spectrometric procedure was conducted at the Bavarian Centre for Biomolecular Mass Spectrometry at TUM, supervised by Dr. Karin Kleigrewe. *Italic text indicates protocol details generously supplied by Dr. Karin Kleigrewe.* Caecal samples were analysed using unbiased positive and negative HILIC (Hydrophilic Interaction Liquid Chromatography) and UPLC-TOF-MS (Ultra-Performance Liquid Chromatography – Time-of-Flight Mass Spectrometry), including additional analysis for short-chain acid abundances. Mean weight of content was 21.0 mg (Max: 23.3 mg, Min: 9.9 mg; one sample had to be excluded).*Approximately 20 mg of mouse caecal content was weighed in a 2 mL bead beater tube (FastPrep-Tubes, Matrix D, MP Biomedicals Germany GmbH, Eschwege, Germany). 1 mL of methanol-based dehydrocholic acid extraction solvent (c=1.3 µmol/L) was added as an internal standard for work-up losses. The samples were extracted with a bead beater FastPep-24TM 5G, MP Biomedicals Germany GmbH, Eschwege, Germany) supplied with a CoolPrepTM (MP Biomedicals Germany, cooled with dry ice) for 3 times each for 20 seconds of beating at a speed of 6 m/sec and followed by a 30 seconds break.* One has to hereby notice that this type of analysis cannot differentiate between metabolites that are derived from the host metabolism i.e. the mouse itself, or the metabolism of the bacteria present in sample i.e. the caecal microbiota.

Untargeted mass spectrometric measurement: The untargeted analysis was performed using a Nexera UHPLC system (Shimadzu, Duisburg, Germany) coupled to a Q-TOF mass spectrometer (TripleTOF 6600, AB Sciex, Darmstadt, Germany).[166] *Separation of the faecal samples was performed using a UPLC BEH Amide 2.1 × 100 mm, 1.7 µm analytic column (Waters, Eschborn, Germany) with a 400 µL/min flow rate. For the HILIC-separation the settings were as follows: The mobile phase was 5 mM ammonium acetate in water (eluent A) and 5 mM ammonium acetate in acetonitrile/water (95/5, v/v) (eluent B). The gradient profile was 100% B from 0 to 1.5 min, 60% B at 8 min and 20% B at 10 min to 11.5 min and 100% B at 12 to 15 min. A volume of 5 µL per sample was injected. The autosampler was cooled to 10 °C and the column oven heated to 40 °C. Every tenth run a quality control (QC) sample which was pooled from all samples was injected. The samples were measured in a randomised order and in the Information Dependent Acquisition (IDA) mode. MS settings in the positive mode were as follows: Gas 1 55, Gas 2 65, Curtain gas 35, Temperature 500 °C, Ion Spray Voltage 5500, declustering potential 80. The mass range of the TOF MS and MS/MS scans were 50–2000 m/z and the collision energy was ramped from 15–55 V. MS settings in the negative mode were as follows: Gas 1 55, Gas 2 65, Cur 35, Temperature 500 °C, Ion Spray Voltage –4500, declustering potential –80. The mass range of the TOF MS and MS/MS scans were 50–2000 m/z and the collision energy was ramped from –15–55 V.*

Targeted short chain fatty acid (SCFA) measurement. The 3-NPH method was used for the quantitation of SCFA.[167] *Briefly, 40 µL of the faecal extract and 15 µL of isotopically labelled standards (ca 50 µM) were mixed with 20 µL 120 mM EDC HCl-6% pyridine-solution and 20 µL of 200 mM 3-NPH HCL solution. After 30 min at 40°C and shaking at 1000 rpm using an Eppendorf Thermomix (Eppendorf, Hamburg, Germany), 900 µL acetonitrile/water (50/50, v/v) was added. After centrifugation at 13000 U/min for 2 min the clear supernatant was used for analysis. The same system as described above was used. The electrospray voltage was set to -4500 V, curtain gas to 35 psi, ion source gas 1 to 55, ion source gas 2 to 65 and the temperature to 500°C. The MRM-parameters were optimised using commercially available standards for the SCFAs. The chromatographic separation was performed on a 100 × 2.1 mm, 100 Å, 1.7 µm, Kinetex C18 column (Phenomenex, Aschaffenburg, Germany) column with 0.1% formic acid (eluent A) and 0.1% formic acid in acetonitrile (eluent B) as elution solvents. An injection volume of 1 µL and a flow rate of 0.4 mL/min was used.*

The gradient elution started at 23% B which was held for 3 min, afterward the concentration was increased to 30% B at 4 min, with another increase to 40%B at 6.5 min, at 7 min 100% B was used which was hold for 1 min, at 8.5 min the column was equilibrated at starting conditions. The column oven was set to 40°C and the autosampler to 15°C. Data acquisition and instrumental control were performed with Analyst 1.7 software (Sciex, Darmstadt, Germany).

Data processing to was carried out using the Xcms Viewer tool (an online version that allows access to the functions of the X-Chromosome Mass Spectrometry analysis software package for users that cannot run the full Xcms package locally) at http://10.195.4.22:8080/app/xcmsviewer, to which password-protected access was generously granted by Dr. Kleigrewe.

The "msconvert" from ProteoWizard were used to convert raw files to mzXML (de-noised by centroid peaks). The bioconductor/R package xcms was used for data processing and feature identification. More specifically, the matched filter algorithm was used to identify peaks (full width at half maximum set to 7.5 s). Then the peaks were grouped into features using the "peak density" method. The area under the peaks was integrated to represent the abundance of features. The retention time was adjusted based on the peak groups presented in most of the samples. To annotate possible metabolites to identified features, the exact mass and MS2 fragmentation pattern of the measured features were compared to the records in HMBD and the public MS/MS database in MSDIAL, referred to as MS1 and MS2 annotation, respectively. The QC samples were used to control and remove the potential batch effect, t-test was used to compare the features' intensity between the groups.

Data visualisation is presented in the Results section. Full SCFA analysis was conducted by Dr. Kleigrewe. After identifying significantly deregulated metabolites, particularly SCFAs, unbiased metabolite lists were inputted into the free MetaboAnalyst[168] webpage, version 6.0, available in autumn 2023. Pathway analysis of annotated compound names was performed using the KEGG pathway libraries for *Mus musculus*, *Bacillus subtilis*, and *Escherichia coli*, all publicly accessible in autumn 2023. Due to its suspected high abundance in caecal samples, only the comparison with the *E. coli* KEGG pathway library is presented, as detailed pathway analyses would exceed the scope of this thesis. The visualisation method employed was a scatter plot testing significant features, with a Hypergeometric Test for enrichment and Relative-betweenness Centrality for topology analysis (all default options). The

reference metabolome was chosen as described above. Analysis reports were retrieved as PDFs, and annotated pathway overviews are included in the figures in the Results section of this thesis.

Brightfield microscopy of immunohistochemically labelled paraffin embedded tissue

Sample preparation for immunohistochemical (IHC) staining followed standard procedures with support from the Comparative Experimental Pathology Department (CEP) at Technical University Munich. Tissue samples, including the ileum, colon, liver, spleen, and mesenteric lymph nodes (mLn), were retrieved from euthanised mice, briefly washed in PBS to remove contaminants, and transferred to 4% paraformaldehyde (pFA).

For “Swiss roll”[169] processing of ileal and colonic tissue, the intestinal section was straightened, and the exterior was superficially washed with cold PBS. Faecal matter was gently expelled from one end, and the intestine was flushed with 2-3 mL of cold PBS via a 1 mL pipette tip. The intestine was then cut open longitudinally, laid flat to expose the lumen, and rolled from distal to proximal around a wooden stick. All tissues were fixed in 4% pFA for approximately 72h, then transferred to IHC cassettes for dehydration, paraffin embedding, and microtome sectioning, following CEP protocols.

In addition to standard stains like H&E and PAS, CD3 and TLR5 expressing cells were enumerated using specific antibodies (see chapter “Antibodies” for specifications). Slides were scanned, and oedema scores (developed with trained pathologist Dr. Katja Steiger) along with cell enumeration were conducted manually using Aperio ImageScope Software (Leica Biosystems) by a scientist blinded to the genotype and treatment of the mice.

Confocal microscopy of immunofluorescently labelled cryo conserved tissues

Cryopreservation of tissues, cryotome sectioning, immunofluorescent labelling, and confocal imaging were conducted following modified standard procedures. Tissues of interest, primarily distal ileum, proximal colon, liver, spleen, and mesenteric lymph nodes (mLn), were isolated from euthanised mice, washed in cold PBS to remove contaminants, and transferred to 4% pFA. Tissues were fixed for 3-4 hours at room

temperature, rinsed with PBS, and incubated in 30% sucrose in PBS at 4°C overnight to prevent ice crystal formation. Samples were embedded in Tissue-Tek O.C.T. Compound using appropriately sized pre-labelled plastic cryomolds (Sakura Finetek Europe), ensuring correct orientation for experimental goals, and then stored at -80°C until fully hardened.

Samples were sectioned at 30 µm thickness on a Leica CM3050 S cryostat (Leica Biosystems GmbH) and transferred to pre-coated slides (Menzel Gläser, SuperFrost Plus, Thermo Fisher Scientific). The slides were treated with a gelatin and $CrK(SO_4)_2$ coating solution to enhance adherence. After drying at room temperature, samples were stored at -80°C until staining. For immunofluorescent staining, sections were thawed, dried at room temperature for 45 minutes, and kept hydrated with buffers. Sections were circled using a ReadyProbes™ Hydrophobic Barrier Pap Pen (Thermo Fisher Scientific) and treated with acetone for 10 minutes at room temperature for additional fixation and antigen retrieval, improving staining success of myeloid cell markers. Acetone was washed off with TBS buffer, and sections were washed, permeabilised with 0.1% Triton-X 100, and blocked with 2% bovine serum albumin (BSA) using TBS buffers.

Slides were blocked for about 1 hour at room temperature with 10% mouse serum in TBS-B before primary antibody staining. Primary or pre-conjugated antibodies were diluted in TBS-B and incubated overnight at 4°C in the dark. Antibody surplus was washed off the following day with TBS-B. Depending on the marker panel and compatibility of species, secondary antibodies were added in conjunction with pre-conjugated antibodies, also incubating overnight as previously described. If no pre-conjugated antibodies were used, secondary antibodies were applied for a minimum of 2 hours at room temperature, and DAPI counterstain was added if applicable. Sections were washed multiple times with TBS buffers to remove unbound antibodies, dipped in water to eliminate salts, and quickly mounted using Fluoromount-G Mounting Media (Invitrogen, Thermo Fisher Scientific). Cover slips were applied, avoiding air bubbles, and slides were dried for up to 48 hours in the dark on a flat surface before storage at 4°C until confocal imaging.

All slides were imaged on a Leica TCS SP8 inverted confocal microscope using a 63x glycerine wet-objective and 10x ocular magnification. Staining sequences, including laser power and exposure times, were standardised using a wild-type control slide, ensuring consistency across all samples, regardless of time point, treatment,

age, or sex. Confocal images were processed with IMARIS software (Imaris 9.7.2, Bitplane).

Isolation of immune cells from secondary lymphoid tissue

Immune cells were dissociated from intestinal tissues (Lamina propria (LP) and intraepithelial (IE)), mesenteric lymph nodes (mLn), and spleen for multicolour flow cytometric analysis using a modified protocol based on the "Lamina Propria Dissociation Kit, mouse" (Miltenyi Biotec, catalogue number 130-097-410).
Pre-digestion, digestion, and washing buffers were prepared per the manufacturer's protocol (version 140-003-623.03) and stored as follows: pre-digestion and washing buffers at 4°C for up to 2 months, and digestion enzymes at -20°C until use. Additionally, 40% and 80% Percoll gradients were prepared using 100% human Percoll, 10x DPBS, RPMI, and 20% FCS, all warmed to 37°C before extraction.

Mice (12-20 weeks old) were euthanised via cervical dislocation after brief Isoflurane exposure. The spleen and mLn were removed and stored in cold PBS on ice. The ileum was approximated by removing the full small intestine and dividing it into three parts, retaining the section closest to the caecum. The intestinal content was flushed with cold PBS, and the ileum was cut open longitudinally for cleaning. Remaining mucus was gently scraped off, and tissue pieces were transferred to a clean 50 mL tube containing pre-warmed pre-digestion buffer with EDTA. After 20 minutes of shaking at 37°C, the pieces were vortexed for mechanical dissociation and strained to obtain the first IE immune cell fraction in the supernatant. This pre-digestion process was repeated to recover a second IE immune cell fraction.

The resulting tissue pieces were washed with the washing buffer to remove EDTA. The IE fractions were allowed to settle, strained to remove debris, pooled, and centrifuged at 300g for 10 minutes to yield a pellet containing intraepithelial immune cells. This pellet was resuspended in 40% Percoll and layered onto 80% Percoll for gradient centrifugation at 2200g for 20 minutes at room temperature, forming a ring of IE immune cells between the layers. These cells were filtered through a 70 µm filter and kept on ice until staining.

Washed ileal pieces were digested in digestion buffer containing enzymes A, D, and R, following the manufacturer’s instructions. The GentleMACS program 37_m_LPDK_1 was run for dissociation. Spleen and mLn were also added to C tubes with 1.5 mL of digestion buffer, disrupted with scissors, and processed with the same

program. The ileal tubes were then detached, and mLn and spleen samples were processed using the m_intestine_01 program.

All samples were transferred to fresh 50 mL tubes, supplemented with RPMI + 20% FCS, and centrifuged. The mLn and spleen pellets were resuspended, strained to remove clumps, and stored on ice until staining. LP immune cells underwent a Percoll gradient similar to the IE immune cells, and were pelleted, resuspended, and stored on ice for staining. Cell numbers were determined, with approximately 1,000,000 cells seeded in a 96-well V-bottom microtitre plate for multicolour flow cytometric analysis. For single stain references, about 200,000 cells were seeded per well.

Multicolour flow cytometric analysis of immune cell populations from secondary lymphoid tissues

All samples were measured using a Sony SP6800 Spectral Cell Analyser. Cells were seeded in individual wells of a 96-V-bottom microtitre plate at the specified densities, spun down, and resuspended in cold PBS with a multichannel pipette. They were stained with a live/dead stain to indicate cell membrane breakdown and cell death, incubating in the dark at room temperature for 20 to 30 minutes. After washing with cold FACS buffer (see “Reagents”), if an unconjugated antibody was used, it was added and incubated for another 20 to 30 minutes as for the live/dead stain. Following a second wash, a fluorochrome-conjugated secondary antibody was added and incubated for 20 to 30 minutes. After another wash, a mixture of pre-conjugated antibodies was added, with a final incubation of 20 to 30 minutes before washing again. Cells were resuspended in 120 µL of FACS buffer and transferred to flow cytometric sampling tubes. For details on antibody targets, clone specificity, fluorochrome conjugates, and dilutions, see “Antibodies.” Single stains were performed for each antibody to adjust the compensation matrix, and control stains using only secondary antibodies were included to assess non-specific staining. Photomultiplier tube (PMT) voltage was optimised for each measurement. All events from the intraepithelial and Lamina propria fractions were recorded to analyse rare populations, while a maximum of about 500,000 events was recorded for mLn and spleen samples.

Single cell RNA sequencing (scRNAseq) analysis of murine intestinal immune cells

10X Genomics based scRNAseq was carried out in cooperation with the laboratory of Prof. Dr. Peter Vandenabeele at the Cell Death and Inflammation Unit at VIB-Centre for Inflammation Research in Ghent, Belgium. The following passages (indicated in italics) were abbreviated from in the Methods section of Wahida *et al.*[170]

Intestinal cell isolation: Small intestines from 3 wild-type mice were flushed with RPMI containing 5% heat-inactivated FCS. Peyer's patches were removed, and the intestines were cut open longitudinally and then into 0.5 cm pieces. The epithelial layer was removed by incubation in HBSS with HEPES, $NaHCO_3$, FCS, and DTE. This step was repeated, and the cells were collected by centrifugation. The cell pellet was resuspended in 37.5% Percoll and centrifuged. The top layer was removed, and the pellet containing intraepithelial lymphocytes and epithelial cells was removed. The remaining tissue pieces were incubated in HBSS with HEPES and EDTA and digested in RPMI with FCS, $MgCl_2$, $CaCl_2$, DNAse I, and collagenases. The cells were collected by centrifugation, resuspended in 37.5% Percoll, and centrifuged. The resulting cell pellet of Lamina propria lymphocytes was processed further for cell sorting. Single cells were stained for CD45 and DAPI and sorted using BD FACSAria™ II and BD FACSAria™ III cell sorters.

Single-cell RNA sequencing: Sorted single-cell suspensions were loaded on a Chromium GemCode Single Cell Instrument to generate single-cell gel beads-in-emulsion (GEM). Biological replicates were multiplexed per lane using TotalSeq-A Cell Hashing Antibodies. The scRNA libraries were prepared using the GemCode NextGEM Single Cell 3' Gel Bead and Library kit. The cDNA content of pre-fragmentation and post-sample index PCR samples was analysed using the 2100 BioAnalyser. Sequencing libraries were loaded on an Illumina NovaSeq flow cell.

Single-cell RNA sequencing data analysis: In total, three samples were processed using the CellRanger v6.0.0 pipeline. The resulting count matrix was filtered based on number of genes per cell, number of unique molecular identifiers (UMI's), and percentage of mitochondrial reads. The filtered data was processed using Seurat v3 in R. Principal component analysis was performed on the highly variable genes to reduce the dimensionality of the data. Unsupervised clustering was performed, and the data was visualised in two-dimensional scatter plots with Uniform Manifold Approximation and Projection (UMAP). Cells were annotated using a combination of

well-known markers genes from the literature and differential gene expression analysis per cluster.

Single-cell barcode demultiplexing: TotalSeq-A Cell Hashing Antibody data was normalised using the centred log ratio (CLR) normalisation method in Seurat.
Differential gene expression analysis: Differential gene expression was assessed with the Wilcoxon rank sum test as implemented in the FindMarkers() function in Seurat.

Computational tools and statistics

Statistical analyses were performed using R Studio, GraphPad prism, Xcms viewer web interface and Namco Microbiome Explorer (for details on R packages please visit respective wegpages, described above). ScRNAseq data was processed and visualised using the R BiocManager package. The dissimilarities between experimental groups were evaluated using statistical tests, resulting p values calculated as indicated in the individual figures.

Results

Germfree (gf) Xiap-deficient mice develop signs of small intestinal inflammation upon targeted colonisation

In the first step, small intestinal tissue, specifically the terminal ileum proximal to the caecum, of wild type (Wt) and Xiap-deficient (*Xiap*$^{-/-}$) mice housed under germfree (gf) conditions was compared to mice colonised via faecal matter transplantation (FMT) using faeces from conventional housing. As previously introduced, paediatric XLP2 patients lacking functional XIAP exhibit early-onset IBD symptoms resembling Crohn's disease. Hence, as outlined in the methods section, three histopathological parameters based on prior observations in adult *Xiap*$^{-/-}$ mice from conventional housing featuring an ileal inflammatory phenotype[170] were established. It was hypothesised that tissue inflammation was directly dependent on the presence of a microbiome even in a genetically susceptible host such as *Xiap*$^{-/-}$ mice.

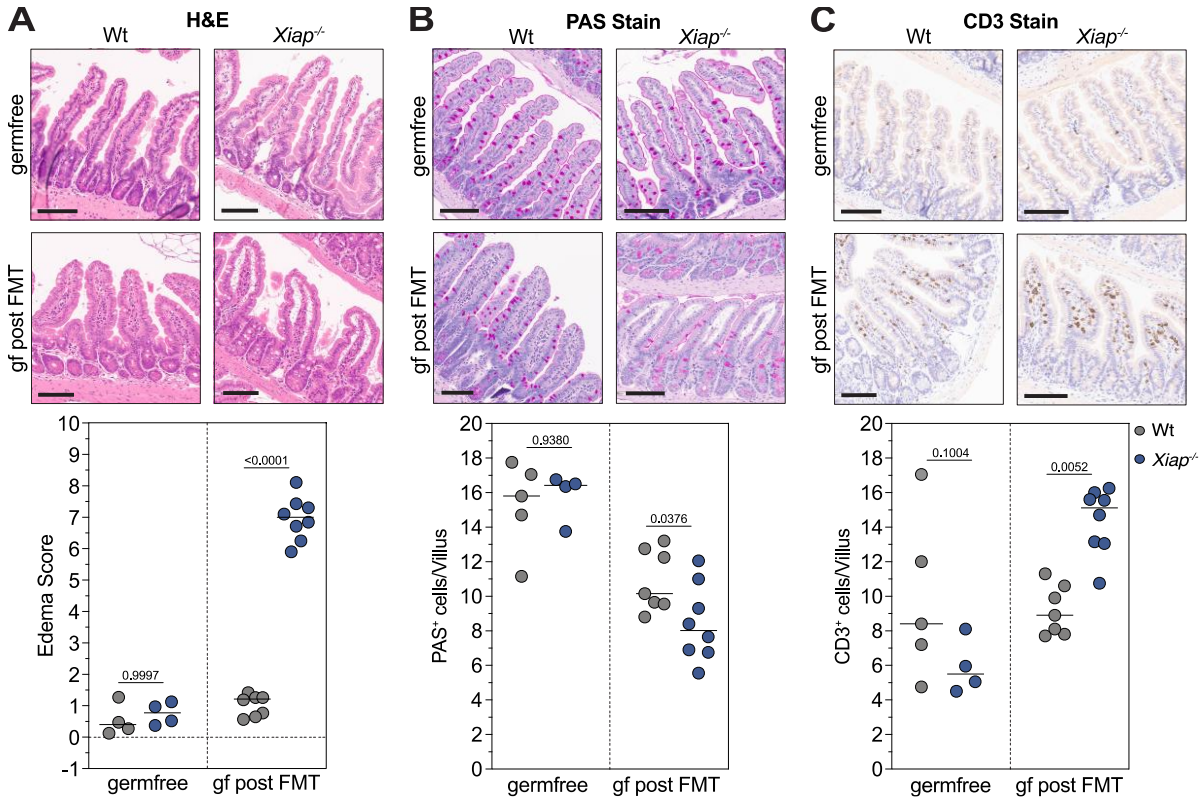

Figure 9. Targeted colonisation via FMT leads to the development of histological signs of ileal tissue inflammation in gf*Xiap*$^{-/-}$ mice. Representative IHC stain of paraffin-embedded ileal tissue and evaluation of depicted features of tissue inflammation i.e. (A) H&E Stain / (B) PAS Stain / (C) CD3 Stain in gfWt (grey) and gf*Xiap*$^{-/-}$ (blue) mice, and post FMT. Scale bars depict 100 µm. Data (A) to (C) were analysed by one-way ANOVA ($p<0.0001$) and reported p values include *post hoc* with Holm-Šidák's correction. Each dot represents one mouse, n = 4 – 8.

A semi-quantitative score indicating the formation of villus oedema was enumerated based on H&E-stained ileal Swiss rolls, reflecting both the severity and extent of fluid influx due to epithelial detachment. Goblet cell numbers indicated the capacity to produce the protective mucus layer separating the intestinal epithelium from the luminal content, and microbiota therein. Lastly, increased numbers of $CD3^+$ T cells in the lamina propria (LP) were assumed to be correlated with an ongoing recruitment of adaptive immune cells.

Prior to FMT (**Figure 9**A), neither gfWt nor gf*Xiap*$^{-/-}$ mice exhibited signs of tissue inflammation, such as villus oedema (p=0.9997). Goblet cell numbers, assessed via PAS staining (**Figure 9**B), showed no significant differences between the groups (p=0.9380). Additionally, the numbers of $CD3^+$ T cells did not significantly differ between the two genotypes (p=0.1004) (**Figure 9**C).

Faeces from adult non-inflamed Wt and symptomatic *Xiap*$^{-/-}$ mice from conventional housing were collected and prepared for transplantation. The pooling of samples allowed for the establishment of a microbiome reflective of the non-inflamed Wt mice in gf*Xiap*$^{-/-}$ mice, a principle which will be discussed later on. Both groups of gf mice were orally gavaged once and then housed separately for 4 weeks. Following FMT, both genotypes were referred to as “post FMT”.

Colonisation resulted in ileal oedema formation exclusively in gf*Xiap*$^{-/-}$ mice post FMT (p<0.0001) (**Figure 9**A). Both Wt and *Xiap*$^{-/-}$ mice post FMT displayed reduced numbers of Goblet cells, with *Xiap*$^{-/-}$ mice post FMT losing significantly more mucus-producing cells than Wt mice post FMT (p=0.0376) (**Figure 9**B). Tissue inflammation in *Xiap*$^{-/-}$ mice post FMT correlated with an increased number of T cells in the ileal LP (p=0.0052) (**Figure 9**C).

In summary, colonisation of adult germ-free mice with a conventional microbiome via FMT induces ileal tissue inflammation specifically in non-inflamed gf*Xiap*$^{-/-}$ mice. This highlights not only the critical role of XIAP in maintaining intestinal homeostasis, but also the essential contribution of the microbiome to the fruition of this phenotype.

Epithelial Paneth cells in the crypts of inflamed *Xiap*$^{-/-}$ mice present with an altered transcriptome

In addition to the protective role of mucus-producing Goblet cells, epithelial Paneth cells are crucial for safeguarding the intestinal stem cell compartment. Paneth cells produce antimicrobial peptides, stored in intracellular vesicles, to maintain a microbe-free crypt environment, denoting them to carry an innate immune-like function. These protective vesicles can be visualised using the lectin Ulex europaeus agglutinin-1 (UEA-1) to approximate Paneth cell functionality. It was hypothesised that Paneth cell dysfunction may leave epithelial stem cells vulnerable to microbial insults, which may directly contribute to the onset of tissue inflammation such as observed in *Xiap*$^{-/-}$ mice (**Figure 9**).

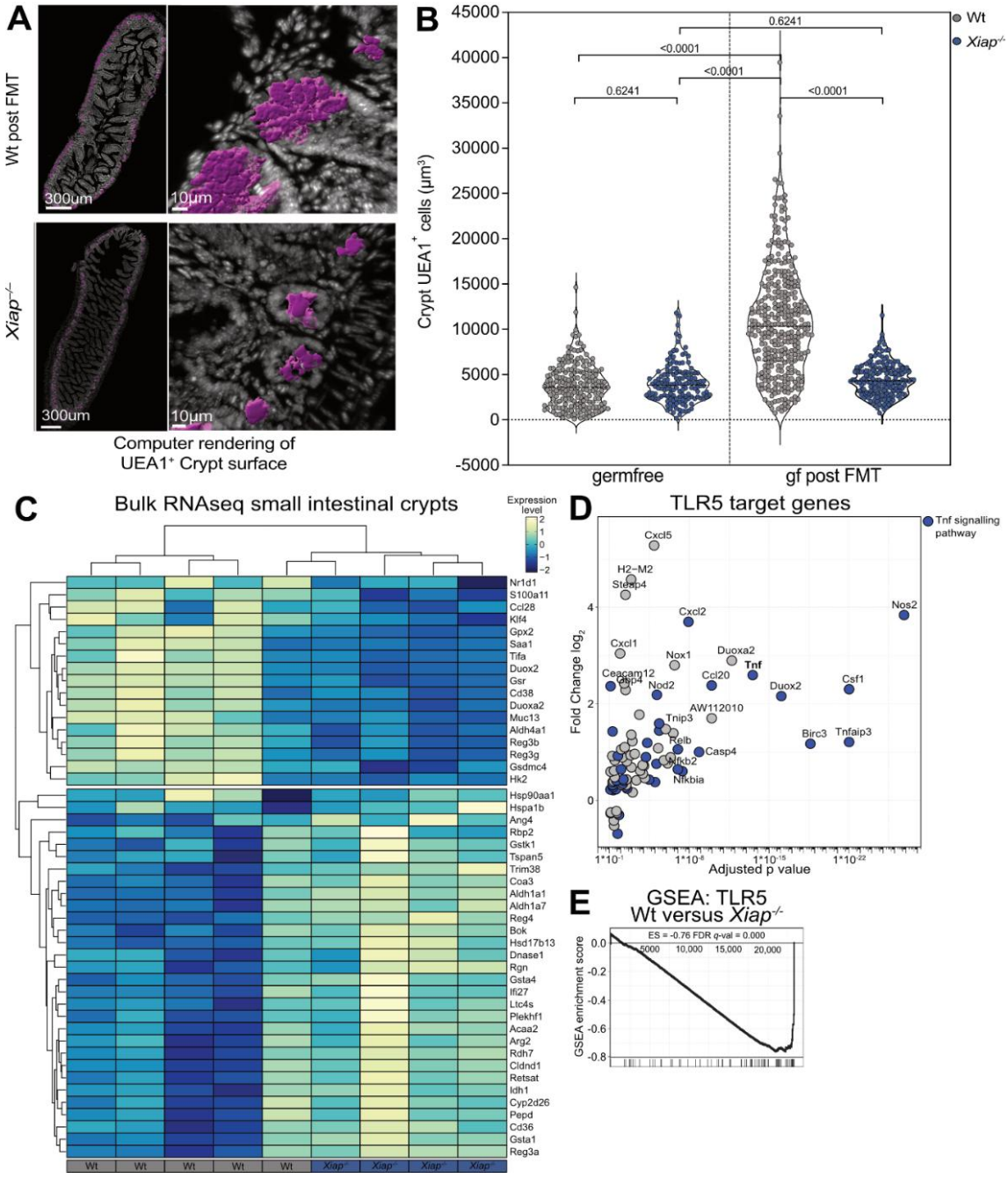

Figure 10. Intestinal tissue inflammation in conventionalised *Xiap*$^{-/-}$ mice correlates with loss of UAE1^{+} vesicle production by Paneth cells; Paneth cells from inflamed *Xiap*$^{-/-}$ mice feature transcriptional changes in genes related to TLR5 signalling and TNF signalling. (A) Computer-assisted rendering of Paneth cell volume (labelled by UAE1^{+} area (in purple)) in intestinal crypt area of Wt and *Xiap*$^{-/-}$ mice post FMT (counterstain of cell nuclei in grey). (B) Quantification of UEA1^{+} volume in intestinal crypts of gfWt (grey) and gf*Xiap*$^{-/-}$ (blue) mice and post FMT. Data was obtained from one slide each for n = 3 per genotype and housing condition. Data (B) was analysed by one-way ANOVA ($p<0.0001$) and reported p values include post hoc with Holm-Šidák's correction. Surface rendering was generated using Imaris software package. (C) Heatmap of selected deregulated genes from bulk RNAseq analysis (GSE182934) of ileal crypts isolated from 5 adult Wt and 4 adult *Xiap*$^{-/-}$ mice from conventional housing. (D) Dot plot of Tlr5 target genes highlighting members of the Tnf signalling pathways in blue, based on GSE117772. (E) GSEA signature comparing Tlr5 gene signature (based on GSE117772) in bulk RNA isolated from ileal crypts of adult Wt versus *Xiap*$^{-/-}$ mice from conventional housing (GSE182934)

Depicted in **Figure 10**A, a computer-assisted surface rendering tool within the Imaris software was employed to quantify the volume of UEA-1$^+$ signal in Paneth cells of gfWt and gf*Xiap*$^{-/-}$ mice, as well as Wt and *Xiap*$^{-/-}$ mice post FMT (**Figure 10**B). No significant differences in the volume of UEA-1$^+$ vesicles in the crypts were observed between gfWt and gf*Xiap*$^{-/-}$ mice (p=0.6241). Upon microbiome establishment, the volume of UEA-1$^+$ vesicles in Paneth cell increased significantly in Wt mice, indicating an adaptive response to microbial antigens increasing antimicrobial peptide production (p<0.0001). In contrast, the volume of UEA-1$^+$ vesicles did not increase in *Xiap*$^{-/-}$ mice post FMT (p=0.6241) and remained significantly lower than in Wt counterparts (p<0.0001). This reduction in the volume of UEA-1$^+$ vesicles suggests a compromised ability of Paneth cells to mount an appropriate response to microbiome introduction, rendering the stem cell compartment vulnerable to microbial exposure.

Based on this, transcriptional differences in Paneth cells between non-inflamed Wt and inflamed *Xiap*$^{-/-}$ mice were investigated. The transcriptome of isolated intestinal crypts from adult mice from conventional housing was analysed via bulk RNA sequencing (GSE182934). Notably, crypts of inflamed *Xiap*$^{-/-}$ mice exhibited deregulation of several metabolic pathways (**Figure 10**C). Downregulation was observed in genes related to oxidative stress response (e.g., Duox2), innate immune response (e.g., S100a11, Ccl28), transcriptional regulation and cell differentiation (e.g., Klf4, Gpx2), and Paneth cell function (e.g., Reg3b, Reg3g). Conversely, higher expression levels of genes associated with mitochondrial function and energy metabolism (e.g., Coa3, Acaa2), heat shock proteins (e.g., Hsp90aa1, Hspa1b), detoxification and antioxidant defence (e.g., Gstk1, Gsta4, Gsta1), and apoptosis regulators (e.g., Bok, Dnas1) were noted. This expression pattern suggests that the tissue is undergoing a stress response, immune activation, and repair activities, indicative of ongoing Paneth cell dysfunction.

The extent to which a stress response is selectively elicited in Paneth cells in the absence of XIAP remains to be elucidated. Based on previous findings linking aberrant TNF signalling downstream of TLR induction to excessive cell death in *Xiap*-deficient immune cells[153,156], it was postulated that a similar mechanism might underlie the epithelial cell phenotype.

To elucidate the connection between TLR induction and TNF signalling, the intestinal epithelial map based on TLR-reporter mice published by Price *et al.*[171] was utilised. This study demonstrated that *Tlr5* expression in murine small intestinal

epithelium is exclusive to Paneth cells. Analysis of their publicly available dataset (GSE117772), which targeted TLR5 through flagellin stimulation in Paneth cell-enriched small intestinal organoids, revealed that TLR5 stimulation resulted in the upregulation of numerous genes associated with TNF signalling (**Figure 10**D). This finding is particularly relevant, given that XIAP is crucial for mediating signalling downstream of TNF induction (see respective Introduction chapter for details). Additionally, gene set enrichment analysis of a TLR5 target gene signature (based on GSE117772, **Figure 10**E) indicated distinct downregulation of TLR5 target genes in crypts of inflamed *Xiap*$^{-/-}$ mice compared to Wt mice, correlating with a dysfunctional phenotype and transcriptional profile in TLR5^{+} Paneth cells of *Xiap*$^{-/-}$ mice.

Ultimately, the aberrant Paneth cell phenotype observed in inflamed *Xiap*$^{-/-}$ mice suggests a functional link between TLR5 activation and TNF signalling in the epithelium, a hypothesis confirmed by Wahida *et al.*[170] While *TLR5* expression is widespread in human cells of various origins, only specific cell types express *Tlr5* in mice. Thus, an investigation into other cell types, particularly innate immune cells, was initiated to determine which might be affected by the interplay between TLR5 stimulation and downstream TNF signalling, potentially sensitising TLR5^{+} cells to loss of *Tlr5* expression or cell death.

XIAP deficiency correlates with a loss of TLR5-expressing Lamina propria immune cells

As shown in **Figure 10**, the absence of XIAP affects TLR5-expressing Paneth cells in the murine intestinal epithelium, and transcriptomic changes in Paneth cells revealed a link between TLR5 induction and downstream TNF target genes. However, as the focus of this thesis lay in the immune cell compartment, it was investigated whether TLR5-associated TNF signalling might additionally influence immune cells characterised by the expression of TLR5, potentially contributing to the inflammatory intestinal phenotype in *Xiap*$^{-/-}$ mice. Hereby, a role for TNFR2 was explored, building on *in vitro* findings by Yabal *et al.* suggesting an involvement of TNFR2 in inflammatory cell death downstream of TLR induction in the absence of XIAP.[153]

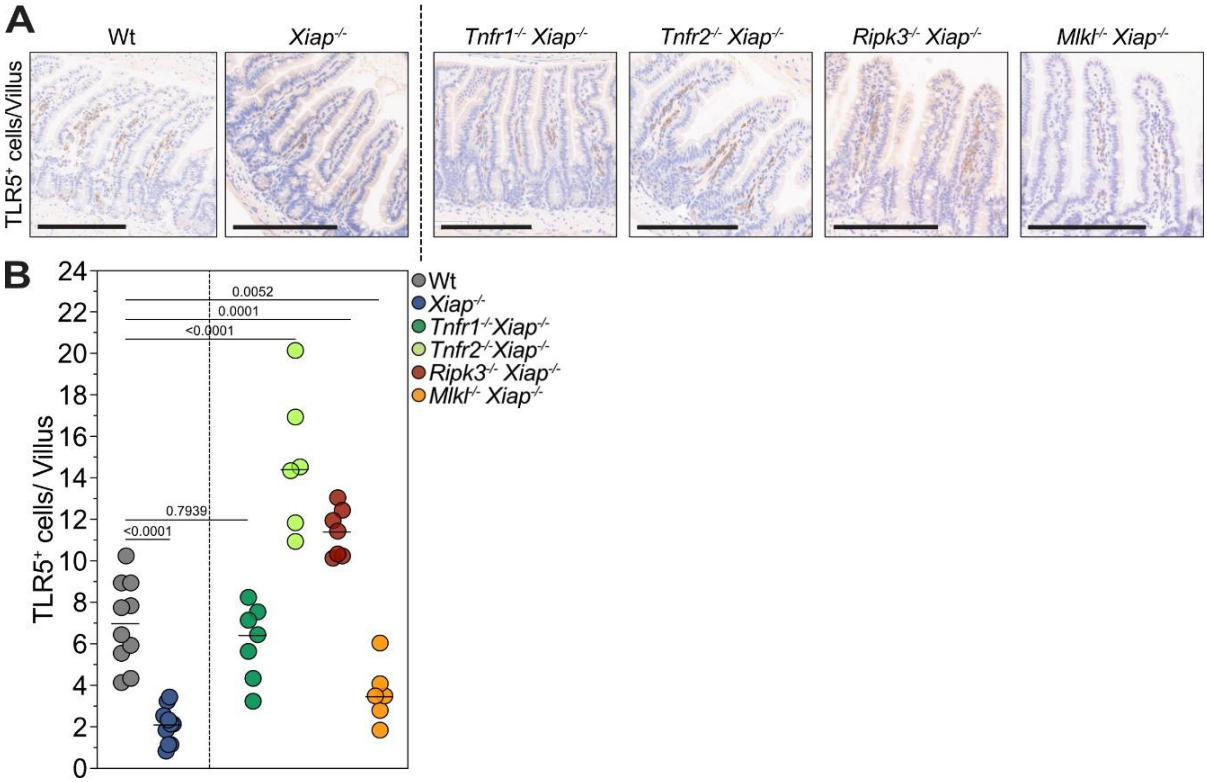

Figure 11. Loss of TLR5 expression in villus immune cells in *Xiap*$^{-/-}$ mice from conventional housing is rescued by genetic ablation of TNFR2, or the upstream inducer of necroptosis RIPK3, but appears to be independent of the presence of MLKL. Representative IHC stain of paraffin-embedded ileal tissue (A) and quantification of TLR5 expressing cells(B) of Wt (grey) versus genetically modified mice of depicted genotypes (i.e. *Xiap*$^{-/-}$ mice = blue, *Tnfr1*$^{-/-}$ *Xiap*$^{-/-}$ = dark green, *Tnfr2*$^{-/-}$ *Xiap*$^{-/-}$ = light green, *Ripk3*$^{-/-}$*Xiap*$^{-/-}$ = dark red , *Mlkl*$^{-/-}$*Xiap*$^{-/-}$ = orange). Scale bars depict 200 µm. Data was analysed by one-way ANOVA ($p<0.0001$) and reported p values include *post hoc* with Holm-Šidák's correction. Each dot represents one mouse, n = 6 – 10.

As visualised using an IHC-stain, TLR5^{+} cells in the ileum were exclusively localised in the lamina propria (LP) (**Figure 11**A, quantified in B), with genotype-

dependent differences in frequency. Notably, significantly fewer TLR5$^+$ LP cells were found in inflamed *Xiap*$^{-/-}$ mice than in Wt controls (p<0.0001). Both in *Tnfr1*$^{-/-}$ *Xiap*$^{-/-}$ mice and *Tnfr2*$^{-/-}$ *Xiap*$^{-/-}$ mice, housed in conventional conditions, numbers of TLR5$^+$ cells were rescued up to Wt levels, with *Tnfr2*$^{-/-}$ *Xiap*$^{-/-}$ mice even exceeding numbers found in Wt mice (p<0.0001). These findings indicate a role for both TNF receptors in maintaining TLR5$^+$ cell populations in the absence of XIAP, aligning with the previously identified Paneth cell phenotype, with a stronger effect executed via TNFR2.

Given existing data suggesting RIPK3 involvement in TNF-driven myeloid cell loss via necroptosis[153], the role of this kinase was evaluated. As shown in **Figure 11**B, *Ripk3*$^{-/-}$ *Xiap*$^{-/-}$ mice displayed a significant increase in TLR5$^+$ cells in the LP beyond Wt levels (p=0.0001), suggesting an involvement of RIPK3 in this cellular mechanism. Conversely, *Mlkl*$^{-/-}$ *Xiap*$^{-/-}$mice showed no significant rescue of TLR5$^+$ cells (p=0.0052) compared to *Xiap* $^{-/-}$ mice, an unexpected finding given the typical role of MLKL as an executor in RIPK3-mediated necroptosis.

These findings demonstrate that an XIAP deficiency affects TLR5$^+$ immune cells in the LP. While the involvement of TNF signalling was expected, surprisingly, the extent of the phenotype rescue due to the ablation of TNFR2 exceeded that of TNFR1. Additionally, RIPK3 was implicated in the cellular mechanism affecting TLR5$^+$ immune cells in the absence of XIAP, though interestingly MLKL appeared non-essential.

Trl5 expressing immune cells in the Lamina propria align with a dendritic cell identity

Apparent in **Figure 10** and **Figure 11**, TLR5 expression in mice is restricted to specific cell populations, namely Paneth cells and lamina propria (LP) immune cells, in the intestine. It was furthermore shown that TLR5$^+$ LP immune cells are significantly affected in inflamed *Xiap*$^{-/-}$ mice. To understand the functional contribution of these specialised immune cells to the inflammatory phenotype, it was of vital importance to elucidate their identity.

In a first step, transcriptomic analysis was employed to investigate TLR5$^+$ cells of Wt mice, examining their co-expression of other markers to clarify their identity and function in the intestine. A scRNAseq dataset of CD45$^+$ immune cells (GSE183885) from the intestinal epithelium (IE) and LP of the small intestine, as well as from the colon and mesenteric lymph nodes, served as the basis for identifying TLR5$^+$ immune cells that may share or display unique transcriptional markers. Since **Figure 11** suggested that TLR5$^+$ cell loss in the LP of *Xiap*$^{-/-}$ mice was rescued through TNFR2 ablation, the analysis furthermore focused on TNFR2$^+$ subpopulations across the intestine.

Although this scRNAseq data covered only Wt cells, hence precluding direct comparison with *Xiap*$^{-/-}$ mice, these findings would provide a foundation for the next phase comparing cell surface protein markers in Wt and *Xiap*$^{-/-}$ mice, to further investigate the identity and function of intestinal immune cell populations involved in the intestinal inflammatory phenotype.

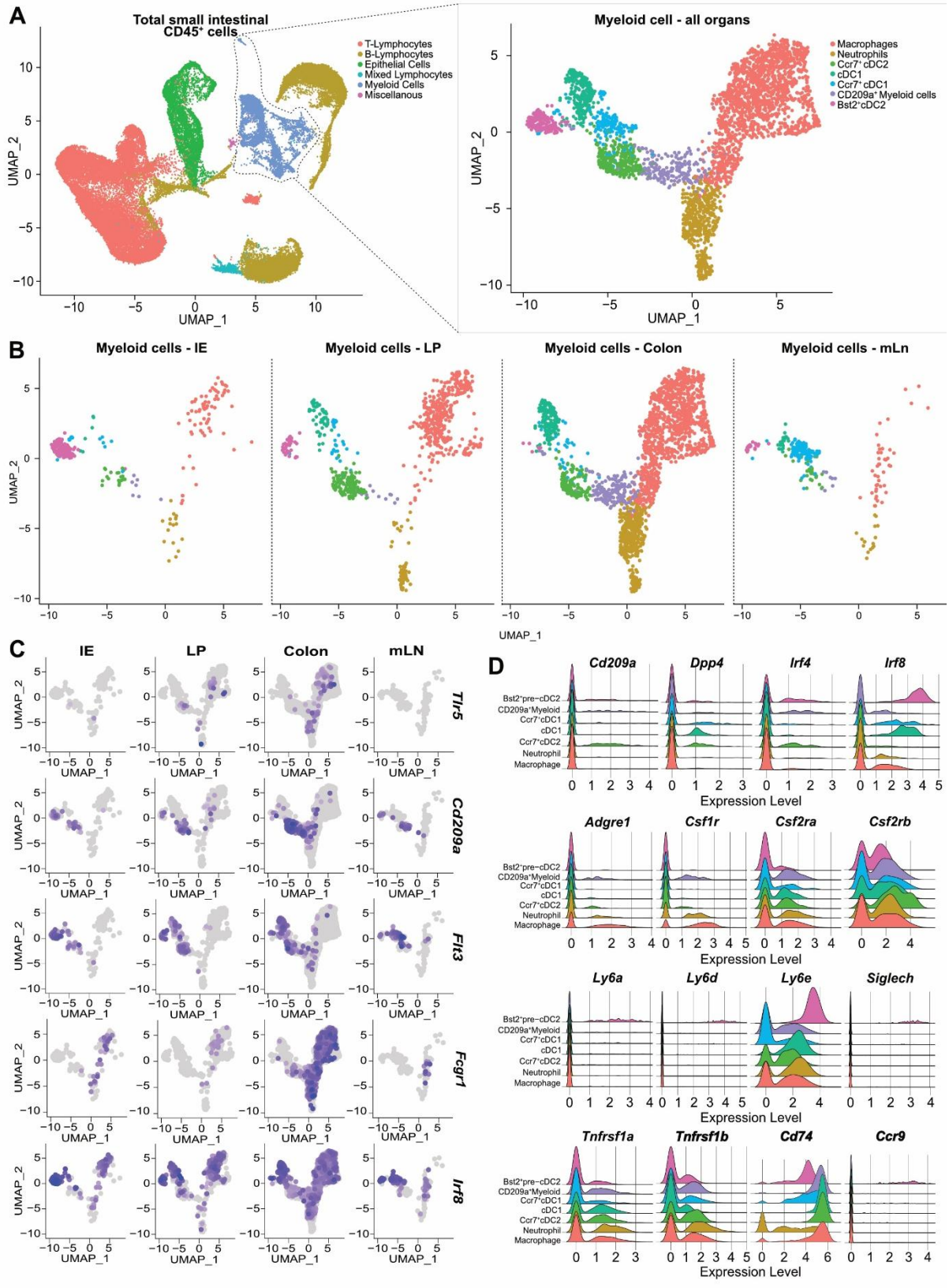

Figure 12. *Tlr5*⁺ DC isolated from the Lamina propria (LP) express *Cd209a,* and *bona fide* cDC2 markers, *Tlr5*⁺ DC cannot be isolated from the ileal epithelium (IE). scRNAseq of immune cells from small intestinal IE, LP, colon (IE and LP) and mesenteric lymph nodes (mLn) depicted as (A) UMAP of unsupervised clustering of all *Prprc*⁺ cells (all immune cells) and manual annotation of major immune population dependent on expression tables, and UMAP of re-clustered manually annotated myeloid

populations pooled from all organs. (B) UMAP of myeloid clusters separated by tissue origin. (C) Feature plot depicting expression of genes of interest (*Tlr5*, *Cd209a*, DC-development marker *Flt3*, macrophage marker *Fcgr1* (encoding CD64) and cDC marker *Irf8*) in previously identified myeloid clusters split by tissue origin. (D) Ridge plot depicting expression levels of genes of interest (serving the identification of specific DC subpopulations) in previously identified myeloid clusters. Extracted cells were pooled from 3 Wt littermate mice, raw data accessible via GSE183885.

Figure 12	Cluster name	# of cells in scRNAseq
A	T cell cluster	19300
	B cell cluster	12593
	Epithelial cell cluster	5913
	Mixed T-B cell cluster	631
	Myeloid cell cluster	4509
	Misc.	135
D	Macrophage cluster (red)	1583
	Neutrophil cluster (dark yellow)	499
	Ccr7+ cDC2 cluster (grass green)	311
	cDC1 cluster (turquoise)	248
	Ccr7+ cDC1 cluster (light blue)	214
	Cd209a+ myeloid cluster (violet)	207
	Bst2+ pre-cDC2 cluster (pink)	204

Table 2. Numbers of cells included in scRNAseq analysis, forming clusters as illustrated in **Figure 12**.

As shown in **Figure 12**A and B, unsupervised clustering analysis focused on sorted CD45$^+$ cells, with T and B cells excluded to isolate myeloid populations. High expression of the transcription factor (TF) *Mafb* defined a macrophage cluster in both IE and LP (**Figure 12**C and D), which also expressed *Fcgr1* (encoding CD64) along with markers *Adgre1* (F4/80) and *Csf1r* (M-CSF receptor), indicating a *bona fide* macrophage lineage. A distinct cluster of neutrophils, characterised by *Clec4e* expression, was also detected in both compartments.

The small intestine is known to host unique DC populations, some with niche-specific roles in the IE versus the LP.[47] In the depicted analysis, five distinct DC-like populations were identified, each expressing *Dpp4*, a pan-DC marker, and the TF *Flt3*, distinguishing them from the macrophage and neutrophil clusters. Further, cDC1 populations were identified by *Xcr1* expression as it became apparent that *Irf8* did not serve as an exclusive marker for cDC1. *Ccr7*$^+$ cDC1 and *Ccr7*$^+$cDC2 populations were also detected, with the latter expressing *Cd209a* and the cDC2 TF *Irf4*. High *Ccr7* expression, a marker associated with DC migration to lymph nodes. This notion was corroborated by high *Cd74* expression, an MHCII molecule typically upregulated upon DC activation, suggesting a role for these cells in antigen presentation and naïve T-cell priming, both local and in mLn.

Focusing on *Tlr5* expression, it was found that in the small intestine, *Tlr5*$^+$ expression was prominently featured in *Ccr7*$^+$cDC2 in the LP; this subset further featured Cd209a expression, a potential marker of functional specialisation within intestinal DC populations, and high expression levels of *Tnfrsf1b* encoding TNFR2.

Tlr5^{+} cells were not observed in the IE, aligning with prior immunohistochemical results (**Figure 11**), and supporting a compartmentalisation of TLR5 expression. Interestingly, in the colon, *Tlr5* expression was primarily found in the macrophage and neutrophil clusters. However, as the *Xiap*-dependent intestinal inflammatory phenotype was specifically located in the small intestine, colon clusters did not become the focus of the presented research but may be investigated at a later time point. mLN were devoid of *Tlr5*$^{+}$ cells. *Tlr5*$^{+}$ cell counts were low overall, possibly due to cell death as a result of the mechanical stress of tissue isolation, a limitation addressed later in this thesis.

A separate *Cd209a*$^{+}$ DC population in the IE, characterised by high *Irf8* expression but lacking *Xcr1*, also expressed *Irf4*, in addition to markers dogmatically associated with plasmacytoid DC (pDC) lineage (*Bst2*, *Siglech*, *Ccr9*). The shared *Cd209a* expression between *Tlr5*$^{+}$LP DC and these *Tlr5*$^{-}$IE DC led to the speculation that *Cd209a*$^{+}$ IE versus LP populations might represent functional stages within a developmental continuum rather than strictly separate lineages. Based on the high transcriptional plasticity proposed in DC ontogeny according to current research, *Cd209a*$^{+}$ *Bst2*$^{+}$ DC in the IE may represent a pre-cDC2 subtype, corroborated by the expression of the progenitor marker *Ly6a*.[56]

The scRNAseq data, along with the recent understanding of DC diversity, led to the hypothesis that the absence of TLR5^{+} cells in the IE might reflect the immaturity of IE DC compared to their LP counterparts. *Cd209a* was identified as an important marker, linking *Tlr5*$^{+}$ DC in the LP with certain IE DC populations, supporting the hypothesis that these DC subsets might represent different functional stages rather than distinct populations. These cells could be particularly susceptible to inflammation-driven cell death in the absence of XIAP, a hypothesis supported by high *Tnfrsf1b* expression, linking their depletion to TNFR2 as previously observed.

CD209a^{+}DC exhibit intestinal niche-specific but related developmental characteristics

Building on the markers established in scRNAseq analyses of intestinal DC in Wt mice, the current analysis sought to evaluate the hypothesis that XIAP loss disrupts the maturation dynamics of compartmentalised intestinal DC subpopulations. Specifically, it was proposed that *Cd209a*$^{+}$ *Tlr5*$^{-}$ IE pre-cDC2 populations encounter antigens due to their proximity to the intestinal lumen. Speculatively, they upregulate TLR5 upon migrating into the LP to communicate with resident DC and T cells; a cascade of events interrupted in the absence of XIAP.

To analyse myeloid populations from IE and LP, two flow cytometry panels were developed, with immune cells isolated from mLn as control. For this, adult Wt mice and *Xiap*$^{-/-}$ mice from conventional housing were compared, as they had previously been shown to harbour histological signs of small intestinal inflammation.[170] Given that myeloid isolation protocols can influence population survival and cell-surface marker expression, flow cytometry findings will be corroborated with additional confocal staining in later sections of this thesis. Additionally, one has to acknowledge the methodological limitation that isolation protocols involving consecutive digestion steps cannot guarantee a clean separation between IE versus LP populations.

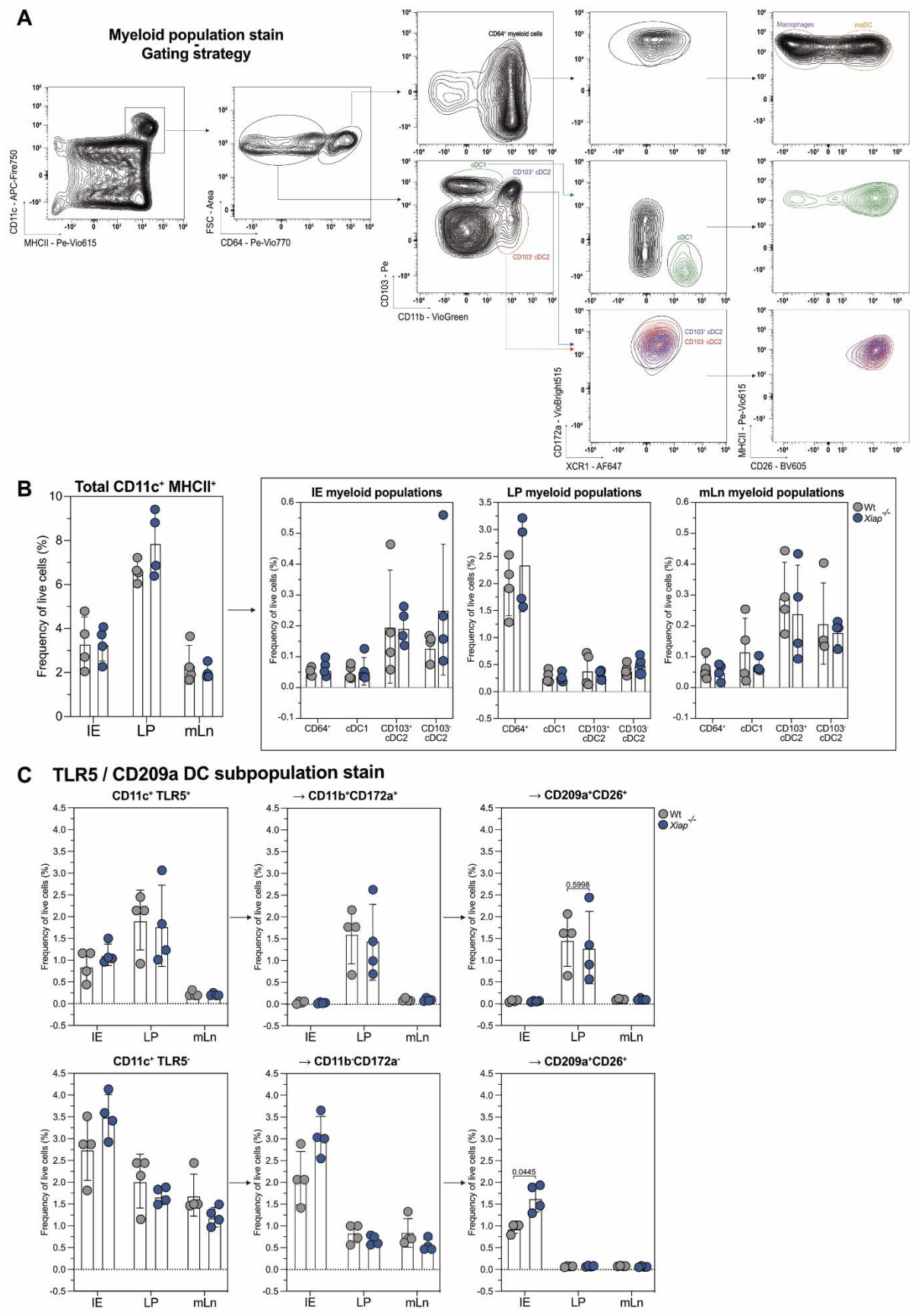

Figure 13. Both intraepithelial (IE) TLR5$^-$ CD209a$^+$ and Lamina propria (LP) TLR5$^+$ CD209a$^+$ are tendentially dysregulated in absence of XIAP. Flow cytometric analysis of isolated immune cells

from IE, LP and mesenteric lymph nodes (mLn), (A) gating strategy for detection of major DC populations and (B) quantification of DC populations. P values of differences between mean of population frequencies of myeloid populations according to multiple unpaired t tests with Welch correction not significant (C) Quantification of TLR5$^+$ CD209a$^+$ LP DC population versus CD209a$^+$ IE preDC population (based on scRNAseq data depicted in **Figure 12**) in adult Wt versus *Xiap*$^{-/-}$ mice from conventional housing, n = 4. Cells are quantified as percentage of live cells per stain, determined by live/dead stain, a total 1.5*10^5 events recorded for IE/LP samples, and 1*10^6 events recorded for mLn samples. P values of differences between mean of population frequencies of TLR5$^-$CD209a$^+$ IE and TLR5$^+$ CD209a$^+$ LP populations according to paired t test depicted in graph.

As a first step, a staining mix was applied based on established markers that classify myeloid cells in the intestine into traditionally recognised populations (**Figure 13**A).[36,172] Previous studies have shown intestinal myeloid cells generally express MHCII and CD11c. **Figure 13**B shows that LP has the highest MHCII$^+$ CD11c$^+$ cell population (7.8% in inflamed *Xiap*$^{-/-}$ mice vs 6.6% in Wt mice), while IE yielded fewer cells. Five distinct myeloid subsets were identified using the canonical macrophage marker CD64, the cDC1 marker XCR1 and cDC2 maker CD172a, as well as the integrins CD11b and CD103. Consistent with prior studies, a population so CD11b$^+$ CD103$^+$ double positive DC2 were identified, unique to the intestine and draining lymph nodes.[173,174] Numbers of these mostly IE cells did not differ between genotypes. In both IE and LP, CD11b$^+$ DC lacking CD64 were observed, with a modest increase of CD11b$^+$ CD103$^-$ DC2 in *Xiap*$^{-/-}$ mice IE (0.24% vs 0.12% in Wt). Among the CD64$^+$ populations, cells expressing CD26 were identified, suggestive of an activated phenotype consistent with inflammatory context, as described in recent findings[51]. The LP also exhibited a subset of CD64$^+$ CD26$^-$ cells, likely macrophages, alongside CD64$^+$ CD26$^+$ cells designated as monocyte-derived DC. Notably, CD64$^+$ cells were almost absent in IE of both genotypes. Therefore, staining overall myeloid populations did not suffice to identify specialised IE and LP DC populations affected by the absence of XIAP.

Conventionalised *Xiap*$^{-/-}$ mice feature a loss of LP immune cells characterised by the expression of TLR5 (**Figure 11**). scRNAseq offered first insights into the potential cDC2 ontogeny of these cells, and CD209a was established as a marker offering a potential functional link between IE DC and LP DC populations. Hence, a second stain combining the cDC2 marker CD172a with TLR5 and Cd209a was established.

As depicted, TLR5$^+$ CD209a$^+$ cDC2 in LP were confirmed as slightly reduced in *Xiap*$^{-/-}$ mice (1.3% vs 1.5% in Wt). Flow cytometry, supported by scRNAseq, further

confirms that TLR5^{+} CD209a^{+} cells were primarily CD11b^{+}, expressing CD26 and the cDC2 marker CD172a. TLR5^{+} CD209a^{+} cells were primarily featured in the LP. In contrast, TLR5^{-} CD209a^{+} DC populations were significantly elevated in the IE of *Xiap*$^{-/-}$ mice (1.6% vs 0.9% in Wt), and notably negative for both CD11b and CD172a supporting the hypothesis that IE DC display a more immature phenotype.

In summary, while overall myeloid population changes were fairly modest and statistically not significant comparing *Xiap*$^{-/-}$ mice and Wt mice, flow cytometry confirms a predominant localisation of TLR5^{+} DC in LP in both genotypes. CD209a marks specialised and potentially plastic DC subsets in both IE and LP, with TLR5^{+} CD209a^{+} LP DC tendentially reduced and TLR5^{-} CD209a^{+} IE DC significantly increased in *Xiap*$^{-/-}$ mice. These results somewhat strengthen the hypothesis that the absence of XIAP may affect upstream DC subsets in IE, potentially impacting downstream TLR5^{+} LP DC functionality.

IE DC populations with a suspected pDC-like, pre-DC2 phenotype have gained attention, showing plasticity in marker expression across different DC populations.[56] Previous beliefs in the field of DC ontogeny considered the transcription factor IRF8 as merely indicative of a cDC1 fate. Recent findings established a more broad use of IRF8 indicative of early pre-DC priming.[51,55] Thus, the following flow cytometric strategy included IRF8, providing a broader assessment of IE DC heterogeneity using IRF8-Venus reporter mice. It was hypothesised that CD209^{+} IE cells, low in typical DC markers, express CX3CR1 and BST2, a marker associated with pDC, and may represent pre-DC2 that develop fully only upon antigen encounter.

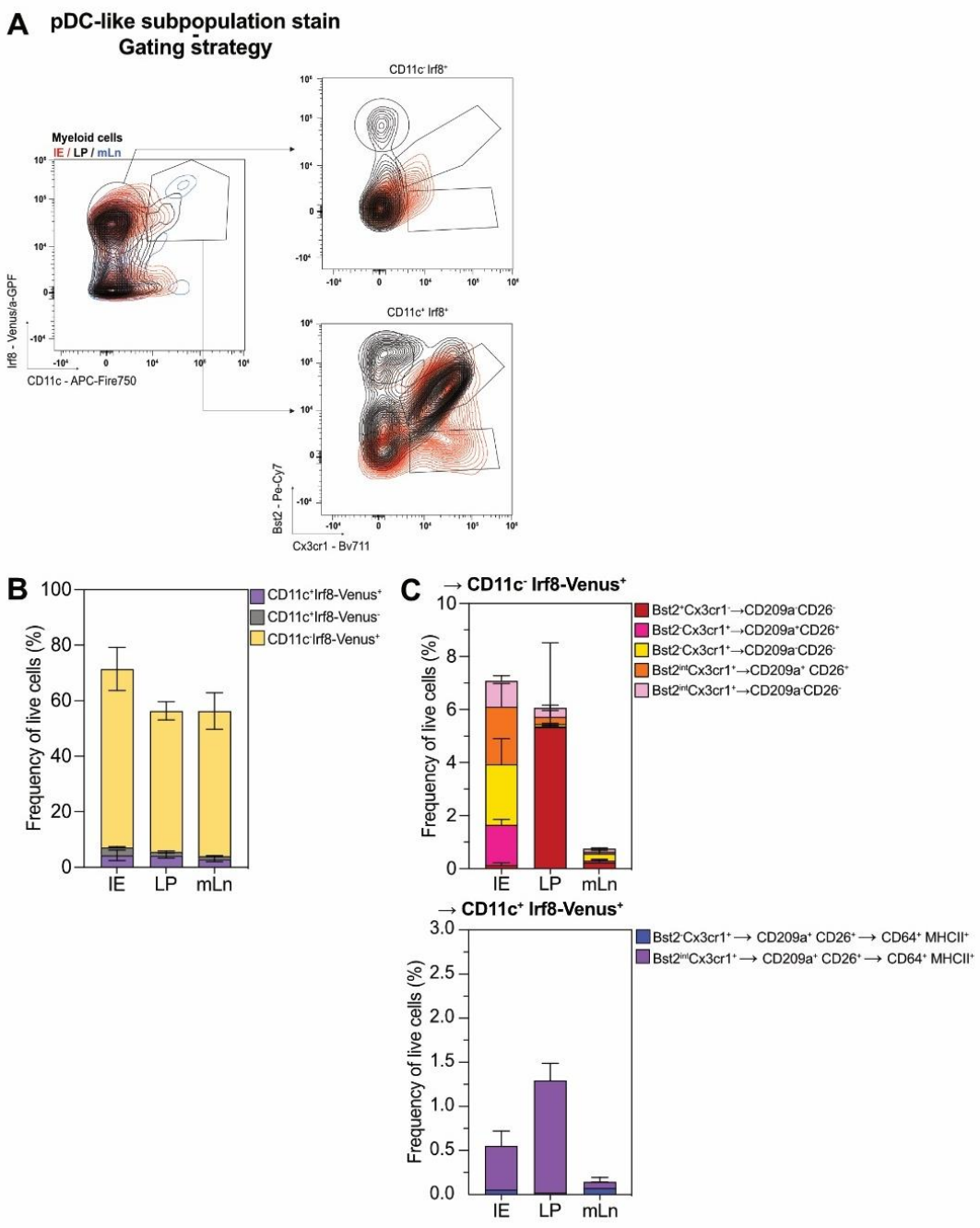

Figure 14. Some IRF8$^+$ CD209a$^+$ IE DC express markers indicative of a pDC-like pre-cDC2 phenotype. Flow cytometric analysis of isolated immune cells from IE (red), Lamina propria (LP) (black) and mesenteric lymph nodes (mLn,) (blue). (A) Gating strategy for analysis and (B and C) quantification of IRF8-expressing DC subpopulations in adult IRF8-Venus reporter mice from SPF housing, n = 3. Cells are quantified as percentage of live cells, determined by live/dead stain, a total 1.5*10^5 events recorded for IE/LP samples, and 1*10^6 events recorded for mLn samples.

Figure 14A and B indicate that all three populations, IRF8$^+$ CD11c$^-$, IRF8$^+$ CD11c$^+$ and IRF8$^-$ CD11c$^+$ cells were present in IE and LP. Informed by previously depicted results, which showed elevated frequencies of TLR5$^-$ CD209a$^+$ in

the IE of *Xiap*$^{-/-}$ mice that were also characterised by CD11c expression (**Figure 13**C), a particular interest lay in the characterisation of the IRF8^{+} CD11c^{+} population.

Within both the IE and LP, the largest frequency of CD11c^{+} IRF8^{+} cells (0.4% and 1.3%, respectively) were found to express both CX3CR1 and BST2 (albeit at intermediate levels), alongside CD209a and CD26. The additional expression of activation marker MHCII, and CD64, is somewhat supportive of the proposed hypothesis of a plastic population of pDC-like pre-DC2 that mature upon antigen encounter in the IE. Briefly, CD11c^{-} IRF8^{+} DC populations in the IE were predominantly CX3CR1^{+}. However, most of these cells did not express both BST2 and CD209a, hence, deciphering their specific function lies outside of the goal of above-proposed hypothesis. The largest CD11c^{-} IRF8^{+} LP population (5.3%) was found to express BST2. It was hypothesised that this population may represent a locally resident LP population that replenished DC pools in LP.

In summary, flow cytometric analysis, informed by previous scRNAseq results, substantiates the presence of distinct CD209a^{+} DC subsets in the intestinal IE and LP layer, suggesting that IE DC populations, particularly the IRF8^{+} subset, may represent a pDC-like, immature pre-cDC2 phenotype. Although no significant quantitative differences emerged between Wt mice and *Xiap*$^{-/-}$ mice with regard to the frequency of TLR5^{+} LP in this assay, the dysregulation in TLR5^{-} IE DC in the absence of XIAP could reflect an upstream stage in the functional development of TLR5^{+} LP DC, hence offer a mechanistic explanation for previous results regarding TLR5^{+} immune cells based on IHC. This observation aligns with emerging evidence that DC phenotypes in the intestinal environment are shaped by compartment-specific cues rather than rigid ontogeny[47], with these cells displaying an antigen-driven plasticity that likely supports stage-specific roles across tissue layers. Currently, ongoing functional and scRNAseq studies, including experiments in gf*Xiap*$^{-/-}$ mice outlined in the following chapters, aim to clarify these complex maturation and activation dynamics, hypothesised as the underlying mechanisms by which rare DC populations contribute to intestinal inflammation in the absence of XIAP.

Microbiome-dependent TLR5 deregulation correlates with early tissue inflammation in XIAP deficiency

To clarify the temporal relationship between microbiota introduction, TLR5-expressing immune cell emergence and tissue inflammation, an additional colonisation experiment was conducted. Non-inflamed germfree Wt and *Xiap*$^{-/-}$ mice were passively exposed to a conventional microbiome, allowing for the observation of histological changes in ileal tissue over time. This approach was employed to lead to a more precise understanding of the sequential events occurring in the absence of XIAP, compared to endpoint measurements from FMT (**Figure 9**) or mice raised in conventional housing from birth[170].

Young, 3- to 4-week-old, sex-matched gfWt and gf*Xiap*$^{-/-}$ mice were transferred into a conventional housing facility, where they rested for one day before baseline samples were collected. Passive colonisation was initiated by introducing dirty litter from adult Wt and *Xiap*$^{-/-}$ mice housed in the conventional facility. Mice were sacrificed at days 5, 8, and 15 post colonisation onset. Macroscopically, stool consistency and colour changed from black and liquid to a firmer, light brown appearance, typical of conventionally housed mice of this genetic background. This observation suggested successful conventionalisation, even in the absence of direct FMT.

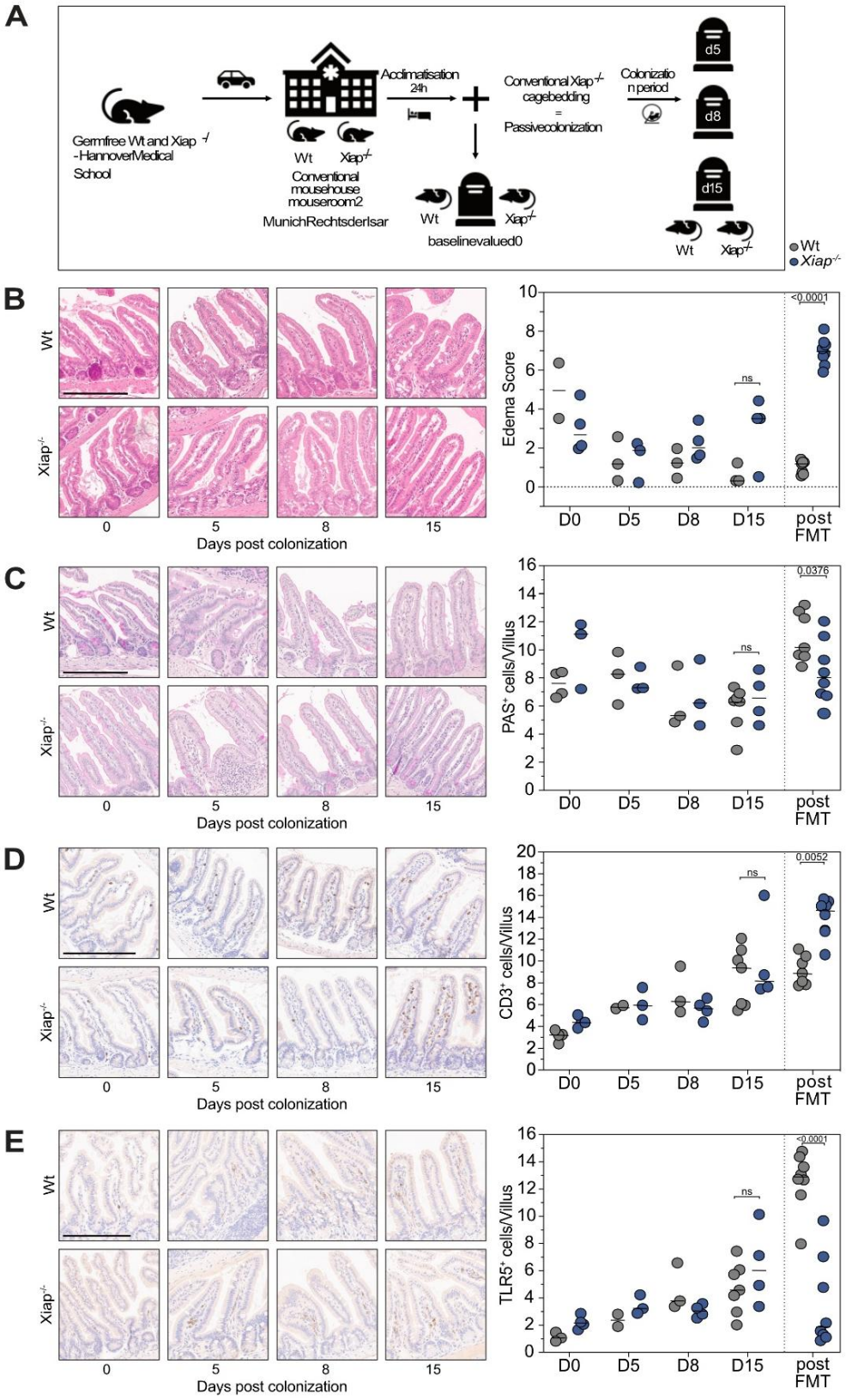

Figure 15. Passive conventionalisation of young germfree *Xiap*$^{-/-}$ mice induces first signs of intestinal epithelial barrier dysfunction within 15 days, but fails to emulate the phenotype of *Xiap*$^{-/-}$ mice 4 weeks post FMT. Graphical summary of experimental setup for passive conventionalisation experiment (A) and representative IHC stains of paraffin-embedded ileal tissue and

evaluation of time kinetics (D0 until D15, and post FMT) of depicted features of tissue inflammation i.e. (B) H&E / (C) PAS Stain / (D) CD3 Stain / (E) TLR5 in gfWt (grey) and gf*Xiap*$^{-/-}$ mice (blue) and post passive colonisation. P values depicted in graph were analysed via one way ANOVA including *post hoc* analysis with Holm-Šidák's correction, ns indicates a p value exceeding >0.9999. Scale bars depict 180-200 µm. Each dot represents one mouse, n = 2 – 8.

As shown in **Figure 15**B, young germfree mice exhibited a more loose epithelial tissue structure at D0, regardless of genotype. This observation is likely attributable to increased intestinal permeability in infant mice at around two weeks of age, compared to adults at twelve weeks.[175] Over time, transcription of barrier-forming tight junction markers such as Claudin 3, Occludin, and Zonula occludens-1 increases, while pore-forming markers like Claudin 2 and 5 decrease. The influence of dietary and bacterial components on tight junction expression has also been documented.[176] Therefore, it can be assumed that the oedema-like appearance observed in H&E stains of germfree mice likely reflects a desired barrier permeability rather than active inflammation. Following colonisation, the oedema score in Wt mice steadily decreased from D5 to D15. However, in *Xiap*$^{-/-}$ mice, the oedema score initially decreased similarly but began to rise by D8, surpassing that of Wt mice. By D15, *Xiap*$^{-/-}$ mice exhibited a tendentially higher oedema score than their conventionalised Wt counterparts and exceeded baseline levels observed at D0. Nevertheless, this score remained lower than that of mice colonised via a single oral FMT followed by a four-week resting period (**Figure 15**B).

The presence of mucus-producing Goblet cells, assessed using PAS staining (**Figure 15**C), revealed a tendency for higher Goblet cell numbers in gf*Xiap*$^{-/-}$ mice mice compared to Wt at D0. Over 15 days, only marginal differences in Goblet cell numbers were observed between *Xiap*$^{-/-}$ mice and Wt mice at each time point. Consistent with the oedema observations, higher PAS^{+} cell numbers were recorded in adult mice of both genotypes post FMT (see also **Figure 9**), suggesting that Goblet cell dynamics are not fully captured within 15 days. Regarding immune cell recruitment in the ileal tissue, indicated by CD3^{+} T cell counts per villus, germfree mice showed markedly low immune cell numbers in villi. Colonisation led to an overall increase in immune cell numbers in both Wt and *Xiap*$^{-/-}$ mice (**Figure 15**D), which was also corroborated by confocal analysis of myeloid populations (data not shown). No differences in recruited T cell numbers were noted between Wt and *Xiap*$^{-/-}$ mice within the 15 day period. In contrast, *Xiap*$^{-/-}$ mice post FMT did exhibit higher CD3^{+} T cell counts per villus.

Lastly, a particular interest lay in the temporal relationship between alterations in TLR5 expression in myeloid cell populations correlating with histological signs of tissue inflammation. The dynamics of TLR5-expressing LP immune cells following microbiota introduction into young gfWt and gf*Xiap*$^{-/-}$ mice were assessed (**Figure 15**E). At D0, both genotypes exhibited low numbers of TLR5^{+} cells within intestinal villi. Over the 15 days of passive colonisation, TLR5^{+} cell numbers increased in both Wt and *Xiap*$^{-/-}$ mice, with *Xiap*$^{-/-}$ mice unexpectedly showing a higher number of TLR5+ cells by D15. Even at D15, TLR5^{+} cell numbers in both genotypes remained lower than those observed in Wt and *Xiap*$^{-/-}$ mice post FMT. These findings suggest that TLR5^{+} cells infiltrate or mature more rapidly in the villi of *Xiap*$^{-/-}$ mice compared to Wt mice upon microbiome exposure.

Crucially, the absence of TLR5-expressing cells did not correspond to histological inflammation in germfree *Xiap*$^{-/-}$ mice, indicating that TLR5 deficiency alone is not sufficient to drive inflammation. Instead, the inflammatory phenotype in *Xiap*$^{-/-}$ mice is strictly dependent on the presence of a microbiome. Previous research by Chassaing et al. demonstrated that *Tlr5*$^{-/-}$ mice developed metabolic syndrome and CD-like inflammation in the large intestine, and exhibited altered microbial composition. In contrast, TLR5$^{\Delta DC}$ mice, with TLR5 ablation specifically under the CD11c promoter, did not develop intestinal inflammation or dysbiosis, suggesting that absence of TLR5 expression in CD11c^{+} myeloid cells alone does not precipitate inflammation. Consistently, as shown in **Figure 9**, neither gfWt nor gf*Xiap*$^{-/-}$ mice displayed ileal inflammation before FMT colonisation, despite low initial TLR5^{+} cell numbers. A significant increase in TLR5^{+} cells was observed in Wt mice post FMT, however absence of TLR5^{+} cells alone does not explain the heightened inflammation risk in absence of XIAP.

Speculatively, these observations suggest that in genetically pre-disposed mice, loss of epithelial integrity leads to excessive interaction between IE DC and the intestinal microbiome, leading to TLR5^{+} DC emergence and subsequent loss in the LP, potentially through inflammation-driven cell death in absence of XIAP. However, the 15 day passive conventionalisation period was insufficient to replicate the full extent of the inflammatory progression observed in *Xiap*$^{-/-}$ mice four weeks post FMT. This underscores the need to extend observation time points in future experiments to fully capture the dynamics of microbiome-dependent inflammation development in a genetically predisposed environment.

Passive conventionalisation alters CD209a$^+$ intraepithelial and TLR5$^+$ lamina propria DC frequencies

scRNAseq of Wt intestinal immune cells, complemented by flow cytometric analysis of intestinal myeloid populations from adult Wt and *Xiap*$^{-/-}$ mice, identified CD209a as a potential marker distinguishing unique DC subtypes. These findings were suggestive of a functional separation: DC located in the intestinal epithelium express CD209a but lack TLR5, whereas those in the LP express both markers. This proposed compartmentalisation indicated that epithelial CD209a$^+$ DCs, hypothesised to be immature plasmacytoid-like pre-cDC2 (**Figure 14**), might be maintained in a hyporesponsive state by the epithelial cytokine milieu, a mechanism supported by Rivera *et al*.[53] Their maturation and subsequent migration into the LP would only be induced upon microbial interaction, where they gain TLR5 expression and potentially adopt roles in immune regulation. Furthermore, it should be noted that experimentally, scRNAseq and flow cytometry suffer from clear limitations, as they require cell isolation, which can influence cell viability and the expression of surface markers. A shortcoming of particular importance in *Xiap*$^{-/-}$ mice, in which a central mediator of cell death has been ablated.

Therefore, to investigate the proposed effects of the interaction between an emerging microbiome on specialised compartmentalised DC populations *in situ*, a staining protocol using CD209a and TLR5 markers was developed. Immunofluorescently labelled ileal cryosections were imaged using confocal microscopy comparing gfWt and gf*Xiap*$^{-/-}$ mice at D0, and at D15 post conventionalisation. Pre-conjugated anti-CD209a and primary-secondary antibody staining for TLR5 were applied. Imaris software was used to create 3D-rendered surfaces of CD209a$^+$ cells, and co-expression with TLR5 was evaluated. Potential artefacts were excluded based on sphericity and size to ensure individual cell analysis.

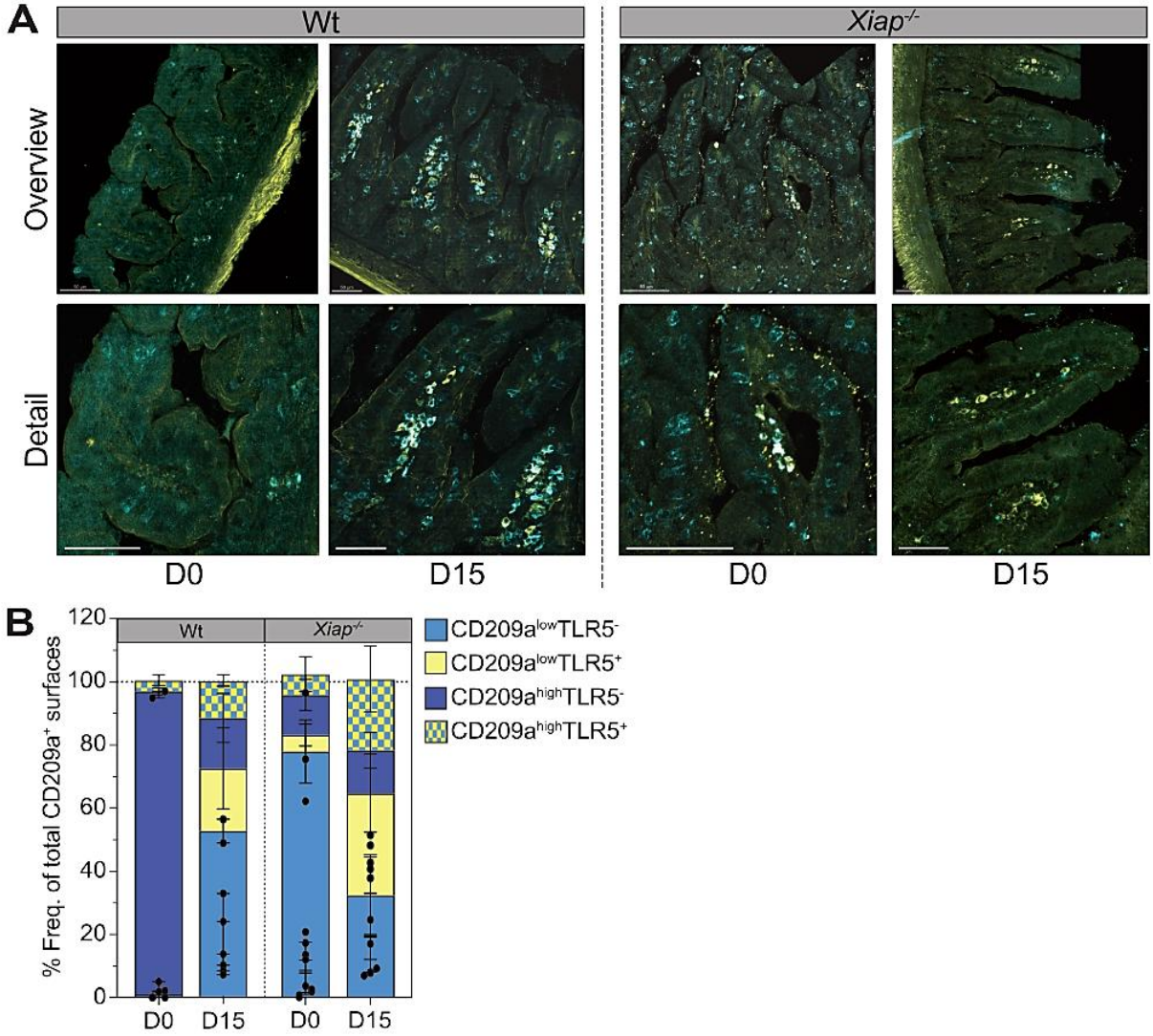

Figure 16. Passive conventionalisation of gf*Xiap*$^{-/-}$ mice correlates with a tendential reduction of intraepithelial (IE) CD209a$^+$ DC and a simultaneous increase in numbers of CD209a$^+$TLR5$^+$ DC in the LP. (A) Representative pictures (overview and detail) of *in situ* confocal analysis of immunofluorescently labelled ileal cryosections stained with pre-conjugated anti-CD209a antibody (signal in cyan) and anti-TLR5 antibody (signal in yellow) of gfWt and gf*Xiap*$^{-/-}$ mice at D0 and at D15 post conventionalisation. (B) Frequency analysis of computer-assisted surface rendering of ileal immune cells based on expression of CD209a (low expression depicted in light blue, high expression dark blue) and co-expression of TLR5 (depicted in yellow, double positive cells depicted as pattern). Depicted is SEM of frequencies of n = 2-3 mice per time point and genotype, adjusted p value determined using Kruskal-Wallis ANOVA not significant. Surfaces were rendered using Imaris software package.

At D0, the abundance of IE-localised CD209a$^+$ cells (in cyan) was high in both gfWt and gf*Xiap*$^{-/-}$ mice, while TLR5 expression was nearly absent (**Figure 16**A). This finding was in accordance with low numbers of TLR5$^+$ cells in germfree mice as found in IHC stains depicted above (**Figure 15**). Quantitative analysis (**Figure 16**B) showed that in gfWt mice, 96.0% of CD209a$^+$ surfaces were TLR5$^-$, with only a small fraction

(3.4%) co-expressing TLR5. In contrast, gf*Xiap*$^{-/-}$ mice had a lower percentage (78.1%) of CD209a^{+} cells, generally expressing lower CD209a levels. Additionally, 12.8% of CD209a^{+} surfaces were found in the LP, with minimal co-expression of TLR5.

Upon microbial colonisation, both Wt and *Xiap*$^{-/-}$ mice exhibited a marked increase in total numbers of LP immune cells (data not depicted). In Wt mice, 52.5% of surfaces were CD209a^{low}TLR5^{-} (suggestive of immature DCs in the IE), while 16.0% were CD209a^{high}TLR5^{-} in the LP. In *Xiap*$^{-/-}$ mice, a higher frequency (22.6%) of CD209a^{high}TLR5^{+} cells was observed in the LP, compared to 11.8% in Wt mice. Notably, very few CD209a+ cells remained in the IE of *Xiap*$^{-/-}$ mice at D15. Cells expressing TLR5 but low in CD209a were prevalent in the LP (19.9% in Wt versus 32.4% in *Xiap*$^{-/-}$ mice).

These results support the proposed existence of compartmentalised CD209a^{+} DC populations, in confirmation of the hypothesis that CD209a^{+} TLR5^{-} DCs are maintained in an immature state within the IE and mature upon migration to the LP. This aligns with prior scRNAseq and flow cytometry data, establishing CD209a as a marker of distinct DC subtypes with potential roles in immune tolerance and inflammation.

Furthermore, these findings indicate a more rapid recruitment of CD209a^{+} TLR5^{-} IE DC and maturation of CD209a^{+} TLR5^{+} LP DC in *Xiap*$^{-/-}$ mice upon microbiome exposure, compared to Wt mice. Speculatively, the hyperresponsiveness of these intestinal immune cells offers a potential explanation for the intestinal inflammatory phenotype in these mice. However, as previously discussed, differences established within only 15 days of conventionalisation remained below statistical significance.

Germfree *Xiap*$^{-/-}$ mice establish a dysbiotic microbiome upon passive conventionalisation

Significant signs of tissue inflammation were specific to *Xiap*$^{-/-}$ mice featuring a conventional microbiome, with neither SPF-housed nor germfree *Xiap*$^{-/-}$ mice exhibiting any inflammatory phenotype, as shown in **Figure 9**, and Wahida *et al.*[170]. Moreover, microbial exposure was found to be necessary to induce TLR5 expression in LP DC in both Wt and *Xiap*$^{-/-}$ mice (**Figure 15**), further emphasising a critical role for the microbiome in inflammation development in the absence of XIAP. The interaction between the microbiome and intraepithelial DC is noteworthy. IE DC are essential for scavenging antigens and shaping immune responses. This highlights that the inflammatory phenotype observed in *Xiap*$^{-/-}$ mice is highly dependent on the presence of a microbiome, and provides a mechanistic explanation of the proposed connection between specialised IE DC, TLR5^{+} LP DC and downstream inflammatory consequences.

Building on these observations, microbial changes during passive conventionalisation in young gfWt and gf*Xiap*$^{-/-}$ mice were investigated. It was hypothesised that a dysbiotic microbiome established in absence of XIAP would induce excessive immune responses in IE DC. Hence, the aim was to identify which bacteria initially colonised germfree mice in a conventional facility, how these communities evolved over time, and how their establishment diverged in comparison between Wt and *Xiap*$^{-/-}$ mice. Samples of ileal and caecal contents, as well as fresh faecal pellets from the distal colon, were collected at days 0, 5, 8, and 15. Absolute abundances were calculated based on sample spiking (for assay details, see “Methods”). Since the mice were delivered germfree, it was assumed that the proposed effects of the maternal microbiome were negligible[177]. Instead, the bacterial load and composition observed must have originated from exposure to cage bedding and faecal pellets of adult Wt and *Xiap*$^{-/-}$ mice from conventional housing, as well as from the air, water, food pellets, and cages provided. Macroscopic monitoring of passive conventionalisation in germfree mice was conducted, revealing a gradual reduction in abdominal swelling, a typical feature of germfree mice caused by caecal enlargement due to undigested fibre. Changes in faecal pellet appearance were also noted, indicating successful microbial colonisation within 15 days.

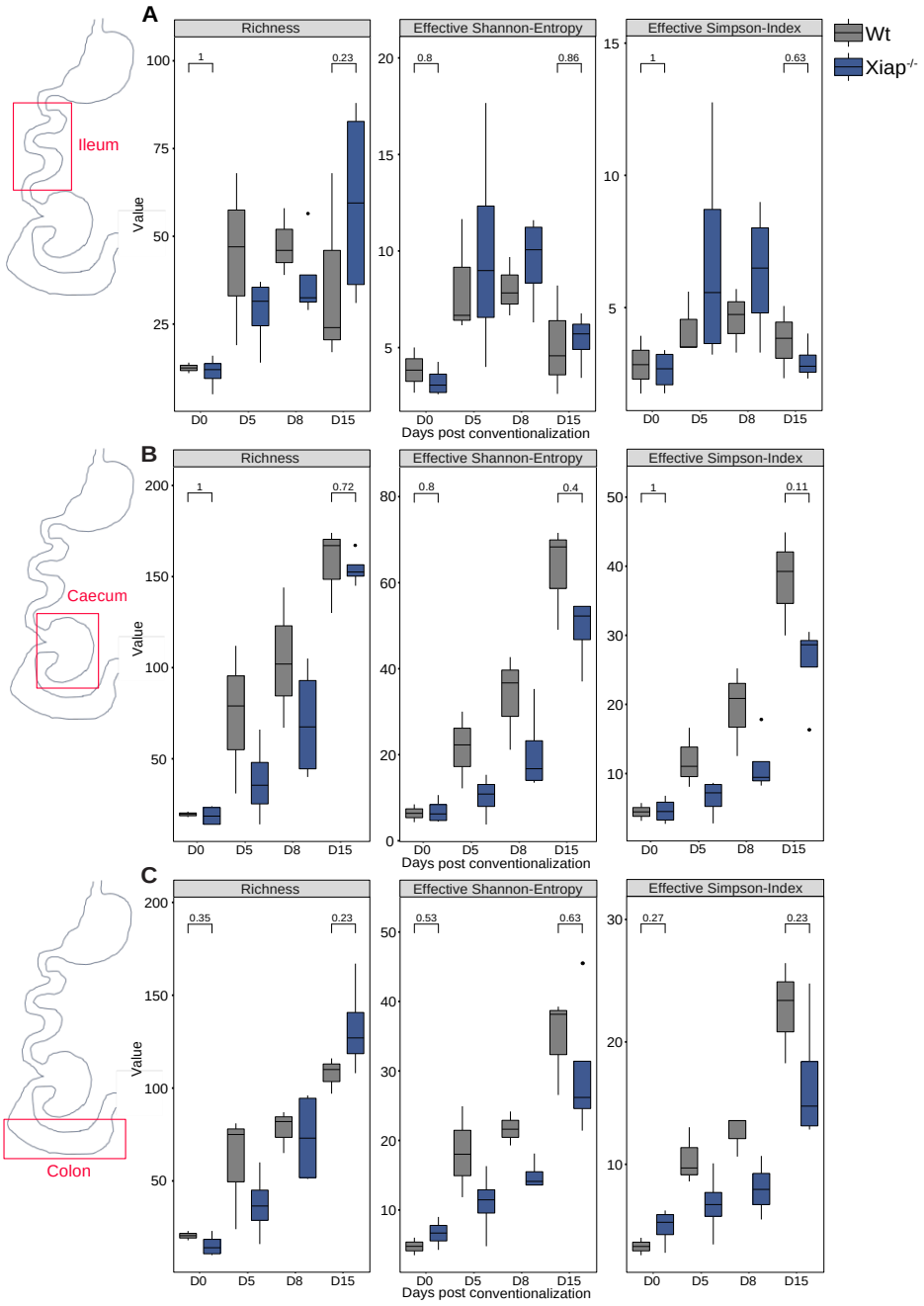

Figure 17. Passively conventionalised *Xiap*$^{-/-}$ mice show a tendential reduction in bacterial species diversity. Richness, Effective Shannon-Entropy (H) and Effective Simpson-Index (D) based on 16S rRNA sequencing analysis (A) ileal, (B) caecal and (C) colonic content of Wt (grey) versus *Xiap*$^{-/-}$ (blue) mice at baseline and throughout a 15 day period post colonisation (n = 2-4 per timepoint and genotype). Groups at depicted timepoints underwent pairwise comparison via Wilcoxon signed-rank test; individual p-values are depicted in respective graphs. Sampling sites are schematically indicated.

As illustrated in **Figure 17**, the maximum species richness for either Wt (grey) or *Xiap*$^{-/-}$ mice (dark blue) depended strongly on the sampling site; overall, however, *Xiap*$^{-/-}$ mice exhibited lower species richness compared to conventionally housed adult Wt mice, even at day 15 post-conventionalisation. Approximately 150 species

were identified in the caecal content of both Wt and *Xiap*$^{-/-}$ mice at day 15, while ileal content richness peaked at fewer than 60 species in *Xiap*$^{-/-}$ mice and below 50 species for Wt mice at day 8. The colon contained about 107 species for Wt and a mean of 132 for *Xiap*$^{-/-}$ mice. In contrast, 16S rRNA sequencing of the caecal content of adult *Xiap*$^{-/-}$ mice from conventional housing revealed over 150 species, with Wt mice showing significantly higher diversity, exceeding 300 species. However, this study did not systematically analyse ileal content and colonic faeces.[170]

Several explanations could account for the reduced species diversity found in this study, including the limited observational timeframe of 15 days. The rate and extent of colonisation solely through exposure to non-sterile housing conditions and the litter of adult inflamed *Xiap*$^{-/-}$ mice, without oral FMT application, warrant further investigation.

To assess species evenness and dominant species representation, Effective Shannon-Entropy (H) and Effective Simpson-Index (D) were calculated (**Figure 17**). Effective indices were selected as they consider both species richness and individual species representation; traditional diversity indices often assume even distribution among species. Briefly, Effective Shannon-Entropy measures randomness in a system, where higher values indicate greater diversity. The Effective Simpson-Index reflects the likelihood that two randomly selected individuals belong to the same species, thus negating the influence of infrequent species; a lower Effective Simpson-Index indicates higher diversity and reduced dominance by individual species. Differences in diversity indices were marginal between Wt and *Xiap*$^{-/-}$ mice, particularly in the ileum. In the caecum, Effective Shannon-Entropy was higher in Wt mice (H = 62.98) compared to *Xiap*$^{-/-}$ mice (H = 49.01) at day 15, while the Effective Simpson-Index was lower in *Xiap*$^{-/-}$ mice (D = 26.02) than in Wt mice (D = 38.04). A similar trend was observed in colonic samples (Wt H = 34.66 vs *Xiap*$^{-/-}$ H = 29.81; *Xiap*$^{-/-}$ D = 16.77 vs Wt D = 22.67). Consequently, at day 15 of conventionalisation, diversity was slightly but not significantly different between genotypes, contrasting findings reported for adult inflamed *Xiap*$^{-/-}$ mice maintained in conventional housing.[170]

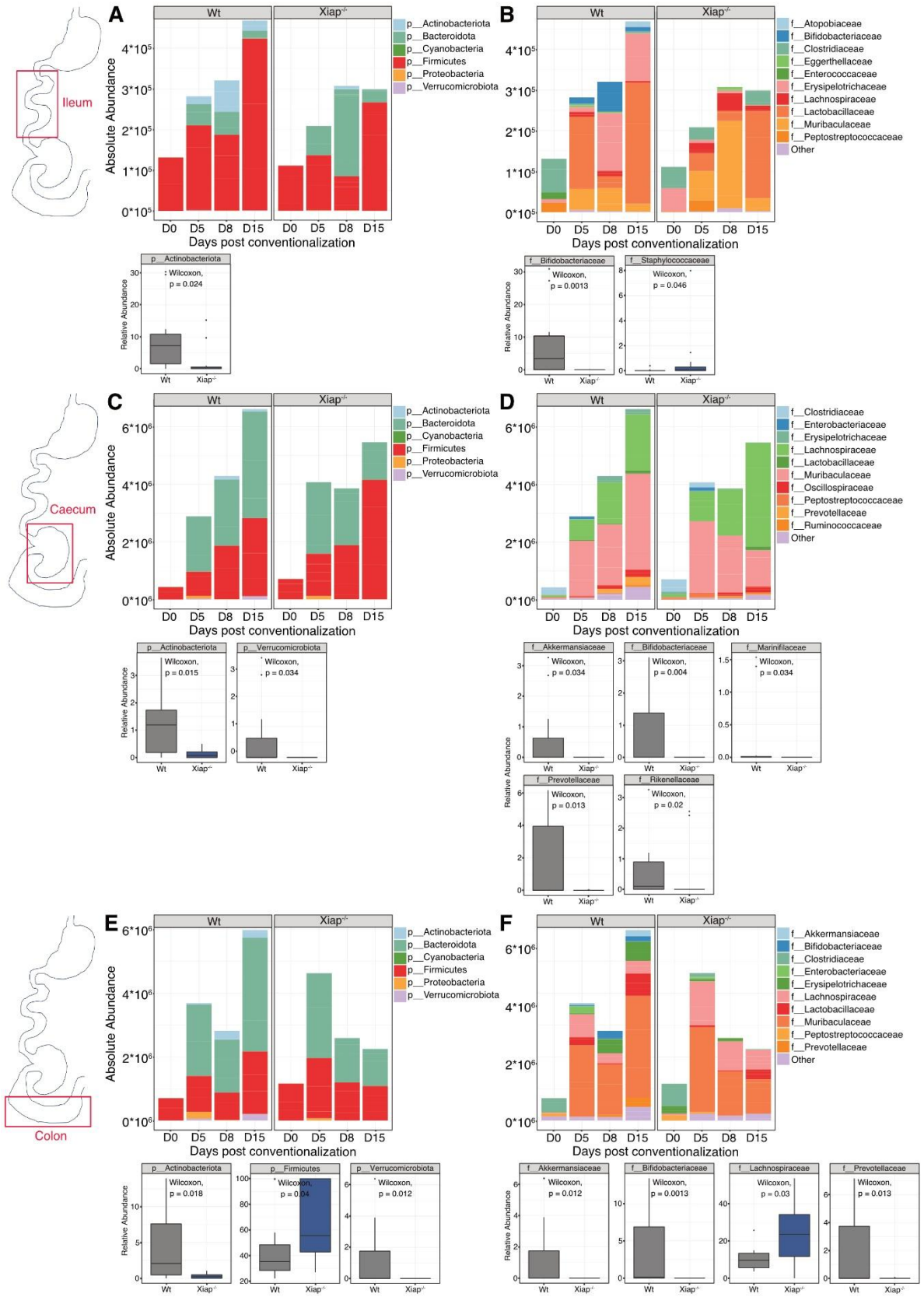

Figure 18. Passively conventionalised *Xiap*$^{-/-}$ mice show reduced absolute bacterial load, and loss of distinct species abundance within 15 days of conventionalisation onset throughout the

intestine. Taxonomic binning of relative abundances of bacterial phyla (A, C, E) and families (B, D, F), and statistically different relative abundances of phyla (A, C, E) and families (B, D, F) discovered via 16S rRNA sequencing analysis in (A and B) ileal content, in (C and D) caecal content, in (E and F) colonic content of Wt versus *Xiap*$^{-/-}$ mice at baseline and throughout a 15 day period post colonisation (n = 2-4 per timepoint and genotype). Significantly different species were determined via Wilcoxon signed-rank test; individual p values are depicted in respective graphs. Sampling sites are schematically indicated.

Interestingly, as depicted in **Figure 18**, bacterial load in the ileum at day 0 ($13x10^4$ for Wt and $10.9x10^4$ for *Xiap*$^{-/-}$ mice) was notably lower than in caecal ($4.2x10^5$ for Wt and $6.8x10^5$ for *Xiap*$^{-/-}$ mice) and colonic content ($6.9x10^5$ for Wt and $9.6x10^5$ for *Xiap*$^{-/-}$ mice). Even at day 15, ileal bacterial load ($4.6x10^5$ for Wt versus $2.9x10^5$ for *Xiap*$^{-/-}$ mice) remained comparable to or below initial levels seen in caecal and colonic samples, independent of genotype. Throughout the sampling period, *Xiap*$^{-/-}$ mice consistently exhibited lower bacterial loads than Wt mice at almost all time points. At day 15, *Xiap*$^{-/-}$ mice featured a distinctly lower bacterial mass in ileal ($4.6x10^5$ for Wt versus $2.9x10^5$ for *Xiap*$^{-/-}$ mice), caecal ($6.6x10^6$ for Wt versus $5.5x10^6$ for *Xiap*$^{-/-}$ mice), and colonic content ($5.9x10^6$ for Wt versus $2.3x10^6$ for *Xiap*$^{-/-}$ mice). This reduced diversity and bacterial load may make the ileal microbiome more susceptible to disturbances, potentially explaining the specific localisation of inflammation development in the ileum of *Xiap*$^{-/-}$ mice.

At the phylum level, both Wt and *Xiap*$^{-/-}$ mice presented six main phyla during the 15-day conventionalisation period: Firmicutes (red in **Figure 18** A, C, and E), Bacteroidota (light green), Actinobacteriota (light blue), Proteobacteria (yellow), Cyanobacteria (bright green), and Verrucomicrobiota (violet). At day 0, ileal, caecal, and colonic samples of both genotypes did not differ significantly in microbiota composition, with Firmicutes being the dominant phylum. As colonisation progressed, *Xiap*$^{-/-}$ mice exhibited a significantly reduced relative abundance of Actinobacteriota across all sampling sites, with Verrucomicrobiota also diminished in caecal and colonic samples.

Firmicutes remained dominant throughout the conventionalisation period, regardless of sampling site. This phylum was of particular interest specifically because of the marked loss of *Clostridium*, a genus within Firmicutes, previously observed in conventionally housed adult Wt and *Xiap*$^{-/-}$ mice. Interestingly, the relative abundance of Firmicutes appeared increased in *Xiap*$^{-/-}$ mice during this passive conventionalisation experiment, which contrasts findings reported by Wahida *et al.*[170]. However, as demonstrated in **Figure 18**E, the absolute abundance of Firmicutes

exceeded Wt levels only at day 5 post conventionalisation, with overall levels not consistently surpassing those of Wt. Furthermore, neither Actinobacteriota nor Verrucomicrobiota were established in caecal content of *Xiap*$^{-/-}$ mice and the Proteobacteria phylum remained below Wt levels, resulting in an overrepresentation in relative proportions of Firmicutes in *Xiap*$^{-/-}$ mice.

To gain further insight into compositional changes among the ileal, caecal, and colonic microbiomes of Wt and *Xiap*$^{-/-}$ mice, the overall 709 discovered OTUs at the family level were compared. Notably, *Xiap*$^{-/-}$ mice exhibited significantly reduced relative abundance of Bifidobacteriaceae (Actinobacteria) in all investigated intestinal compartments. Additionally, consistent with previous findings[170], *Xiap*$^{-/-}$ mice displayed a marked loss of *Akkermansia*, a family within Verrucomicrobiota. Both Prevotellaceae (reduced in caecum and colon of *Xiap*$^{-/-}$ mice, see **Figure 18**D and F) and Rikenellaceae (reduced in caecum of *Xiap*$^{-/-}$ mice, see **Figure 18**D) are common members of the intestinal microbiome and are known to produce acetic acid, propionic acid, and succinic acid for the host. Rikenellaceae has been associated with obesity-related white adipose tissue inflammation and linked to lower butyrate levels[178].

While overall bacterial load was clearly reduced in *Xiap*$^{-/-}$ mice, the impact on the intraepithelial DC that scavenge antigens and the subsequent immune response warrants further exploration. This indicates that the observed phenotypic consequences in *Xiap*$^{-/-}$ mice are intricately tied to the dynamics of the microbiome, which significantly influences the functionality of DC in the gut.

Microbial dysbiosis in *Xiap*$^{-/-}$ mice affects caecal metabolome composition

Spiked 16S rRNAseq analysis of species abundances in the intestinal content *Xiap*$^{-/-}$ mice (**Figure 18**) confirmed features of microbial dysbiosis upon exposure to a conventional microbiome, corroborating previous findings from adult inflamed *Xiap*$^{-/-}$ mice.[170] Compositional changes within the microbiome are particularly relevant for IE DC as key players in luminal antigen scavenging. These alterations furthermore disrupt the intricate balance within the local ecological niche, wherein distinct species symbiotically exchange metabolic compounds, thereby supporting the survival of others during ecological succession. Moreover, the intestinal microbiome produces vital metabolites that play essential roles in intestinal homeostasis and can influence immune responses by modulating immune cell differentiation. It was therefore hypothesised that a skewed metabolome composition downstream of microbial dysbiosis could exacerbate a dysfunctional phenotype in IE DC, additionally contributing to Paneth cell dysfunction as proposed in Wahida *et al*.[170]

16S rRNA analysis has clear limitations in elucidating the functional consequences of dysbiosis with regard to metabolome composition. To further explore the functional implications of the above-observed compositional changes, caecal content from conventionalised *Xiap*$^{-/-}$ mice was analysed via mass spectrometry, given that Metabolic features were compared using the xcms viewer tool. In MS analysis, polar organic metabolites are eluted in both positive and negative HILIC; positive HILIC typically yields amino acids, while fatty acids are predominantly found in negative HILIC (**Figure 19**). Additionally, a separate analysis focused on measuring short-chain fatty acids (SCFA) (**Figure 20**).

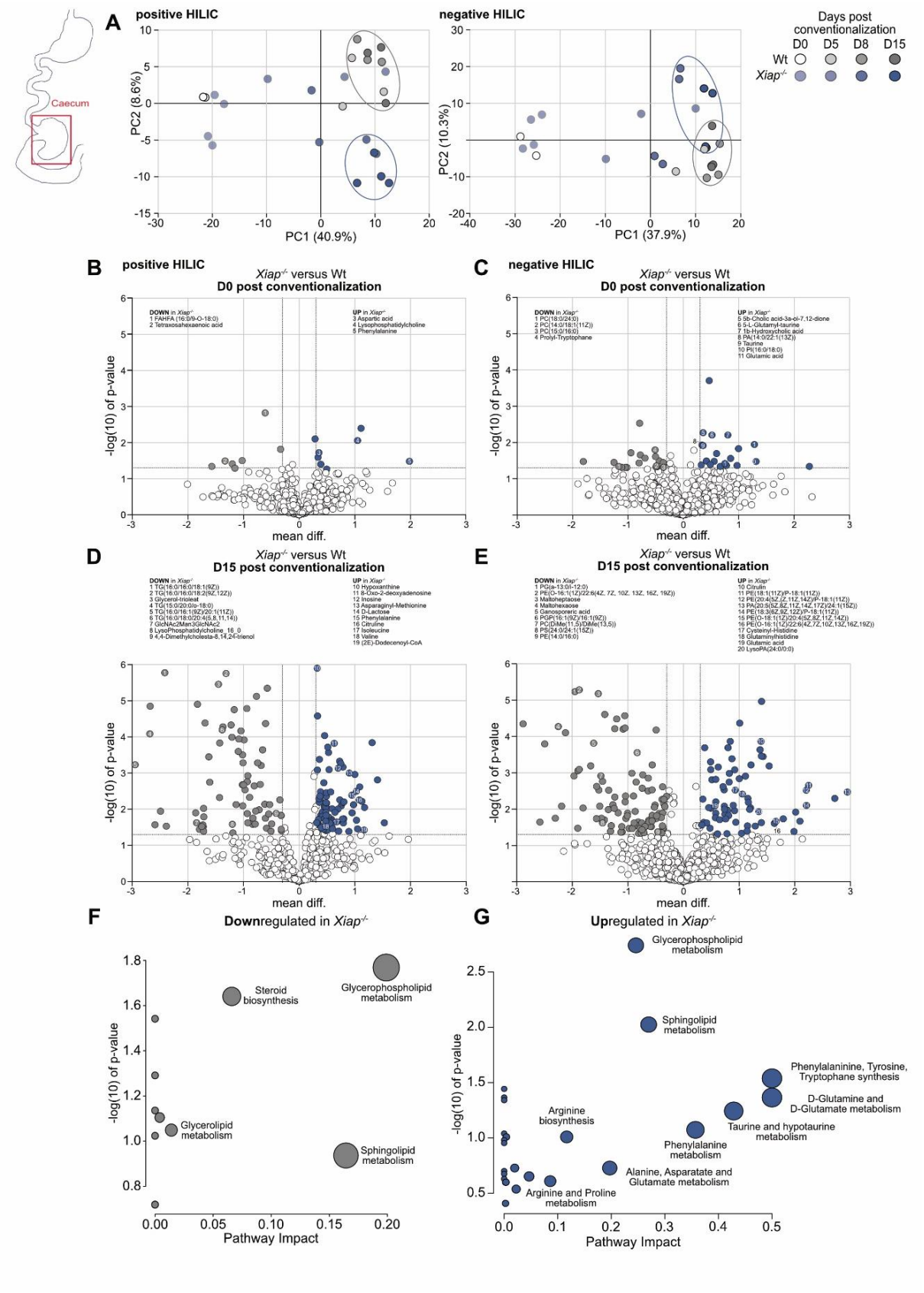

Figure 19. Passive conventionalisation of *Xiap*$^{-/-}$ mice correlates with downregulation of cell membrane components and increased amino acid levels in the caecal metabolome. (A) PCA of timekinetics of metabolites resulting from positive HILIC and negative HILIC of caecal luminal content of passively colonised Wt and *Xiap*$^{-/-}$ mice, and (B-D) volcano plot of significantly differentially

expressed metabolic features (x-cut = $log_{10}(2)$, y-cut = $-log_{10}(0.05)$ from positive and negative HILIC of caecal luminal content of (B and C) gfWt and gf*Xiap*$^{-/-}$ mice, and (D and E) Wt and *Xiap*$^{-/-}$ mice after 14 days of colonisation (n = 2-4 per timepoint and genotype). (F and G) KEGG Pathway comparison using MetaboAnalyst depicting downregulated (F) and upregulated (G) metabolic pathways in caecal content of Wt versus *Xiap*$^{-/-}$ mice after 14 days of colonisation. Data shows n = 2 – 4 mice pooled per genotype and timepoint.

As shown in **Figure 19**A, Principal Component Analysis (PCA) indicated no significant differences in caecal metabolome signature between Wt (in grey) and *Xiap*$^{-/-}$ mice (in blue) mice at D0 through D5. Distinct metabolic features were observed on D5 compared to D0, but Wt and *Xiap*$^{-/-}$ mice did not exhibit clear separation. By D8 and D15, however, the metabolic composition in *Xiap*$^{-/-}$ mice changed significantly compared to Wt mice, as indicated by the separation of samples in PCA (encircled in light blue for *Xiap*$^{-/-}$ mice and light grey for Wt). This suggests that while mice begin establishing their microbiome and intestinal metabolome within 5 days of conventionalisation onset, the dynamic changes in the microbiome of *Xiap*$^{-/-}$ mice may lead to a distinct metabolomic signature compared to Wt mice. This supports the notion that microbial species composition is not the only concern; rather, it is the expressed metabolites that may support the host or act as antigens detectable by immune cells such as DC, mediating the immunological response and ultimately leading to the onset of intestinal inflammation.

The analysis aimed to elucidate specific metabolites responsible for the observed differences. A total of 534 metabolic features were discovered in positive HILIC, while negative HILIC yielded 883 features; however, due to technical limitations of MS analysis and compound libraries, not all of them were accurately annotated. In conjunction with histological findings and 16S rRNAseq results (**Figure 18**), the metabolic data illustrates the successful conventionalisation of young germfree mice using cage bedding and ambient microbiota. At D0 (**Figure 19**B and C), only a few metabolites were significantly different between genotypes before conventionalisation (19 metabolites in positive HILIC, 39 metabolites in negative HILIC). However, after conventionalisation, vastly different metabolic profiles emerged between Wt and *Xiap*$^{-/-}$ mice (**Figure 19** D and E, 169 metabolites in positive HILIC, 174 in negative HILIC). Hence, while some underlying differences due to the genetic ablation of XIAP were found at D0, the vast majority of differences may be attributed to the metabolic activity of the microbiota after conventionalisation.

First, to explore genotype-dependent differences in host metabolome independent of microbiota presence, differences in caecal metabolites at D0 were analysed. Notably, gf*Xiap*$^{-/-}$ mice displayed upregulated levels of amino acids (blue circles in B and C) such as aspartic acid and glutamic acid, while showing lower levels of various lipid-related metabolites (grey circles in **Figure 19**B and C), including (fatty acid esters of hydroxy fatty acids) FAHFA and different phosphatidylcholines (PC). An increased baseline level of lysophosphatidylcholine (LPC) was observed, a biomarker for ongoing cell stress.[179]

At D15 post conventionalisation, amino acids remained upregulated in *Xiap*$^{-/-}$ mice, with additional amino acids and derivatives detected. These findings reflect those of Bjerrum *et al.*, who associated increased amino acids in IBD patients with malabsorption and microbial dysbiosis.[180] Compounds involved in nucleotide synthesis, such as hypoxanthine and inosine, were also elevated, suggesting barrier leakiness that may hinder adequate absorption of amino acids into the host's bloodstream.[181] Interestingly, in contrast to D0, various phospholipid membrane compounds, specifically phosphatidylethanolamines (PE), were increased in *Xiap*$^{-/-}$ mice at D15, accompanied by a downregulation of triglycerides (TG) and related compounds.

Using the MetaboAnalyst Pathway Analysis webtool, potential KEGG pathways affected by the metabolites were assessed (see **Figure 19**E and F). *Xiap*$^{-/-}$ mice demonstrated a potentially defective metabolism of cell membrane components, including glycerophospholipids and sphingolipids. Pathways leading to the synthesis and metabolism of various amino acids were clearly upregulated in conventionalised *Xiap*$^{-/-}$ mice.

Given the distinct loss of butyrate-producing species and consequential lower levels of butyrate in caecal content reported in adult *Xiap*$^{-/-}$ mice from conventional housing[170], differences in caecal luminal SCFA levels between passively conventionalised Wt and *Xiap*$^{-/-}$ mice were evaluated in a targeted MS analysis.

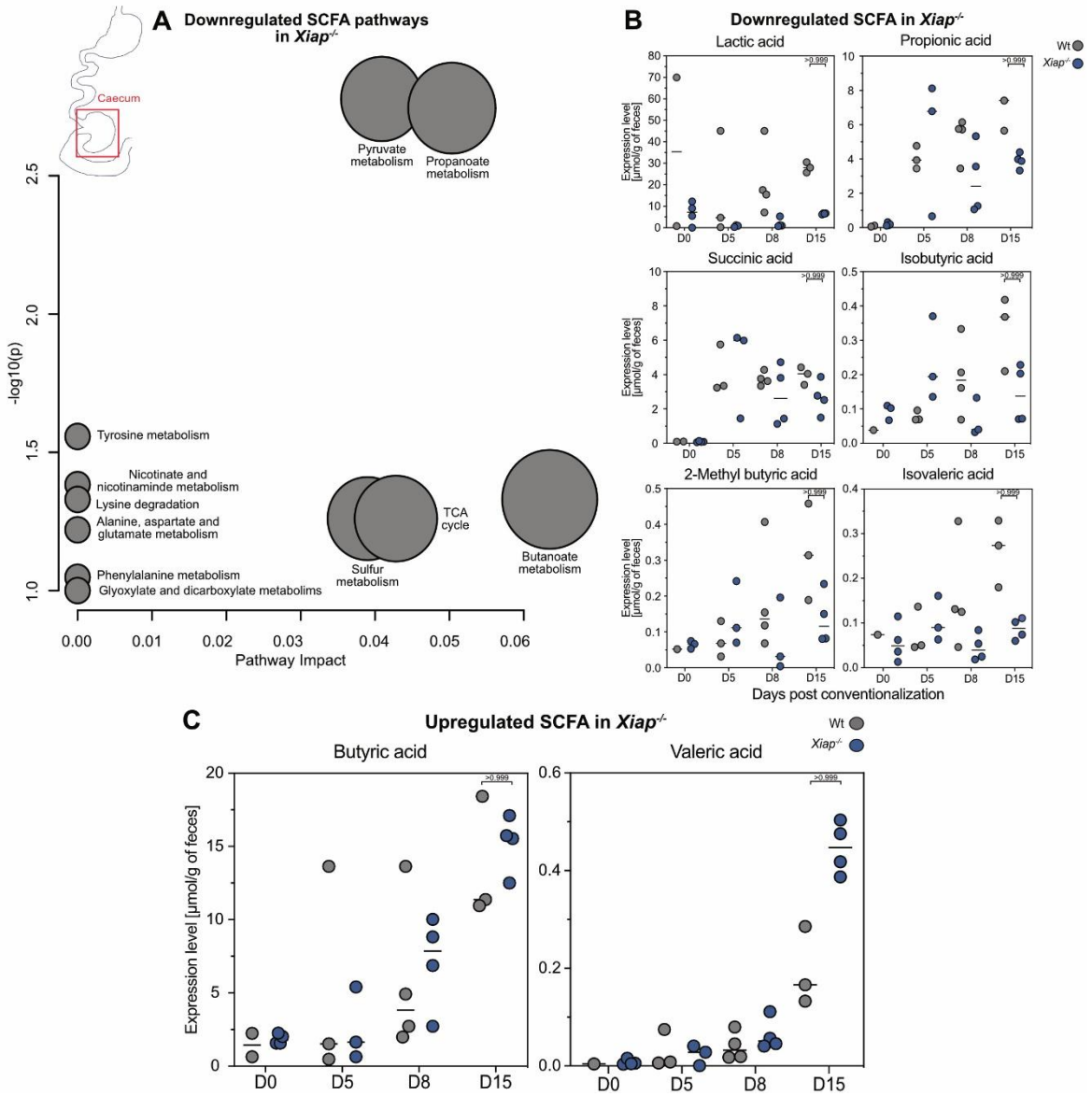

Figure 20. Passively conventionalised *Xiap*$^{-/-}$ mice exhibit a tendency for dysregulated short-chain fatty acid levels in caecal content within 15 days of conventionalisation. KEGG Pathway comparison using MetaboAnalyst depicting downregulated (A) metabolic pathways and timekinetics of levels of related SCFA (B) in caecal content of *Xiap*$^{-/-}$ mice versus Wt mice throughout 15 days of colonisation, (C) tendentially upregulated SCFA in *Xiap*$^{-/-}$ mice versus Wt mice throughout 15 days of colonisation. Depicted adjusted p value determined using Kruskal-Wallis ANOVA were not significant. Data present n = 2 – 4 mice as individual dots per genotype and timepoint.

As can be seen in **Figure 20**A, when determining potentially affected KEGG pathways, many of the SCFA found to be reduced in caecal content of *Xiap*$^{-/-}$ mice feed directly into amino acid metabolism. Additionally, SCFA crucially contribute to epithelial barrier integrity preventing malabsorption and intestinal leakiness, mutually corroborating above depicted (**Figure 19**) accumulation of various amino acids in the caecal content of conventionalised *Xiap*$^{-/-}$ mice.

As illustrated in **Figure 20**B, most highly abundant SCFA levels were decreased in *Xiap*$^{-/-}$ mice (depicted in dark blue). Lactic acid concentrations were decreased in *Xiap*$^{-/-}$ mice (28.1 µmol/g for Wt versus 6.5 µmol/g for *Xiap*$^{-/-}$ mice). Propionic and succinic acid were similarly reduced, with minimal concentrations of isobutyric acid, 2-methyl butyric acid, and isovaleric acid detected, all of which were lower in *Xiap*$^{-/-}$ mice. Merely valeric acid appeared upregulated in *Xiap*$^{-/-}$ mice.

In contrast to previous findings in adult inflamed *Xiap*$^{-/-}$ mice, butyrate levels were not significantly affected in *Xiap*$^{-/-}$ mice 15 days after conventionalisation. As depicted in **Figure 19**, at the endpoint of passive colonisation at D15, no differences in the abundance of Firmicutes, prominent butyrate producers, e, were found. An increase in the relative abundance of Lachnospiraceae, a family within Firmicutes, may explain these experimental discrepancies.

In conclusion, it was established that after D5 of conventionalisation, the caecal metabolome of *Xiap*$^{-/-}$ mice significantly diverged from that of Wt mice, exhibiting distinct upregulation of amino acids and dysregulated synthesis of cell membrane components, along with a significant reduction in lactic and propionic acids. Metabolic changes within 15 days of colonisation of germfree Wt versus *Xiap*$^{-/-}$ mice did not fully replicate the differences observed in conventionally housed adult Wt versus *Xiap*$^{-/-}$ mice, particularly regarding SCFA butyrate levels in caecal content. However, it became evident that that the previously established differences in microbial composition mount clear functional discrepancies in *Xiap*$^{-/-}$ mice already within 15 days post conventionalisation, which may, in turn, impair adequate immune responses lead to tissue inflammation.

Discussion

The data presented in this study using *Xiap*$^{-/-}$ mice as a model for early-onset IBD highlights a significant role for specialised myeloid populations, namely DC. The findings suggest that DC may be crucial to this monogenic form of IBD, but also contribute to the broader understanding of conventional IBD, particularly the under-explored role of innate immunity. These results may allow for extrapolation to human patients, providing valuable insights into early-onset IBD phenotypes, particularly for XLP2 patients.

XIAP deficiency sensitises mice to the development of Crohn's-like ileitis

The study highlights the utility of *Xiap*$^{-/-}$ mice as a spontaneous model for early-onset and conventional IBD presenting as Crohn's disease (CD), wherein genetic susceptibility and microbial environment jointly influence the intestinal phenotype. In IBD research, large intestinal colitis models, such as the DSS-induced model, are commonly used. These models typically emphasise T cell dysfunction as a major driver of inflammation. Severe colonic phenotypes also occur in IL-10 or IL-10 receptor deficiency models, as seen in IL-10-deficient mice, which develop colonic inflammation even under specific pathogen-free (SPF) conditions.[119]

Findings show that a deficiency in XIAP alone does not induce small-intestinal inflammation, as young and adult germfree *Xiap*$^{-/-}$ mice did not display signs of intestinal inflammation, supporting previous research that XIAP deficiency-dependent inflammation is also microbiome-dependent.[170] The conundrum of the lack of a phenotype observed in *Xiap*$^{-/-}$- mice under SPF conditions,[134] is suggestive of the fact that XIAP deficiency merely predisposes mice to ileitis, which only develop inflammation in response to a microbial trigger. In the publication by Wahida *et al.*[170] underlying the herein presented data, as well as in parallelly conducted research by Strigli *et al.*[182]*,* inflammation was associated with the dysregulation of Proteobacteria, particularly *Helicobacter*, across facilities housing *Xiap*$^{-/-}$ mice.

The data suggest that XIAP deficiency sensitises mice to ileitis only under specific microbial conditions. To track dysbiosis and inflammation development, passive conventionalisation was performed. Exposure to a conventional microbiome

induced inflammation within 15 days, though it did not fully replicate the inflammatory phenotype seen in conventionally housed adult *Xiap*$^{-/-}$ mice or those inoculated via a targeted faecal microbiota transplant (FMT).

Both the passive conventionalisation and targeted FMT used the combined microbiota from non-inflamed Wt and inflamed *Xiap*$^{-/-}$ mice from conventional housing, allowing the additional assessment of whether germfree *Xiap*$^{-/-}$ mice could establish a non-inflammatory microbiome. This approach also tested if germfree Wt mice lacking any genetic predisposition, exposed to the dysbiotic microbiome from inflamed *Xiap*$^{-/-}$ mice, would develop inflammation. Conclusively, the presented findings indicate that inflammation occurred only in genetically susceptible *Xiap*$^{-/-}$ mice, with distinct microbial communities developing as compared to their Wt counterparts.

Experimental conventionalisation of *Xiap*$^{-/-}$ mice for 15 days remains exploratory

Over recent decades, microbiome research has surged, driven by potential microbiome-based therapies like FMT, colonisation with defined microbial communities, and probiotic treatments.[183] A key limitation remains the lack of a definition of the “dysbiotic microbiome” for individual diseases. While it is generally accepted that dysbiosis involves a loss of species diversity[78], often correlated with IBD, specific microbial changes concerning distinct species, families or phyla are not easily mapped to disease pathology.

In this study, the microbiome of conventionalised *Xiap*$^{-/-}$ mice was analysed in the ileum, caecum, and colon, expanding upon prior research that focused solely on caecal content.[170] Some microbiome was already present one day after non-sterile facility exposure, consistent with El Aidy *et al.*, who reported full microbial community establishment one day after FMT-based colonisation.[184] However, contrasting studies by Choo and Rogers reported peak bacterial loads in germfree mice four to seven days post FMT.[185] Of note, the passive exposure used in the herein presented experiments differs from FMT, and may limit comparisons to previous work. Here, the bacterial load increased incrementally over 15 days in passively conventionalised Wt mice, suggesting microbiome acquisition through coprophagy[186] and grooming, which may more closely resemble the natural process of microbiome establishment in perinatal mice.[187]

Analysis of germfree mice confirmed that microbiota establishment began upon arrival in the non-sterile facility, even before bedding introduction from conventionally housed mice, suggesting that forced inoculation by FMT is not strictly necessary to establish a microbiome.

The sampling period of 15 days, as utilised in the herein presented experimental regime, was found to represent a clear limitation, and ongoing experiments (outside this thesis) are now extending to 60 days to better capture the full phenotype seen in adult *Xiap*$^{-/-}$ mice raised in conventional facilities. Conventionalised germfree *Xiap*$^{-/-}$ mice displayed a slight reduction in species diversity, contrasting with prior findings where adult inflamed *Xiap*$^{-/-}$ mice showed significant species diversity loss. The intestinal phenotype in Wahida *et al*.[170] and Strigli *et al*.[182] was seen only in conventionally housed *Xiap*$^{-/-}$ mice featuring dysregulated *Helicobacter* species, and differences in the caecal microbiomes of conventionally housed adult *Xiap*$^{-/-}$ mice versus Wt mice included a loss of *Clostridium* genus members.

Notably, while co-housing inflamed *Xiap*$^{-/-}$ mice with Wt mice transiently rescued the tissue inflammatory phenotype, adult *Xiap*$^{-/-}$ mice retained reduced *Clostridium* levels from the Firmicutes phylum.[170] In contrast, in the current study, conventionalised young *Xiap*$^{-/-}$ mice showed an increase in other Firmicutes members, specifically Lachnospiraceae and Staphylococcaceae, mirroring microbial changes observed in human IBD patients.[188]

As discussed in the introduction, defining a “healthy” eubiotic microbiome remains challenging, given high donor variability and the lack of precise standards beyond a general human core microbiome.[72] Links between dysbiosis and IBD remain largely correlative. A loss of species richness specifically affected inflamed *Xiap*$^{-/-}$ mice in conventional housing but not those in SPF facilities, which did not display inflammation. These studies primarily involve adult mice with germline mutations in *Birc4*, already featuring both tissue inflammation and established dysbiosis in the caecum, making it difficult to fully elucidate the parallel progression of dysbiosis and inflammation.

In summary, the herein presented work expands on existing knowledge of XIAP-deficient intestinal phenotypes and establishes conventionalised germfree *Xiap*$^{-/-}$ mice as an effective model for studying the establishment of aberrant microbial niches and inflammatory onset over time. Previous studies focused on adult mice

around 10-12 weeks, while future research demands a comparison of conventionalised young germfree Wt and *Xiap*$^{-/-}$ mice with young mice of either genotype raised in the conventional facility. This is particularly relevant as research suggests a critical period for microbiome establishment begins at weaning, which could influence immune development and susceptibility to inflammation.[90,189,190]

The dysbiosis in XIAP deficiency may be due to species with high metabolic independence

It has become increasingly apparent that the establishment of the intestinal microbiome relies on a complex cascade of consecutively occurring events termed ecological succession. Throughout this process, cross-feeding species generate vital metabolites that serve as the basis for the growth of secondarily arising species. Analysis of the microbiome via 16S rRNA sequencing does not elucidate effects on the bacterial metabolism at protein level. Therefore, an MS-based metabolome analysis of caecal content was employed, as it would offer insights into the actual translational metabolic output. However, this method cannot differentiate between the metabolites generated by the murine host, as compared to those of the bacteria. Ultimately, it offers a snapshot overview of the reciprocal and multifaceted process, in which changes in the host's intestinal physiology may have altered the niche of the bacteria, and how the bacteria themselves have metabolically adapted to those changes.

The notably elevated amino acid levels in conventionalised *Xiap*$^{-/-}$ mice, even prior to conventionalisation, represent possible host-intrinsic effects due to genetic ablation of XIAP. Increased caecal amino acids, like phenylalanine, aspartic acid, and glutamic acid, may reflect nutrient retention issues due to compromised barrier integrity, a symptom hypothesised to be linked to a "leaky gut."[191] This theory is further supported by tendentially lower levels of short-chain fatty acids (SCFA) such as lactic and propionic acid in *Xiap*$^{-/-}$ mice, as Jaworska *et al*. proposed an increased blood-to-faecal SCFA ratio as a potential IBD marker, highlighting how intestinal lesions allow for SCFA "leakage" into the circulation.[192] To elucidate this hypothesis, additional analyses of blood serum focussed on expected faecal metabolites would be necessary.

Further evidence for compromised barrier integrity in *Xiap*$^{-/-}$ mice includes the findings of elevated purine derivatives, hypoxanthine, and 8-oxo-2-deoxyadenosine. This finding is corroborated by the fact that increased oxidative stress is a known factor in IBD, linked to elevated purine salvage, particularly hypoxanthine, which bacteria use for energy and which plays a role in barrier maintenance.[1] Hence, it was hypothesised that the presented higher hypoxanthine levels may suggest either a compensatory response to epithelial disruption or an inability of dysfunctional epithelial cells to retain essential energy sources.

While intrinsic host factors likely contribute to these metabolic shifts, differences in microbiome composition clearly play a key role, as adult germfree and SPF *Xiap*$^{-/-}$ mice did not develop intestinal inflammation. A recent meta-analysis by Veseli *et al.*[86] of over 400 human intestinal metagenomes identified 33 metabolic modules that distinguish the microbiomes of IBD patients, revealing high metabolic independence (HMI) among these bacterial communities. The survival of microbial species featuring HMI was hypothesised to be uncoupled from the need for cross-feeding or host-derived metabolites, suggestive of adaptation to the harsh conditions in inflammatory niches as present in the intestine of an IBD patient. Thus, the elevated levels of certain metabolites in *Xiap*$^{-/-}$ mice, despite lower bacterial loads, may indicate an HMI-adapted microbiome. The upregulated pathways for “amino acid biosynthesis” and “nucleotide metabolism,” along with increased phospholipids, reflect the modules noted in Veseli *et al.*[86]

Methodological, meta-transcriptomic analysis could offer additional insight into the functional state of these microbial communities, as 16S rRNA sequencing alone only allows taxonomic identification. Meta-transcriptomics is particularly relevant given bacteria’s rapid adaptation to environmental shifts, allowing for the characterisation of microbial metabolic output and adaptation through gene expression changes. This clear limitation in the present data, lacking a meta-transcriptomic analysis, is being considered for future studies outside of the scope of the herein-presented data.

Observed changes in species abundance, such as increased abundance of members of the Bifidobacteriaceae, or metabolic shifts like reduced SCFA, however, are not sufficient to drive the inflammatory phenotype. The introduction of a microbiome of inflamed *Xiap*$^{-/-}$ mice into Wt mice did not onset inflammation. Thus, it is hypothesised that dysregulated luminal antigens stemming from a dysbiotic commensal microbiome activate immune cells, driving tissue inflammation specifically

in genetically susceptible hosts, such as observed for *Xiap*$^{-/-}$ mice featuring a loss of XIAP function.

TLR5 engagement may contribute to local inflammation in the absence of XIAP

Previous studies have shown that certain DC integrate into the epithelial layer by upregulating tight junction markers, extending protrusions into the lumen to sample luminal antigens.[7] In contrast to intraepithelial (IE) DC, lamina propria (LP) DC can be assumed to typically not interact directly with luminal antigens unless epithelial barrier integrity is compromised. Wahida *et al.* identified a population of TLR5^{+} DC in the LP of Wt mice, which was reduced in inflamed *Xiap*$^{-/-}$ mice.[170] This loss was proposed to contribute to local tissue inflammation, although the underlying mechanism remained unclear.

Expanding on Wahida *et al.* findings, the current study aimed to explore the functional role of TLR5-expressing cells and their increased tendency to undergo necroptotic cell death in the absence of XIAP. Analysis of scRNAseq data from Wt mice revealed a distinct transcriptional profile of *Tlr5*$^{+}$ cells from the LP. These cells expressed both the transcription factors *Irf4* and *Irf8*, typically linked to cDC2 and cDC1 differentiation, respectively. A novel discovery was the link between those *Tlr5*$^{+}$ LP DC, and a specialised IE DC population, both featuring the expression of the C-type lectin receptor *Cd209a*. *Cd209*$^{+}$ IE DC were found to exhibit expression of markers of pDC ontogeny, such as *Ly6e* and *Siglech*. It was hypothesised that this may be reflective of the existence of a transitional DC population with cDC2 differentiation potential, consistent with the idea of pDC-like pre-DC2 populations in peripheral organs like the intestine.

Further background is provided by a study by Chassaing *et al.,* which used conditional genetic ablation in mice to investigate the specific role of TLR5 in intestinal epithelial versus CD11c^{+} DC populations in intestinal inflammation and dysbiosis.[193] Their work highlights that TLR5 ablation in epithelial cells reproduced the inflammatory phenotype seen in full body-TLR5-deficient mice, while ablation of TLR5 in CD11c^{+} DC specifically neither induced inflammation nor dysbiosis. This aligns with the herein presented findings that the absence of TLR5^{+} cells in the LP alone did not trigger local inflammation. The numbers of TLR5^{+} cells in both young, non-inflamed germfree Wt

and *Xiap*$^{-/-}$ mice were either below or comparable to those in inflamed adult *Xiap*$^{-/-}$ mice, suggesting that the mere absence of TLR5^{+} DC in the LP does not fully explain the tissue inflammatory phenotype. Rather, the current hypothesis suggests that intestinal inflammation in *Xiap*$^{-/-}$ mice results from an inappropriate immune response to antigen encounters by immature-like pre-cDC2 in the IE compartment, which then migrate to the LP in a hyperresponsive manner. In Wt mice, DC in the LP primarily contribute to coin local antigen cross-presentation and adaptive immune response induction. However, the absence of XIAP may disrupt these processes by increasing TNF signalling in TLR5^{+} cDC2 in the LP downstream of hyperactivation of IE DC populations, leading to local programmed inflammatory cell death and tissue inflammation. This hypothesis of a cascade of events connecting luminal dysbiosis, *Cd209a*$^{+}$ IE DC populations exposed to luminal antigens, resulting in a dysfunction of *Tlr5*$^{+}$ LP DC downstream, also explains the lack of an inflammatory phenotype in germfree Wt and *Xiap*$^{-/-}$ mice, albeit featuring low number of TLR5^{+} DC in their LP.

Moreover, this hypothesis also highlights a limitation of the aforementioned study by Chassaing *et al.* utilising a CD11c-specific TLR5 ablation.[193] The lack of phenotype in this model may be explained by immature IE cDC2 failing to undergo the above-proposed cascade required for TLR5 upregulation, altogether circumventing the onset of tissue inflammatory phenotype due to local inflammatory cell death.

Ultimately, to allow for the experimental manipulation of different steps throughout this proposed inflammatory cascade, future studies necessitate the use of an inducible Cre system. Inducible, targeted ablation of specialised *Cd209a*$^{+}$ IE DC and *Tlr5*$^{+}$ LP DC under different hygienic conditions could clarify their specific roles in XIAP-deficient intestinal inflammation.

Sub-tissular intestinal niches support unique DC phenotypes in confirmation of the LP-specificity of TLR5

A novel finding lay in the observation of compartmentalised DC subpopulations with shared CD209a expression as briefly outlined above, with CD209a^{+} TLR5-negative DC localised mainly in the IE, while CD209a+ DC expressing TLR5 populated the LP. An *Irf8*-Venus reporter mouse model further identified IE-specific immature cDC2 populations marked by differential regulation of the pDC-associated marker BST2 and CD209a. Notably, inflamed *Xiap*$^{-/-}$ mice exhibited an increase in CD209a^{+} TLR5^{-} IE DC, but a reduction in CD209a^{+} TLR5^{+} LP DC. These data support previous findings

that this shift may signify a reprogramming to an inflammatory phenotype in *bona fide* cDC2, which may then contribute to local inflammation.[51]

Mechanistically, the current hypothesis proposes that a population of CD209a$^+$ IE pre-cDC2, upon antigen activation, undergoes maturation, upregulates TLR5, migrates to the LP, and ultimately undergoes inflammatory cell death in the absence of XIAP. This cycle is thought to drive local tissue inflammation and reduce CD209a$^+$ TLR5$^+$ LP DC as apparent in tissue samples from *Xiap*$^{-/-}$ mice. The presence of CD209a$^+$ IE cells was confirmed in germfree conditions prior to microbiome introduction, while subsequent conventionalisation triggered a notable rise in immune cell counts in the LP, especially in TLR5$^+$ LP cells. By day 15 of conventionalisation, CD209a$^+$ TLR5$^+$ LP DC in *Xiap*$^{-/-}$ mice surpassed Wt levels, suggesting a hyper-inflammatory reaction to luminal antigens in genetically susceptible hosts. This process parallels previously observed TLR5$^+$ Paneth cell accumulation in organoids of *Xiap*$^{-/-}$ mice[170]. Conclusively, excessive TLR5 activation in XIAP-deficient DC likely prompts inflammatory cell death and results in tissue inflammation.

However, another proposed possibility lays in that CD209a$^+$ TLR5$^-$ IE DC and CD209a$^+$ TLR5$^+$ LP DC are distinct populations rather than representing continuous stages of DC development, with interactions in the LP ultimately triggering cell death. In this scenario, CD209a$^+$ TLR5$^+$ LP DC may thereby serve as sentinels, monitoring deeper tissue integrity, and being induced by direct interaction with activated CD209a$^+$ TLR5$^-$ IE DC. Adoptive transfers of traceable cells, and refined *in situ* analyses with additional activation markers could elucidate this proposed interaction.

A comprehensive marker set for these specialised DC subpopulations, whether it is the proposed pDC-like hyperresponsive IE pre-cDC2 or hyperactivated TLR5$^+$ LP cDC2, remains crucial as a first step. Future work might aim to generate these DC *in vitro* by mimicking the specific cytokine environment of their sub-tissue origins, enabling targeted manipulations to elucidate their specialised functions in both IE and LP contexts. However, limitations arise with antibody-based methods that may have nonspecific binding, and tissue dissociation for cell isolation can skew surface marker representation, primarily and selectively impacting cells more prone to cell death, in a context in which a central modulator XIAP is missing. The recent generation of a CD209a-reporter mouse may facilitate *in vivo* assessments, reducing the limitations associated with antibody specificity and cell death during cell isolation.

Conceptionally, ongoing discussions in the field are revising long-held paradigms of DC ontogeny. Proposed re-categorisations include subdividing cDC2 into cDC2A and cDC2B[46,49,50] or even introducing a novel cDC3 population[48], posing the question of whether transcription factor- and surface marker-based immune cell categorisation remains a useful tool in the context of myeloid cells in general, and niche-specific DC population plasticity specifically. A shift to functional classification, especially in specific tissue contexts and unique disease-induced cytokine environments, may provide a more effective approach. Such a focus could also enhance the extrapolation of murine models to human autoimmune diseases influenced by innate immune cells, as discussed for the herein presented *Xiap*$^{-/-}$ mice data and the corresponding XLP2 patients below.

Preliminary analysis uncovered a DC subpopulation with an inflammatory transcriptomic profile in an XLP2 patient

Various treatment options exist for classical adult-onset IBD; however, severe cases of intestinal inflammation sometimes require haematopoietic stem cell transplantation (HSCT) to replace the malfunctioning immune cell compartment, despite the risks associated with this procedure. As previously discussed in this thesis, monogenic IBD cases are often severe, and HSCT has become the final attempt at treating XLP2 patients failing to respond to other treatment options. This indicates a significant role for a dysfunctional immune cell compartment in driving intestinal inflammation in the absence of XIAP in humans. Prior research hereby primarily focused on the role of dysfunctional T cells in IBD pathology. Based on the herein presented murine data, it is proposed that the innate myeloid cell compartment, specifically specialised DC subpopulations in distinct sub-tissular compartments, may play a central role in IBD, not only in XLP2 patients specifically, but also potentially in cases of classical adult-onset IBD.

Preliminary evidence from a scRNAseq analysis of an XLP2 patient supports an innate immune system role in intestinal pathology. This analysis of intestinal biopsies identified a unique immune cell cluster annotated as cDC2, characterised by markers like SIRPA and high expression of CD209, the human orthologue to *Cd209a*, and IRF8, with low levels of XCR1 and CLEC9A. TLR5 was excluded as a distinguishable marker due to its ubiquitous expression in various human immune cell types. The patient-specific cDC2 displayed a pDC-like phenotype with high IRF7 and

SICLEC1 expression, along with markers such as MAFB, CD68, CD163, and CD86, indicating hyper-reactivity. Additionally, the cDC3 marker CLEC10A was elevated. Markers of programmed cell death (RIPK1, RIPK3, MLKL, CASP8, AIM2, PYCARD, GSDMB, and GSDMC) suggested these cells were primed for necroptosis or pyroptosis. Though generally, expression of the TLR family was increased, TLR5 was not prominently featured. High TNFR2 expression potentially links these findings to murine data presented in this thesis, where TNFR2 signalling in specialised DC subpopulations was implicated in inflammatory phenotypes in *Xiap*-deficient mice.

Clear limitations in the currently available data must be acknowledged. The proposed sub-tissular DC populations were initially identified based on scRNAseq data. While transcriptomics can offer insights into a cell's phenotype and function, RNA levels alone do not confirm the functional protein repertoire, especially as cell death regulators often undergo extensive post-translational modification, with XIAP notably playing a major role in facilitating ubiquitylation during cell death processes. Additionally, due to the rarity of this monogenic IBD, only one patient was analysed in this manner. Therefore, while offering first hints at the connection between the *Xiap*$^{-/-}$ mouse strain and human XLP2 phenotype, this preliminary data set is not featured in this thesis.

Conclusion

This thesis refines the manipulation of the *Xiap*-deficient monogenic IBD mouse model introduced by Wahida *et al.*[170] The data herein constitutes a first step in exploring how local differentiation of specialised DC may drive intestinal inflammation through TNFR2-mediated inflammatory cell death. The conventionalisation of germfree *Xiap*$^{-/-}$ mice elucidated molecular mechanisms activated in the absence of XIAP and correlated them with TNF signalling via TNFR2. Specialised DC populations were identified, characterised by compartment-specific expression of CD209a in the intestinal epithelium and TLR5 in the LP, suggesting a sensitisation to inflammatory cell death contributing to intestinal inflammation. The conditions in their sub-tissular niches appeared essential for the phenotype of these DC, as indicated by CD209a expression in the epithelium versus TLR5 upregulation in LP-resident DC.

This phenotype was found to be strictly dependent on the presence of a microbiome, and *Xiap*$^{-/-}$ mice were unable to maintain a conventional microbiome

upon both FMT and passive exposure. This underscores the critical role of microbial composition in disease progression and highlights the potential for microbiome-targeted therapies in IBD treatment.

Beyond murine models, a similar DC population characterised by CD209 expression was identified in a preliminary analysis of the intestine of an XIAP-deficient patient with severe early-onset IBD. These findings highlight possible future treatment options for XLP2 patients that may negate the need for HSCT. Blocking key pro-inflammatory cell death pathways, such as those involving RIPK1 or MLKL inhibitors, could be promising research targets.

In summary, this work currently proposes a mechanism wherein immature cDC2 in the IE migrate to the LP following antigen encounters, leading to accelerated expression of PRR, including TLR5, and other maturation markers. This may reveal new insights into the role of specialised innate immune cells in sustaining intestinal inflammation and may be explored as a treatment target for XIAP deficiency and, potentially, for adult-onset IBD.

Appendix

Figure Index

Literature References

1. Sun, T., Nguyen, A. & Gommerman, J. L. Dendritic Cell Subsets in Intestinal Immunity and Inflammation. *J. Immunol.* **204**, 1075–1083 (2020).
2. Agace, W. W. & McCoy, K. D. Regionalized Development and Maintenance of the Intestinal Adaptive Immune Landscape. *Immunity* **46**, 532–548 (2017).
3. Ogino, T. & Takeda, K. Immunoregulation by antigen-presenting cells in human intestinal lamina propria. *Front. Immunol.* **14**, 1138971 (2023).
4. Mörbe, U. M. *et al.* Human gut-associated lymphoid tissues (GALT); diversity, structure, and function. *Mucosal Immunol.* **14**, 793–802 (2021).
5. Brown, H. & Esterházy, D. Intestinal immune compartmentalization: implications of tissue specific determinants in health and disease. *Mucosal Immunol.* **14**, 1259–1270 (2021).
6. Clevers, H. C. & Bevins, C. L. Paneth Cells: Maestros of the Small Intestinal Crypts. *Annu. Rev. Physiol.* **75**, 289–311 (2013).
7. Farache, J. *et al.* Luminal Bacteria Recruit CD103+ Dendritic Cells into the Intestinal Epithelium to Sample Bacterial Antigens for Presentation. *Immunity* **38**, 581–595 (2013).
8. Pastorelli, L., De Salvo, C., Mercado, J. R., Vecchi, M. & Pizarro, T. T. Central Role of the Gut Epithelial Barrier in the Pathogenesis of Chronic Intestinal Inflammation: Lessons Learned from Animal Models and Human Genetics. *Front. Immunol.* **4**, (2013).
9. Barker, N. *et al.* Identification of stem cells in small intestine and colon by marker gene Lgr5. *Nature* **449**, 1003–1007 (2007).
10. Tian, H. *et al.* A reserve stem cell population in small intestine renders Lgr5-positive cells dispensable. *Nature* **478**, 255–259 (2011).
11. Azkanaz, M. *et al.* Retrograde movements determine effective stem cell numbers in the intestine. *Nature* **607**, 548–554 (2022).
12. Sato, T. *et al.* Paneth cells constitute the niche for Lgr5 stem cells in intestinal crypts. *Nature* **469**, 415–418 (2011).
13. Moor, A. E. *et al.* Spatial Reconstruction of Single Enterocytes Uncovers Broad Zonation along the Intestinal Villus Axis. *Cell* **175**, 1156-1167.e15 (2018).
14. Berková, L. *et al.* Terminal differentiation of villus tip enterocytes is governed by distinct Tgfβ superfamily members. *EMBO Rep.* **24**, e56454 (2023).
15. Farin, H. F. *et al.* Paneth cell extrusion and release of antimicrobial products is directly controlled by immune cell–derived IFN-γ. *J. Exp. Med.* **211**, 1393–1405 (2014).
16. Lee, V. H. & Gulati, A. S. Implications of Paneth cell dysfunction on gastrointestinal health and disease. *Curr. Opin. Gastroenterol.* **38**, 535–540 (2022).
17. Wehkamp, J. & Stange, E. F. An Update Review on the Paneth Cell as Key to Ileal Crohn's Disease. *Front. Immunol.* **11**, 646 (2020).
18. McShane, A. *et al.* Mucus. *Curr. Biol.* **31**, R938–R945 (2021).
19. Johansson, M. E. V. *et al.* The inner of the two Muc2 mucin-dependent mucus layers in colon is devoid of bacteria. *Med. Sci.* 6.
20. Gustafsson, J. K. & Johansson, M. E. V. The role of goblet cells and mucus in intestinal homeostasis.

Nat. Rev. Gastroenterol. Hepatol. **19**, 785–803 (2022).
21. Du Halgouet, A. *et al.* Multimodal profiling reveals site-specific adaptation and tissue residency hallmarks of γδ T cells across organs in mice. *Nat. Immunol.* (2024) doi:10.1038/s41590-023-01710-y.
22. Catalan-Serra, I., Sandvik, A. K., Bruland, T. & Andreu-Ballester, J. C. Gammadelta T Cells in Crohn's Disease: A New Player in the Disease Pathogenesis? *J. Crohns Colitis* **11**, 1135–1145 (2017).
23. Esterházy, D. *et al.* Classical dendritic cells are required for dietary antigen–mediated induction of peripheral Treg cells and tolerance. *Nat. Immunol.* **17**, 545–555 (2016).
24. De Kleer, I., Willems, F., Lambrecht, B. & Goriely, S. Ontogeny of Myeloid Cells. *Front. Immunol.* **5**, (2014).
25. Schlitzer, A. *et al.* Identification of cDC1- and cDC2-committed DC progenitors reveals early lineage priming at the common DC progenitor stage in the bone marrow. *Nat. Immunol.* **16**, 718–728 (2015).
26. Liu, Z., Gu, Y., Shin, A., Zhang, S. & Ginhoux, F. Analysis of Myeloid Cells in Mouse Tissues with Flow Cytometry. *STAR Protoc.* **1**, 100029 (2020).
27. Bosteels, C. & Scott, C. L. Transcriptional regulation of DC fate specification. *Mol. Immunol.* **121**, 38–46 (2020).
28. Chen, K. *et al.* Tissue-resident dendritic cells and diseases involving dendritic cell malfunction. *Int. Immunopharmacol.* **34**, 1–15 (2016).
29. Bassler, K., Schulte-Schrepping, J., Warnat-Herresthal, S., Aschenbrenner, A. C. & Schultze, J. L. The Myeloid Cell Compartment—Cell by Cell. *Annu. Rev. Immunol.* **37**, 269–293 (2019).
30. Mowat, A. McI. Anatomical basis of tolerance and immunity to intestinal antigens. *Nat. Rev. Immunol.* **3**, 331–341 (2003).
31. Nguyen, H. D., Aljamaei, H. M. & Stadnyk, A. W. The Production and Function of Endogenous Interleukin-10 in Intestinal Epithelial Cells and Gut Homeostasis. *Cell. Mol. Gastroenterol. Hepatol.* **12**, 1343–1352 (2021).
32. Wei, H.-X., Wang, B. & Li, B. IL-10 and IL-22 in Mucosal Immunity: Driving Protection and Pathology. *Front. Immunol.* **11**, 1315 (2020).
33. Varol, C., Zigmond, E. & Jung, S. Securing the immune tightrope: mononuclear phagocytes in the intestinal lamina propria. *Nat. Rev. Immunol.* **10**, 415–426 (2010).
34. Loschko, J. *et al.* Absence of MHC class II on cDCs results in microbial-dependent intestinal inflammation. *J. Exp. Med.* **213**, 517–534 (2016).
35. He, K. *et al.* Gasdermin D licenses MHCII induction to maintain food tolerance in small intestine. *Cell* S0092867423005779 (2023) doi:10.1016/j.cell.2023.05.027.
36. Tamoutounour, S. *et al.* CD 64 distinguishes macrophages from dendritic cells in the gut and reveals the T h1-inducing role of mesenteric lymph node macrophages during colitis. *Eur. J. Immunol.* **42**, 3150–3166 (2012).
37. Cerovic, V., Bain, C. C., Mowat, A. M. & Milling, S. W. F. Intestinal macrophages and dendritic cells: what's the difference? *Trends Immunol.* **35**, 270–277 (2014).
38. Sheng, J. *et al.* A Discrete Subset of Monocyte-Derived Cells among Typical Conventional Type 2 Dendritic Cells Can Efficiently Cross-Present. *Cell Rep.* **21**, 1203–1214 (2017).
39. Backer, R. A., Probst, H. C. & Clausen, B. E. Classical DC2 subsets and monocyte-derived DC: Delineating the developmental and

functional relationship. *Eur. J. Immunol.* **53**, 2149548 (2023).
40. Kroczek, R. A. Ontogenic, phenotypic, and functional characterization of XCR1+ dendritic cells leads to a consistent classification of intestinal dendritic cells based on the expression of XCR1 and SIRP. *Front. Immunol.* 12.
41. Gurka, S., Hartung, E., Becker, M. & Kroczek, R. A. *Mouse Conventional Dendritic Cells Can Be Universally Classified Based on the Mutually Exclusive Expression of XCR1 and SIRPα*. http://biorxiv.org/lookup/doi/10.1101/012567 (2014).
42. Bain, C. C. *et al.* TGFβR signalling controls CD103+CD11b+ dendritic cell development in the intestine. *Nat. Commun.* **8**, 620 (2017).
43. Niess, J. H. What are CX 3 CR1 + mononuclear cells in the intestinal mucosa? *Gut Microbes* **1**, 396–400 (2010).
44. Niess, J. H. *et al.* CX 3 CR1-Mediated Dendritic Cell Access to the Intestinal Lumen and Bacterial Clearance. *Science* **307**, 254–258 (2005).
45. Papaioannou, N. E. *et al.* Environmental signals rather than layered ontogeny imprint the function of type 2 conventional dendritic cells in young and adult mice. *Nat. Commun.* **12**, 464 (2021).
46. Cabeza-Cabrerizo, M., Cardoso, A., Minutti, C. M., Pereira da Costa, M. & Reis e Sousa, C. Dendritic Cells Revisited. *Annu. Rev. Immunol.* **39**, 131–166 (2021).
47. Rivera, C. A. & Lennon-Duménil, A.-M. Gut immune cells and intestinal niche imprinting. *Semin. Cell Dev. Biol.* **150–151**, 50–57 (2023).
48. Liu, Z. *et al.* Dendritic cell type 3 arises from Ly6C+ monocyte-dendritic cell progenitors. *Immunity* S1074761323003151 (2023) doi:10.1016/j.immuni.2023.07.001.
49. Dutertre, C.-A. A new step in understanding mouse cDC ontogeny. *Nat. Immunol.*
50. Minutti, C. M. Distinct ontogenetic lineages dictate cDC2 heterogeneity. *Nat. Immunol.*
51. Bosteels, C. *et al.* Inflammatory Type 2 cDCs Acquire Features of cDC1s and Macrophages to Orchestrate Immunity to Respiratory Virus Infection. *Immunity* **52**, 1039-1056.e9 (2020).
52. Brown, C. C. *et al.* Transcriptional Basis of Mouse and Human Dendritic Cell Heterogeneity. *Cell* S009286741931116X (2019) doi:10.1016/j.cell.2019.09.035.
53. Rivera, C. A. *et al.* Epithelial colonization by gut dendritic cells promotes their functional diversification. *Immunity* **55**, 129-144.e8 (2022).
54. Bajaña, S., Turner, S., Paul, J., Ainsua-Enrich, E. & Kovats, S. IRF4 and IRF8 Act in CD11c+ Cells To Regulate Terminal Differentiation of Lung Tissue Dendritic Cells. *J. Immunol.* **196**, 1666–1677 (2016).
55. Lança, T. *et al.* IRF8 deficiency induces the transcriptional, functional, and epigenetic reprogramming of cDC1 into the cDC2 lineage. *Immunity* **55**, 1431-1447.e11 (2022).
56. Rodrigues, P. F. *et al.* pDC-like cells are pre-DC2 and require KLF4 to control homeostatic CD4 T cells. *Sci. Immunol.* **8**, eadd4132 (2023).
57. Zhou, W. *et al.* ZBTB46 defines and regulates ILC3s that protect the intestine. *Nature* **609**, 159–165 (2022).
58. Reizis, B. *et al.* Reclassification of plasmacytoid dendritic cells as innate lymphocytes is premature. *Nat. Rev. Immunol.* (2023) doi:10.1038/s41577-023-00864-y.

59. Higashiyama, M., Miura, S. & Hokari, R. Modulation by luminal factors on the functions and migration of intestinal innate immunity. *Front. Immunol.* **14**, 1113467 (2023).
60. Piquer-Esteban, S., Ruiz-Ruiz, S., Arnau, V., Diaz, W. & Moya, A. Exploring the universal healthy human gut microbiota around the World. *Comput. Struct. Biotechnol. J.* **20**, 421–433 (2022).
61. Fusco, W. *et al.* Short-Chain Fatty-Acid-Producing Bacteria: Key Components of the Human Gut Microbiota. (2023).
62. Wexler, H. M. Bacteroides : the Good, the Bad, and the Nitty-Gritty. *Clin. Microbiol. Rev.* **20**, 593–621 (2007).
63. Sharma, M., Wasan, A. & Sharma, R. K. Recent developments in probiotics: An emphasis on Bifidobacterium. *Food Biosci.* **41**, 100993 (2021).
64. Jochum, L. & Stecher, B. Label or Concept – What Is a Pathobiont? *Trends Microbiol.* **28**, 789–792 (2020).
65. Carvalho, F. A. *et al.* Transient inability to manage proteobacteria promotes chronic gut inflammation in tlr5-deficient mice. *Cell Host Microbe* **12**, 139–152 (2012).
66. Bradley, P. H. & Pollard, K. S. Proteobacteria explain significant functional variability in the human gut microbiome. *Microbiome* **5**, 36 (2017).
67. Iwaza, R., Wasfy, R. M., Dubourg, G., Raoult, D. & Lagier, J.-C. Akkermansia muciniphila: The state of the art, 18 years after its first discovery. *Front. Gastroenterol.* **1**, 1024393 (2022).
68. Vartoukian, S. R. Cultivation strategies for growth of uncultivated bacteria. *J. Oral Biosci.* (2016).
69. Clavel, T. From complex gut communities to minimal microbiomes via cultivation. *Curr. Opin. Microbiol.* (2017).
70. Upadhyay, K. G., Desai, D. C., Ashavaid, T. F. & Dherai, A. J. Microbiome and metabolome in inflammatory bowel disease. *J. Gastroenterol. Hepatol.* **38**, 34–43 (2023).
71. Khan, I. *et al.* Alteration of Gut Microbiota in Inflammatory Bowel Disease (IBD): Cause or Consequence? IBD Treatment Targeting the Gut Microbiome. *Pathogens* **8**, 126 (2019).
72. Risely, A. Applying the core microbiome to understand host–microbe systems. *J. Anim. Ecol.* **89**, 1549–1558 (2020).
73. Ruan, W., Engevik, M. A., Spinler, J. K. & Versalovic, J. Healthy Human Gastrointestinal Microbiome: Composition and Function After a Decade of Exploration. *Dig. Dis. Sci.* **65**, 695–705 (2020).
74. Rinninella, E. *et al.* What is the Healthy Gut Microbiota Composition? A Changing Ecosystem across Age, Environment, Diet, and Diseases. (2019).
75. Tang, Q. *et al.* Current Sampling Methods for Gut Microbiota: A Call for More Precise Devices. *Front. Cell. Infect. Microbiol.* **10**, 151 (2020).
76. Mowat, A. McI. To respond or not to respond — a personal perspective of intestinal tolerance. *Nat. Rev. Immunol.* **18**, 405–415 (2018).
77. Li, D. & Wu, M. Pattern recognition receptors in health and diseases. *Signal Transduct. Target. Ther.* **6**, 291 (2021).
78. Kriss, M., Hazleton, K. Z., Nusbacher, N. M., Martin, C. G. & Lozupone, C. A. Low diversity gut microbiota dysbiosis: drivers, functional implications and recovery. *Curr. Opin. Microbiol.* **44**, 34–40 (2018).

79. Gong, D., Gong, X., Wang, L., Yu, X. & Dong, Q. Involvement of Reduced Microbial Diversity in Inflammatory Bowel Disease. *Gastroenterol. Res. Pract.* **2016**, 1–7 (2016).
80. Hiraoka, S., Yang, C. & Iwasaki, W. Metagenomics and Bioinformatics in Microbial Ecology: Current Status and Beyond. *Microbes Environ.* **31**, 204–212 (2016).
81. Stanley, D., Geier, M. S., Chen, H., Hughes, R. J. & Moore, R. J. Comparison of fecal and cecal microbiotas reveals qualitative similarities but quantitative differences. *BMC Microbiol.* **15**, 51 (2015).
82. Xu, X. *et al.* The gut metagenomics and metabolomics signature in patients with inflammatory bowel disease. *Gut Pathog.* **14**, 26 (2022).
83. Rivera-Chávez, F. Depletion of Butyrate-Producing Clostridia from the Gut Microbiota Drives an Aerobic Luminal Expansion of Salmonella.
84. Heinken, A., Hertel, J. & Thiele, I. Metabolic modelling reveals broad changes in gut microbial metabolism in inflammatory bowel disease patients with dysbiosis. *Npj Syst. Biol. Appl.* **7**, 19 (2021).
85. Colgan, S. P., Wang, R. X., Hall, C. H. T., Bhagavatula, G. & Lee, J. S. Revisiting the “starved gut” hypothesis in inflammatory bowel disease. *Immunometabolism* **5**, e0016 (2023).
86. Veseli, I. *et al. Microbes with Higher Metabolic Independence Are Enriched in Human Gut Microbiomes under Stress*. https://elifesciences.org/reviewed-preprints/89862v1 (2023).
87. Watson, A. R. *et al.* Metabolic independence drives gut microbial colonization and resilience in health and disease. *Genome Biol.* **24**, 78 (2023).
88. Baunwall, S. M. D. *et al.* The use of Faecal Microbiota Transplantation (FMT) in Europe: A Europe-wide survey. *Lancet Reg. Health - Eur.* **9**, 100181 (2021).
89. Belvoncikova, P., Maronek, M. & Gardlik, R. Gut Dysbiosis and Fecal Microbiota Transplantation in Autoimmune Diseases. *Int. J. Mol. Sci.* **23**, 10729 (2022).
90. Al Nabhani, Z. *et al.* A Weaning Reaction to Microbiota Is Required for Resistance to Immunopathologies in the Adult. *Immunity* (2019) doi:10.1016/j.immuni.2019.02.014.
91. Lewis, J. D. *et al.* Inflammation, Antibiotics, and Diet as Environmental Stressors of the Gut Microbiome in Pediatric Crohn’s Disease. *Cell Host Microbe* **18**, 489–500 (2015).
92. Shekhar, S. & Petersen, F. C. The Dark Side of Antibiotics: Adverse Effects on the Infant Immune Defense Against Infection. *Front. Pediatr.* **8**, 544460 (2020).
93. Yu, Y. R. & Rodriguez, J. R. Clinical presentation of Crohn’s, ulcerative colitis, and indeterminate colitis: Symptoms, extraintestinal manifestations, and disease phenotypes. *Semin. Pediatr. Surg.* **26**, 349–355 (2017).
94. Conrad, K., Roggenbuck, D. & Laass, M. W. Diagnosis and classification of ulcerative colitis. *Autoimmun. Rev.* **13**, 463–466 (2014).
95. Verstockt, B., Bressler, B., Martinez-Lozano, H., McGovern, D. & Silverberg, M. S. Time to Revisit Disease Classification in Inflammatory Bowel Disease: Is the Current Classification of Inflammatory Bowel Disease Good Enough for Optimal Clinical

Management? *Gastroenterology* **162**, 1370–1382 (2022).
96. Kaplan, G. G. & Windsor, J. W. The four epidemiological stages in the global evolution of inflammatory bowel disease. *Nat. Rev. Gastroenterol. Hepatol.* **18**, 56–66 (2021).
97. Ng, S. C. *et al.* Worldwide incidence and prevalence of inflammatory bowel disease in the 21st century: a systematic review of population-based studies. *The Lancet* **390**, 2769–2778 (2017).
98. Coward, S. *et al.* Past and Future Burden of Inflammatory Bowel Diseases Based on Modeling of Population-Based Data. *Gastroenterology* **156**, 1345-1353.e4 (2019).
99. Zhao, M. & Burisch, J. Impact of Genes and the Environment on the Pathogenesis and Disease Course of Inflammatory Bowel Disease. *Dig. Dis. Sci.* **64**, 1759–1769 (2019).
100. The International IBD Genetics Consortium (IIBDGC) *et al.* Host–microbe interactions have shaped the genetic architecture of inflammatory bowel disease. *Nature* **491**, 119–124 (2012).
101. Rubino, S. J., Selvanantham, T., Girardin, S. E. & Philpott, D. J. Nod-like receptors in the control of intestinal inflammation. *Curr. Opin. Immunol.* **24**, 398–404 (2012).
102. Ananthakrishnan, A. N. *et al.* Lifestyle, behaviour, and environmental modification for the management of patients with inflammatory bowel diseases: an International Organization for Study of Inflammatory Bowel Diseases consensus. *Lancet Gastroenterol. Hepatol.* **7**, 666–678 (2022).
103. Oh-oka, K. *et al.* Induction of Colonic Regulatory T Cells by Mesalamine by Activating the Aryl Hydrocarbon Receptor. *Cell. Mol. Gastroenterol. Hepatol.* **4**, 135–151 (2017).
104. Barrett, K., Saxena, S. & Pollok, R. Using corticosteroids appropriately in inflammatory bowel disease: a guide for primary care. *Br. J. Gen. Pract.* **68**, 497–498 (2018).
105. Shin, J.-Y. *et al.* Thiopurine Prodrugs Mediate Immunosuppressive Effects by Interfering with Rac1 Protein Function. *J. Biol. Chem.* **291**, 13699–13714 (2016).
106. Van Dieren, J. M., Kuipers, E. J., Samsom, J. N., Nieuwenhuis, E. E. & Van Der Woude, J. C. Revisiting the immunomodulators tacrolimus, methotrexate, and mycophenolate mofetil: Their mechanisms of action and role in the treatment of IBD: *Inflamm. Bowel Dis.* **12**, 311–327 (2006).
107. Genaro, L. M. *et al.* Anti-TNF therapy and immunogenicity in.
108. Juillerat, P. *et al.* Positioning biologics in the treatment of IBD: A practical guide – Which mechanism of action for whom? *Curr. Res. Pharmacol. Drug Discov.* **3**, 100104 (2022).
109. Marsal, J. *et al.* Management of Non-response and Loss of Response to Anti-tumor Necrosis Factor Therapy in Inflammatory Bowel Disease. *Front. Med.* **9**, 897936 (2022).
110. Brierley, C. K. *et al.* Autologous Haematopoietic Stem Cell Transplantation for Crohn's Disease: A Retrospective Survey of Long-term Outcomes From the European Society for Blood and Marrow Transplantation. *J. Crohns Colitis* (2018) doi:10.1093/ecco-jcc/jjy069.
111. Lamb, C. A. *et al.* British Society of Gastroenterology consensus guidelines on the management of inflammatory bowel disease in adults. *Gut* **68**, s1–s106 (2019).

112. Zhang, X.-F. *et al.* Clinical effects and gut microbiota changes of using probiotics, prebiotics or synbiotics in inflammatory bowel disease: a systematic review and meta-analysis. *Eur. J. Nutr.* **60**, 2855–2875 (2021).
113. Paramsothy, S. *et al.* Faecal Microbiota Transplantation for Inflammatory Bowel Disease: A Systematic Review and Meta-analysis. *J. Crohns Colitis* **11**, 1180–1199 (2017).
114. Benchimol, E. I. *et al.* Incidence, Outcomes, and Health Services Burden of Very Early Onset Inflammatory Bowel Disease. *Gastroenterology* **147**, 803-813.e7 (2014).
115. Roberts, S. E. *et al.* A Systematic Review and Meta-analysis of Paediatric Inflammatory Bowel Disease Incidence and Prevalence Across Europe. *J. Crohns Colitis* **14**, 1119–1148 (2020).
116. Gettler, K. *et al.* Common and Rare Variant Prediction and Penetrance of IBD in a Large, Multi-ethnic, Health System-based Biobank Cohort. *Gastroenterology* **160**, 1546–1557 (2021).
117. Uhlig, H. H. *et al.* Clinical Genomics for the Diagnosis of Monogenic Forms of Inflammatory Bowel Disease. *J. Pediatr. Gastroenterol. Nutr.* **72**, 456–473 (2021).
118. Uhlig, H. H. *et al.* The Diagnostic Approach to Monogenic Very Early Onset Inflammatory Bowel Disease. *Gastroenterology* **147**, 990-1007.e3 (2014).
119. Zhu, L. *et al.* IL-10 and IL-10 Receptor Mutations in Very Early Onset Inflammatory Bowel Disease. *Gastroenterol. Res.* **10**, 65–69 (2017).
120. KJhn, R., Rajewsky, K. & MOiler, W. Interleukin-lO-Deficient Mice Develop Chronic Enterocolitis.
121. Speckmann, C. *et al.* X-linked inhibitor of apoptosis (XIAP) deficiency: The spectrum of presenting manifestations beyond hemophagocytic lymphohistiocytosis. *Clin. Immunol.* **149**, 133–141 (2013).
122. Esteban, Y. M., De Jong, J. L. O. & Tesher, M. S. An Overview of Hemophagocytic Lymphohistiocytosis. *Pediatr. Ann.* **46**, (2017).
123. Aguilar, C. & Latour, S. X-linked Inhibitor of Apoptosis Protein Deficiency: More than an X-linked Lymphoproliferative Syndrome. *J. Clin. Immunol.* **35**, 331–338 (2015).
124. Latour, S. & Aguilar, C. XIAP deficiency syndrome in humans. *Semin. Cell Dev. Biol.* **39**, 115–123 (2015).
125. Zeissig, Y. *et al.* XIAP variants in male Crohn's disease. *Gut* **64**, 66–76 (2015).
126. Eckelman, B. P., Salvesen, G. S. & Scott, F. L. Human inhibitor of apoptosis proteins: why XIAP is the black sheep of the family. *EMBO Rep.* **7**, 988–994 (2006).
127. Duckett, C. S. *et al.* A conserved family of cellular genes related to the baculovirus iap gene and encoding apoptosis inhibitors. *EMBO J.* **15**, 2685–2694 (1996).
128. Obexer, P. & Ausserlechner, M. J. X-Linked Inhibitor of Apoptosis Protein â€“ A Critical Death Resistance Regulator and Therapeutic Target for Personalized Cancer Therapy. *Front. Oncol.* **4**, (2014).
129. Cong, H. *et al.* Inhibitor of Apoptosis Protein (IAP) Antagonists in Anticancer Agent Discovery: Current Status and Perspectives. *J. Med. Chem.* **62**, 5750–5772 (2019).
130. Scott, F. L. *et al.* XIAP inhibits caspase-3 and -7 using two binding sites: evolutionarily conserved

mechanism of IAPs. *EMBO J.* **24**, 645–655 (2005).
131. Du, C., Fang, M., Li, Y., Li, L. & Wang, X. Smac, a Mitochondrial Protein that Promotes Cytochrome c–Dependent Caspase Activation by Eliminating IAP Inhibition. *Cell* **102**, 33–42 (2000).
132. Bai, L., Smith, D. C. & Wang, S. Small-molecule SMAC mimetics as new cancer therapeutics. *Pharmacol. Ther.* **144**, 82–95 (2014).
133. Eckelman, B. P. & Salvesen, G. S. The Human Anti-apoptotic Proteins cIAP1 and cIAP2 Bind but Do Not Inhibit Caspases. *J. Biol. Chem.* **281**, 3254–3260 (2006).
134. Harlin, H., Reffey, S. B., Duckett, C. S., Lindsten, T. & Thompson, C. B. Characterization of XIAP-Deficient Mice. *Mol. Cell. Biol.* **21**, 3604–3608 (2001).
135. Rigaud, S. *et al.* XIAP deficiency in humans causes an X-linked lymphoproliferative syndrome. *Nature* **444**, 110–114 (2006).
136. Joazeiro, C. A. P. & Weissman, A. M. RING Finger Proteins: Mediators of Ubiquitin Ligase Activity. *Cell* **102**, 549–552 (2000).
137. Krieg, A. *et al.* XIAP mediates NOD signaling via interaction with RIP2. *Proc. Natl. Acad. Sci.* **106**, 14524–14529 (2009).
138. Bertrand, M. J. M. *et al.* Cellular Inhibitors of Apoptosis cIAP1 and cIAP2 Are Required for Innate Immunity Signaling by the Pattern Recognition Receptors NOD1 and NOD2. *Immunity* **30**, 789–801 (2009).
139. Damgaard, R. B. *et al.* The Ubiquitin Ligase XIAP Recruits LUBAC for NOD2 Signaling in Inflammation and Innate Immunity. *Mol. Cell* **46**, 746–758 (2012).
140. Kanduc, D. *et al.* Cell death: Apoptosis versus necrosis (Review). *Int. J. Oncol.* (2002) doi:10.3892/ijo.21.1.165.
141. Taylor, R. C., Cullen, S. P. & Martin, S. J. Apoptosis: controlled demolition at the cellular level. *Nat. Rev. Mol. Cell Biol.* **9**, 231–241 (2008).
142. Ruffolo, P. R. THE PATHOGENESIS OF NECROSIS.
143. Linkermann, A. & Green, D. R. Necroptosis. *N. Engl. J. Med.* **370**, 455–465 (2014).
144. Murphy, J. M. *et al.* The Pseudokinase MLKL Mediates Necroptosis via a Molecular Switch Mechanism. *Immunity* **39**, 443–453 (2013).
145. He, W. *et al.* Gasdermin D is an executor of pyroptosis and required for interleukin-1β secretion. *Cell Res.* **25**, 1285–1298 (2015).
146. Wang, Y. & Kanneganti, T.-D. From pyroptosis, apoptosis and necroptosis to PANoptosis: A mechanistic compendium of programmed cell death pathways. *Comput. Struct. Biotechnol. J.* **19**, 4641–4657 (2021).
147. Gullett, J. M., Tweedell, R. E. & Kanneganti, T.-D. It's All in the PAN: Crosstalk, Plasticity, Redundancies, Switches, and Interconnectedness Encompassed by PANoptosis Underlying the Totality of Cell Death-Associated Biological Effects. *Cells* **11**, 1495 (2022).
148. Pandian, N. & Kanneganti, T.-D. PANoptosis: A Unique Innate Immune Inflammatory Cell Death Modality. *J. Immunol.* **209**, 1625–1633 (2022).
149. Samir, P., Malireddi, R. K. S. & Kanneganti, T.-D. The PANoptosome: A Deadly Protein Complex Driving Pyroptosis, Apoptosis, and Necroptosis (PANoptosis). *Front. Cell. Infect. Microbiol.* **10**, 238 (2020).
150. Bertrand, M. J. M. *et al.* cIAP1 and cIAP2 Facilitate Cancer Cell Survival by Functioning as E3 Ligases that Promote RIP1

Ubiquitination. *Mol. Cell* **30**, 689–700 (2008).
151. Mahoney, D. J. *et al.* Both cIAP1 and cIAP2 regulate TNF␣-mediated NF-□B activation. *CELL Biol.*
152. Vince, J. E. *et al.* Inhibitor of Apoptosis Proteins Limit RIP3 Kinase-Dependent Interleukin-1 Activation. *Immunity* **36**, 215–227 (2012).
153. Yabal, M. *et al.* XIAP Restricts TNF- and RIP3-Dependent Cell Death and Inflammasome Activation. *Cell Rep.* **7**, 1796–1808 (2014).
154. Lawlor, K. E. *et al.* RIPK3 promotes cell death and NLRP3 inflammasome activation in the absence of MLKL. *Nat. Commun.* **6**, 6282 (2015).
155. Wicki, S. *et al.* Loss of XIAP facilitates switch to TNFα-induced necroptosis in mouse neutrophils. *Cell Death Dis.* **7**, e2422–e2422 (2016).
156. Lawlor, K. E. *et al.* XIAP Loss Triggers RIPK3- and Caspase-8-Driven IL-1β Activation and Cell Death as a Consequence of TLR-MyD88-Induced cIAP1-TRAF2 Degradation. *Cell Rep.* **20**, 668–682 (2017).
157. Olayioye, M. A. *et al.* XIAP-deficiency leads to delayed lobuloalveolar development in the mammary gland. *Cell Death Differ.* **12**, 87–90 (2005).
158. Pasparakis, M., Alexopoulou, L., Episkopou, V. & Kollias, G. Immune and inflammatory responses in TNF alpha-deficient mice: a critical requirement for TNF alpha in the formation of primary B cell follicles, follicular dendritic cell networks and germinal centers, and in the maturation of the humoral immune response. *J. Exp. Med.* **184**, 1397–1411 (1996).
159. Rothe, J. *et al.* Mice lacking the tumour necrosis factor receptor 1 are resistant to TNF-mediated toxicity but highly susceptible to infection by Listeria monocytogenes. **364**, (1993).
160. Erickson, S. L. *et al.* Decreased sensitivity to tumour-necrosis factor but normal T-cell development in TNF receptor-2-deficient mice. *Nature* **372**, 560–563 (1994).
161. Newton, K., Sun, X. & Dixit, V. M. Kinase RIP3 Is Dispensable for Normal NF-□Bs, Signaling by the B-Cell and T-Cell Receptors, Tumor Necrosis Factor Receptor 1, and Toll-Like Receptors 2 and 4. *MOL CELL BIOL* **24**, (2004).
162. Schönheit, J. *et al.* PU.1 Level-Directed Chromatin Structure Remodeling at the Irf8 Gene Drives Dendritic Cell Commitment. *Cell Rep.* **3**, 1617–1628 (2013).
163. Woese, C. R. & Fox, G. E. Phylogenetic structure of the prokaryotic domain: The primary kingdoms. *Proc. Natl. Acad. Sci.* **74**, 5088–5090 (1977).
164. Lagkouvardos, I. *et al.* IMNGS: A comprehensive open resource of processed 16S rRNA microbial profiles for ecology and diversity studies. *Sci. Rep.* **6**, 33721 (2016).
165. Dietrich, A. *et al.* Namco: a microbiome explorer. *Microb. Genomics* **8**, (2022).
166. Bolsega, S. *et al.* The Genetic Background Is Shaping Cecal Enlargement in the Absence of Intestinal Microbiota. *Nutrients* **15**, 636 (2023).
167. Han, J., Lin, K., Sequeira, C. & Borchers, C. H. An isotope-labeled chemical derivatization method for the quantitation of short-chain fatty acids in human feces by liquid chromatography–tandem mass spectrometry. *Anal. Chim. Acta* **854**, 86–94 (2015).
168. Xia, J., Psychogios, N., Young, N. & Wishart, D. S. MetaboAnalyst: a web server for metabolomic data

analysis and interpretation. *Nucleic Acids Res.* **37**, W652–W660 (2009).
169. Moolenbeek, C. & Ruitenberg, E. J. The 'Swiss roll': a simple technique for histological studies of the rodent intestine. *Lab. Anim.* **15**, 57–60 (1981).
170. Wahida, A. *et al.* XIAP restrains TNF-driven intestinal inflammation and dysbiosis by promoting innate immune responses of Paneth and dendritic cells. *Sci. Immunol.* **6**, eabf7235 (2021).
171. Price, A. E. *et al.* A Map of Toll-like Receptor Expression in the Intestinal Epithelium Reveals Distinct Spatial, Cell Type-Specific, and Temporal Patterns. *Immunity* **49**, 560-575.e6 (2018).
172. Helft, J. *et al.* GM-CSF Mouse Bone Marrow Cultures Comprise a Heterogeneous Population of CD11c+MHCII+ Macrophages and Dendritic Cells. *Immunity* **42**, 1197–1211 (2015).
173. Flores-Langarica, A. *et al.* Intestinal CD103+CD11b+ cDC2 Conventional Dendritic Cells Are Required for Primary CD4+ T and B Cell Responses to Soluble Flagellin. *Front. Immunol.* **9**, 2409 (2018).
174. Persson, E. K., Scott, C. L., Mowat, A. McI. & Agace, W. W. Dendritic cell subsets in the intestinal lamina propria: Ontogeny and function: HIGHLIGHTS. *Eur. J. Immunol.* **43**, 3098–3107 (2013).
175. Gleeson, J. P. *et al.* The enhanced intestinal permeability of infant mice enables oral protein and macromolecular absorption without delivery technology. *Int. J. Pharm.* **593**, 120120 (2021).
176. Ulluwishewa, D. *et al.* Regulation of Tight Junction Permeability by Intestinal Bacteria and Dietary Components1,2. *J. Nutr.* **141**, 769–776 (2011).
177. Maternal diet and gut microbiome composition modulate early-life immune development.
178. Peters, B. A. *et al.* A taxonomic signature of obesity in a large study of American adults. *Sci. Rep.* **8**, 9749 (2018).
179. Engel, K. M., Schiller, J., Galuska, C. E. & Fuchs, B. Phospholipases and Reactive Oxygen Species Derived Lipid Biomarkers in Healthy and Diseased Humans and Animals – A Focus on Lysophosphatidylcholine. *Front. Physiol.* **12**, 732319 (2021).
180. Bjerrum, J. T. *et al.* Metabonomics of human fecal extracts characterize ulcerative colitis, Crohn's disease and healthy individuals. *Metabolomics* **11**, 122–133 (2015).
181. Shah, R. M. *et al.* Plasma Metabolic and Lipidomic Fingerprinting of Individuals with Increased Intestinal Permeability. *Metabolites* **12**, 302 (2022).
182. Strigli, A. *et al.* Deficiency in X-linked inhibitor of apoptosis protein promotes susceptibility to microbial triggers of intestinal inflammation. *Sci. Immunol.* **6**, eabf7473 (2021).
183. Yadav, M. & Chauhan, N. S. Microbiome therapeutics: exploring the present scenario and challenges. *Gastroenterol. Rep.* **10**, goab046 (2022).
184. El Aidy, S. *et al.* Gut bacteria–host metabolic interplay during conventionalisation of the mouse germfree colon. *ISME J.* **7**, 743–755 (2013).
185. Choo, J. M. & Rogers, G. B. Establishment of murine gut microbiota in gnotobiotic mice. *iScience* **24**, 102049 (2021).
186. Bo, T.-B. *et al.* Coprophagy prevention alters microbiome, metabolism, neurochemistry, and cognitive behavior in a small

mammal. *ISME J.* **14**, 2625–2645 (2020).
187. Bogatyrev, S. R., Rolando, J. C. & Ismagilov, R. F. Self-reinoculation with fecal flora changes microbiota density and composition leading to an altered bile-acid profile in the mouse small intestine. *Microbiome* **8**, 19 (2020).
188. De Caro, C. *et al.* Gut Microbiota Profile Changes in Patients with Inflammatory Bowel Disease and Non-Alcoholic Fatty Liver Disease: A Metagenomic Study. *Int. J. Mol. Sci.* **25**, 5453 (2024).
189. Schloss, P. D. *et al.* Stabilization of the murine gut microbiome following weaning. *Gut Microbes* **3**, 383–393 (2012).
190. Kemp, K. M., Colson, J., Lorenz, R. G., Maynard, C. L. & Pollock, J. S. Early life stress in mice alters gut microbiota independent of maternal microbiota inheritance. *Am. J. Physiol.-Regul. Integr. Comp. Physiol.* **320**, R663–R674 (2021).
191. Yu, S. *et al.* Leaky Gut in IBD: Intestinal Barrier–Gut Microbiota Interaction. *J. Microbiol. Biotechnol.* **32**, 825–834 (2022).
192. Jaworska, K. *et al.* Inflammatory bowel disease is associated with increased gut-to-blood penetration of short-chain fatty acids: A new, non-invasive marker of a functional intestinal lesion. *Exp. Physiol.* **104**, 1226–1236 (2019).
193. Chassaing, B., Ley, R. E. & Gewirtz, A. T. Intestinal Epithelial Cell Toll-like Receptor 5 Regulates the Intestinal Microbiota to Prevent Low-Grade Inflammation and Metabolic Syndrome in Mice. *Gastroenterology* **147**, 1363-1377.e17 (2014).

List of Publications

Wahida A.*, **Müller M*.,** *et al.,* XIAP restrains TNF-driven intestinal inflammation and dysbiosis by promoting innate immune responses of Paneth and dendritic cells; Sci Immunol. 2021 Nov 5;6(65):eabf7235. doi: 10.1126/sciimmunol.abf7235. Epub 2021 Nov 5. PMID: 34739338
* both authors contributed equally to this publication

Griewahn L., **Müller-Foxworth M**., *et al.*, SPATA2 restricts OTULIN-dependent LUBAC activity independently of CYLD; Cell Reports, Jan 2023, doi.org/10.1016/j.celrep.2022.111961